Donald A. Petrash

MCDONNELL DOUGLAS

STUDY AND DESIGN OF A CRYOGENIC PROPELLANT ACQUISITION SYSTEM

Third Quarterly Report
1 JANUARY 1972 THROUGH 31 MARCH 1972

15 APRIL 1972

MDC G2940

PREPARED BY:

G.W. BURGE
PROJECT MANAGER, NAS8-27685
PROPULSION DEPARTMENT

APPROVED BY:

P.L. KLEVATT
CHIEF TECHNOLOGY ENGINEER–PROPULSION
RESEARCH AND DEVELOPMENT
ADVANCE SYSTEMS AND TECHNOLOGY

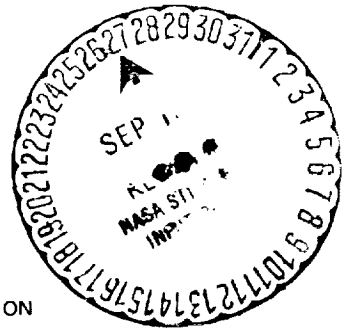

PREPARED FOR
NATIONAL AERONAUTICS AND SPACE ADMINISTRATION
MARSHALL SPACE FLIGHT CENTER
HUNTSVILLE, ALABAMA
CONTRACT NAS8-27685

MCDONNELL DOUGLAS ASTRONAUTICS COMPANY

5301 Bolsa Avenue, Huntington Beach, CA 92647

PREFACE

This is the third quarterly progress report on the program, "Study and Design of a Cryogenic Propellant Acquisition System." The period covered is 1 January to 31 March 1972. This work is being carried out by McDonnell Douglas Astronautics Company (MDAC) for the National Aeronautics and Space Administration, Marshall Space Flight Center, Huntsville, Alabama, under Contract NAS8-27685. Mr. G. M. Young serves as the principal NASA contracting officer representative. The MDAC technical effort is being conducted under the direction of G. W. Burge, Program Manager, and Dr. J. B. Blackmon, Deputy Program Manager. Major contributions to this report were made by J. N. Castle, Dr. C. R. Easton, B. R. Heckman, D. W. Kendle, and Dr. R. A. Madsen.

CONTENTS

FIGURES

TABLES

Section 1
INTRODUCTION

1.1 OBJECTIVES

The objectives of this project are to investigate, define, and demonstrate, through ground testing, an acquisition system for supplying subcooled LH_2 and LO_2 to satisfy integrated cryogenic auxiliary propulsion system (APS) requirements effectively for a vehicle such as a space shuttle. This effort will concentrate on concepts that utilize the favorable surface tension characteristics of fine mesh screens and will significantly advance cryogen acquisition technology in general. The anticipated analytical and experimental results will provide a sound technology base for the subsequent design of a future APS cryogen supply subsystem. These objectives will be achieved by a four-phase program covering 20 months.

1.2 PROGRAM SUMMARY

1.2.1 Phase I—Analysis

The objectives of this phase are to: (1) evolve conceptual designs for candidate APS acquisition systems, (2) formulate the analytical models needed to analyze this class of system, and (3) generate parametric data on overall candidate system performance, characteristics, and operational features in sufficient depth to establish critical design problems and criteria and support a sound system design and evaluation.

1.2.1.1 Task A—Design Studies

Candidate surface-tension-type acquisition systems will be conceptually defined relative to anticipated requirements for a shuttle-class application and studied in detail. This will include not only the acquisition subsystem but also all other subsystems that interact with the acquisition device, such

as the propellant storage, pressurization, and vent subsystem. This will be approached by establishing a workable design for a baseline system using the distributed channel concept; analyzing this system in detail with respect to failure modes, performance, design criteria, and areas of potential and significant improvement; and perturbing or evolving the baseline design in areas where these potential improvements exist and can technically be accomplished. This procedure may thus result in establishing several variations of a system design or several different system designs with individual or specialized characteristics that will ultimately be compared with one another. Analysis and design models and/or procedures will be modified or developed as necessary to support this investigation. The study will include a failure mode analysis for the promising candidates.

1.2.1.2 Task B—Parametric Studies

Critical parametric data will be generated for each promising candidate to identify and define critical design factors and criteria for each concept. Design limits and performance parameters such as head retention capability and weight will be evaluated over a range of conditions so that the impact of variation in system design requirements can be assessed for each promising candidate concept.

1.2.2 Phase II—Design

The objective of this phase will be to use the theoretical models and parametric results generated in Phase I to arrive at (1) a selected acquisition concept and resulting preliminary design for a shuttle-class APS feed system, (2) a test prototype design for a representative APS acquisition subsystem that will permit meaningful ground testing to verify the design concept, and (3) a test plan to control the prototype testing to produce maximum usable results.

1.2.2.1 Task A—Preliminary Design/Comparison

APS feed system preliminary designs will be produced based on the candidate acquisition concepts and the general results from Phase I. These designs will be in sufficient detail to permit a valid performance comparison of the

potential candidates. This task will be completed with the final selection of the recommended feed system design for a shuttle-class APS. Selection criteria will stress the ability to satisfy flexible vehicle mission and duty cycle requirements and compatibility with a minimum-cost, high "probability of success" development program.

Bench testing will be conducted relative to critical problems that must be resolved in order to complete the preliminary designs realistically. These tests will be conducted in parallel with the design activity.

1.2.2.2 Task C—Prototype Design

The objective of this task is to prepare a detailed design for a large-scale prototype acquisition system test apparatus, suitable to support a ground test program, that is compatible with the system selected in Task II-A for the shuttle-class APS. The prototype will be designed and instrumented to demonstrate the critical operational aspects of the system and show that practical fabrication is possible. The current plan is to use an existing, insulated, 105-inch LH_2 tank that will be modified and into which the integrated LH_2 acquisition system will be installed.

A test plan defining the installation and the tests to be conducted will be prepared as part of the design activity.

1.2.2.3 Task D—Reporting

Monthly and quarterly reports, and a final and an interim report will be submitted as defined by the program schedule. This effort will also include oral reviews and status reports.

1.2.3 Phase III—Fabrication

During this phase, the prototype design generated under Task II-C will be fabricated and/or assembled.

1.2.4 Phase IV—Testing

The objective of this task is to coordinate test operations at MSFC to verify the performance of the prototype system and to analyze and evaluate the test

results. Included as part of this phase are a preliminary leak test and checkout of the modified tank, and delivery of the completed prototype.

1.2.4.1 Task A—Checkout and Ship

A leak test will be conducted after completion of the 105-inch tank structural modifications. After final assembly, the completed test prototype will be sent to MSFC.

1.2.4.2 Task B—Test Operation

Engineering support will be provided at MSFC to direct and coordinate installation and performance evaluation testing of the prototype system as outlined in the developed test plan.

1.2.4.3 Task C—Analysis and Reporting

The test results will be analyzed to assess the demonstrated performance and characteristics of the prototype feed system and to compare them with anticipated behavior. These results will be documented in the final report, thus concluding the program.

Section 2
SUMMARY

During the third quarter of this program, work progressed essentially according to schedule and the program plan.

The technical effort during this quarter involved completion of the Phase I - Analysis and initiation of Phase II - Design. The various system elements being considered include the basic cryogen tankage; cryogen thermal storage provisions for in-atmosphere as well as space operation; the acquisition subsystem and its thermal control; pressurization provisions; and the feed subsystem (that portion of the system between the acquisition device and the pump, including interaction between the pump and the acquisition system). These areas are being pursued in sufficient depth to permit the evolution of a well defined feed system preliminary design. Most of the current effort is directed towards a series of bench tests to provide data and design concept substantiation to support this preliminary design effort.

Specific accomplishments for the quarter are listed below:

A. Essentially completed all propellant storage thermal analysis and trade studies relative to the main tankage insulation and thermal control. Unresolved decisions relate to the final vent system selection.
B. Completed most of the parametric data for pressurization system performance and weight penalties.
C. Initiated a detailed study of the internal tank pump/mixer TVS system (about 50 percent complete).
D. Established basic equations for start tank zero gravity "vacuum refill".

E. Initiated a study of a thermodynamic transient pump bypass flow management concept but have not resolved feasibility.

F. Initiated an extensive series of bench tests to provide essential information to support preliminary design effort. Experiments underway include:

- Candidate screen bubble-point tests in LH_2.
- Screen heat transfer tests with retained LH_2 exposed to a warm ullage.
- Screen welding tests.
- Screen/backup structure pressure loss tests with flow.
- Tests to evaluate influence of vibration on retention capability.
- Tests to assess bubble-point degradation brought about by screen pleating.
- Tests to determine influence of screen flexing on bubble-point characteristics.

Details of this work are covered in Section 3 of this report.

Section 3
TECHNICAL DISCUSSION

During the third quarter of this program, work was essentially completed on Phase I - Analysis and initiated on Phase II - Design per the program plan as shown in Figure 1. Work is currently in progress on Task A - Preliminary Design/Comparison and Task B - Bench Testing of the Phase II design efforts. To simplify reporting, the concluding analysis effort from Phase I will be reported along with the preliminary design task of Phase II since these work areas are intimately tied together.

3.1 PHASE II, TASK A - PRELIMINARY DESIGN/COMPARISON

The objective of this task is to evolve preliminary designs for the acquisition concepts identified in Phase I and integrated into total feed systems compatible with advanced H_2/O_2 APS system requirements. A final design will then be selected for prototype evaluation in subsequent program phases. The baseline acquisition concepts were evolved during Phase I and for reference purposes are shown in Figure 2. In discussing the preliminary design, the systems have been broken down into their basic subsystems, even though most of the work is being approached on an integrated system basis.

3.1.1 Thermal Subsystem

3.1.1.1 Space Insulation - Optimization

The original LH_2 tank MLI optimization reported in Reference 1 for the 7-day coast was based on a simplified analytical model using a propellant storage efficiency criteria. This optimization was repeated using the MDAC Space Propulsion Module Sizing and Optimization Program (H109) which takes the entire propulsion module into account and optimizes any selected design variable on the basis of either minimum stage gross weight or maximum stage velocity change. The program was set up using the baseline

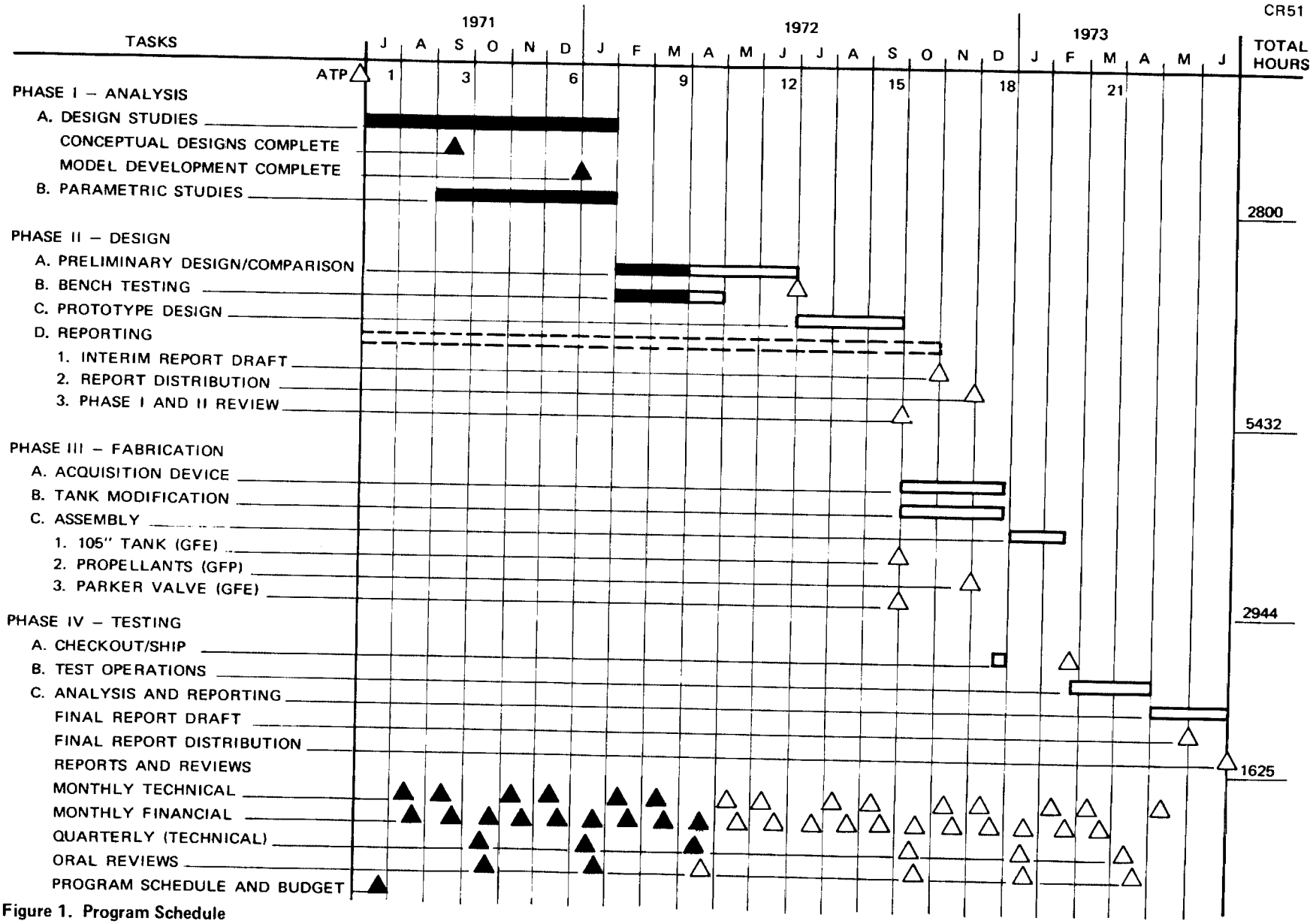

Figure 1. Program Schedule

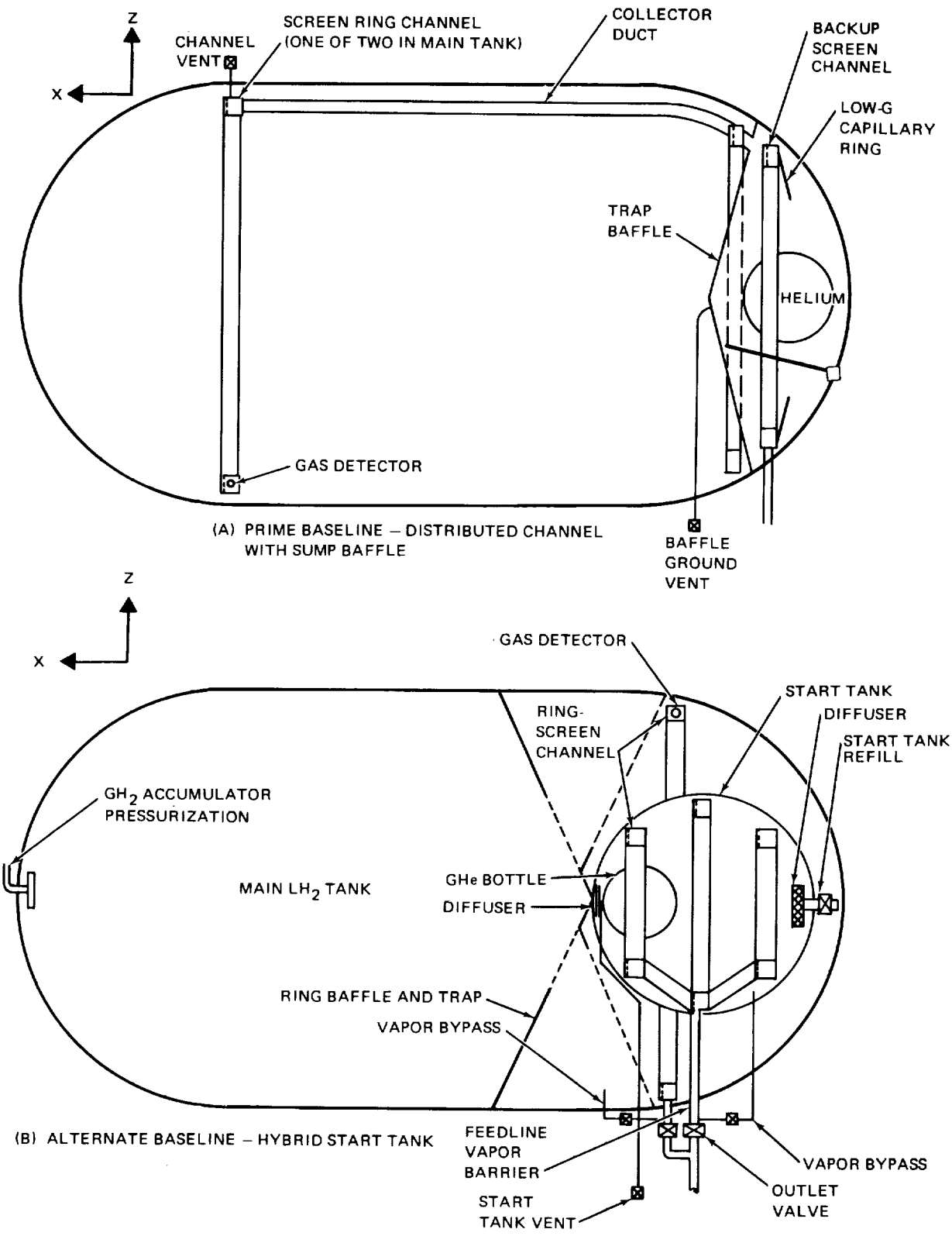

Figure 2. Baseline Acquisition Concepts

vehicle overall geometry, specific insulation parameters, and overall design factors; the vehicle gross weight was evaluated as the number of insulation layer-pairs on the LH_2 tank was varied. Rather than using total vehicle weight, results are presented in terms of vehicle gross weight minus 123,000 kg (270,000 lb). Important assumptions for this analysis are as follows: (1) cold (propellant temperature) helium pressurization, (2) a two-blanket, double-goldized, kapton/dacron (B4A) net insulation (effective design thermal conductivity = 2.42 $\frac{\text{Joules}}{\text{M-Sec°K}}$), (3) a 9-burn duty cycle for an easterly design mission, (4) tankage size based on the data of Tables 1 and 7 of Reference 1, (5) initial ullage of 35 percent, (6) true NPSP tank pressure control maintaining 20.7×10^3 N/m^2 (3 psi) above propellant saturation pressure during expulsion and a hot boundary temperature for the vehicle of 278°K (500°R).

The system was first optimized on the assumption that no heat absorption occurred by LH_2 sensible temperature rise and that all incoming heat resulted in vaporization and direct boiloff at 14.7 psia tank pressure. This represents a continuous venting mode of operation. The overall results as computed by the H109 program are shown in Figure 3 which shows that minimum feed-system weight results with 48 layer-pairs of insulation (just slightly higher than in the initial analysis). It should be noted that at this point in the analysis, the absolute gross weight numbers were not valid; only the relative values or changes were meaningful.

The mode of operation alalyzed above, in which all heat is used to boiloff cryogen at 14.7 psia tank pressure, is conservative because considerable heat can be absorbed by sensible temperature rise of the propellant. A second mode of operation was analyzed by the H109 program in which it was assumed that the LH_2 tank did not vent during the mission and that all incoming heat was absorbed by uniform temperature increase of the tank contents. All other assumptions listed above were retained. It was found, as indicated in Figure 3, that the optimum insulation for this mode of operation consisted of 34 layer-pairs of MLI. For this case, the maximum achieved tank pressure was 170×10^3 N/m^2 (24.6 psia) which occurs just prior

Table 1

COMPARISON OF INSULATION CONCEPTS FOR IN-ATMOSPHERE OPERATION
DISTRIBUTED CHANNEL ACQUISITION SYSTEM

Required LH_2 Storage	Insulation Type	Insulation Thickness (cm)	ΔWeight Insulation (kg)	ΔWeight Boiloff (kg)	Total Weight (kg)
Through boost	Excess helium-purged MLI	0	0	33	33
	Internal foam	1.9 (1)	143	27	170
	External foam	0.64(4)	29	11	40
	Vacuum jacket	0	517(2)	0	517
Through entry	Excess helium-purged MLI	0	0	118	118
	Internal foam	1.9	143	39 or 49(3)	182 or 192
	External foam	0.64	29	31 or 56	60 or 85
	Vacuum jacket	0	517(2)	0.5	517
Through landing	Excess helium-purged MLI	1.27	99	136	235(5) (203)
	Internal foam	1.9	143	61 or 104	204 or 247
	External foam	1.27	57	45 or 79	102 or 136
	Vacuum jacket	0	517(2)	1	518

1. Minimum thickness of internal foam to restrict temperature below LN_2.
2. Outer vacuum jacket weight (Reference 3).
3. First value GN_2/He repressurization: Second value GHe purge only.
4. Minimum layup of insulation.
5. Corrected value in ( ) to account for performance improvement during coast.

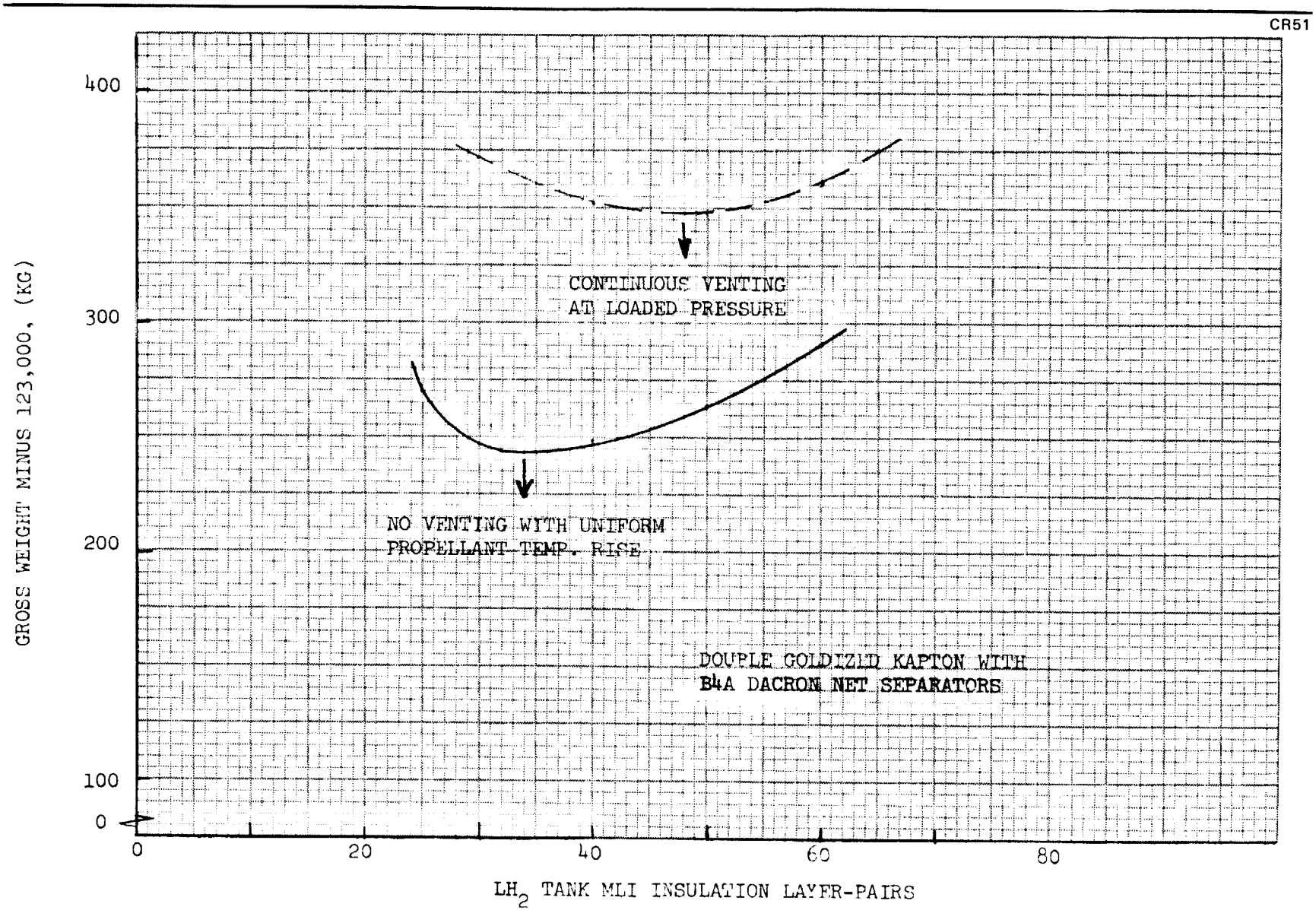

Figure 3. Space MLI Insulation Optimization

to the 8th expulsion step. This pressure will be exceeded if any stratification occurs in the system that is not removed or if local heating results in vapor generation. Thus, this mode of operation is probably optimistic. Therefore the MLI thickness will be selected, at this point, based on the more conservative direct boiloff model. The basic MLI details are shown in Figure 4. For the 48-layer-pair system, the MLI base weight will be 98.7 kg (217.5 lb) consisting of 35 kg for insulation face sheets and 63.7 kg for MLI. For a 34-blanket system, the total weight would be 80.3 kg. The 48 layers will result in a heat load during equilibrium coast of 48.7 watts (166 Btu/hr) and a LH_2 boiloff of 0.39g kg/hr (0.87 lb/hr) or 66.2 kg (146 lb) for the total coast period.

The same basic goldized kapton/dacron B4A net MLI insulation is used on the LO_2 tank. As discussed in Reference 1, weight can be saved if the net heat input to the LO_2 tank is maintained near zero by using the cooling capability of the LH_2 tank vent gases to cool the LO_2 system. In Figure 5 the required GH_2 coolant weight, LO_2 tank insulation weight, and the summation are shown as a function of the number of LO_2 tank insulation layers. The maximum LH_2 tank vent loss, based on the LH_2 tank MLI thickness, is 66.5 kg as noted. If this were all used to cool the LO_2 tank, 22 layer-pairs of MLI are required on the LO_2 tank. However, this does not result in a minimum weight summation; this condition is achieved by using 50 MLI layer-pairs on the LO_2 tank and passing only 29 kg of GH_2 to cool the LO_2 tank. However, if the LH_2 tank is normally vented, this vent loss is not chargable to the LO_2 system and the optimum LO_2 system would be that with minimum layers of MLI compatible with the LH_2 tank vent weight. Thus a 22-layer MLI system is probably the optimum design. If the LO_2 tank MLI were optimized by minimizing system weight assuming no hydrogen cooling and that all incoming heat goes into LO_2 boiloff, 64 layers of MLI (52 kg) would be needed. The LO_2 boiloff would be about 39.8 kg for a total weight of 91.8 kg. Thus the use of GH_2 cooling for the LO_2 tank is quite desirable.

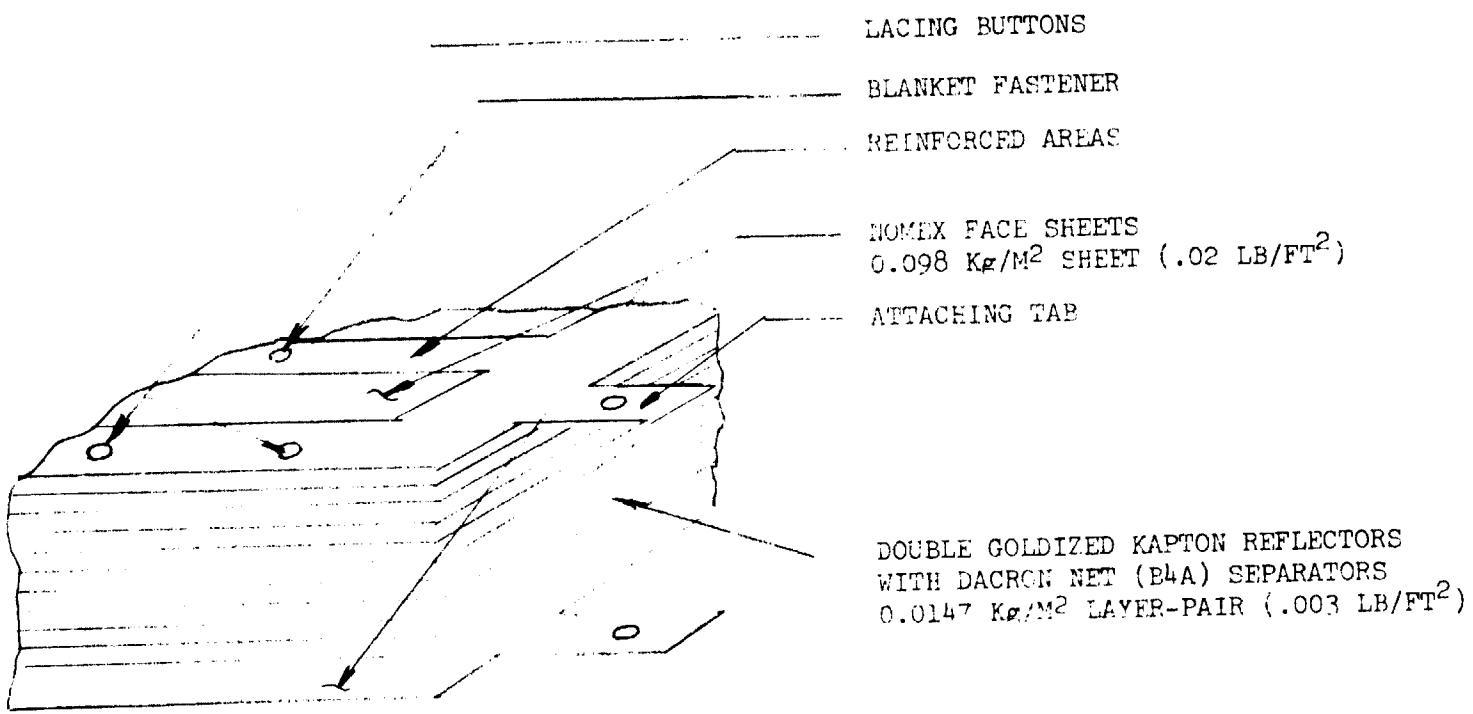

Figure 4. MLI Blanket Configuration/Design

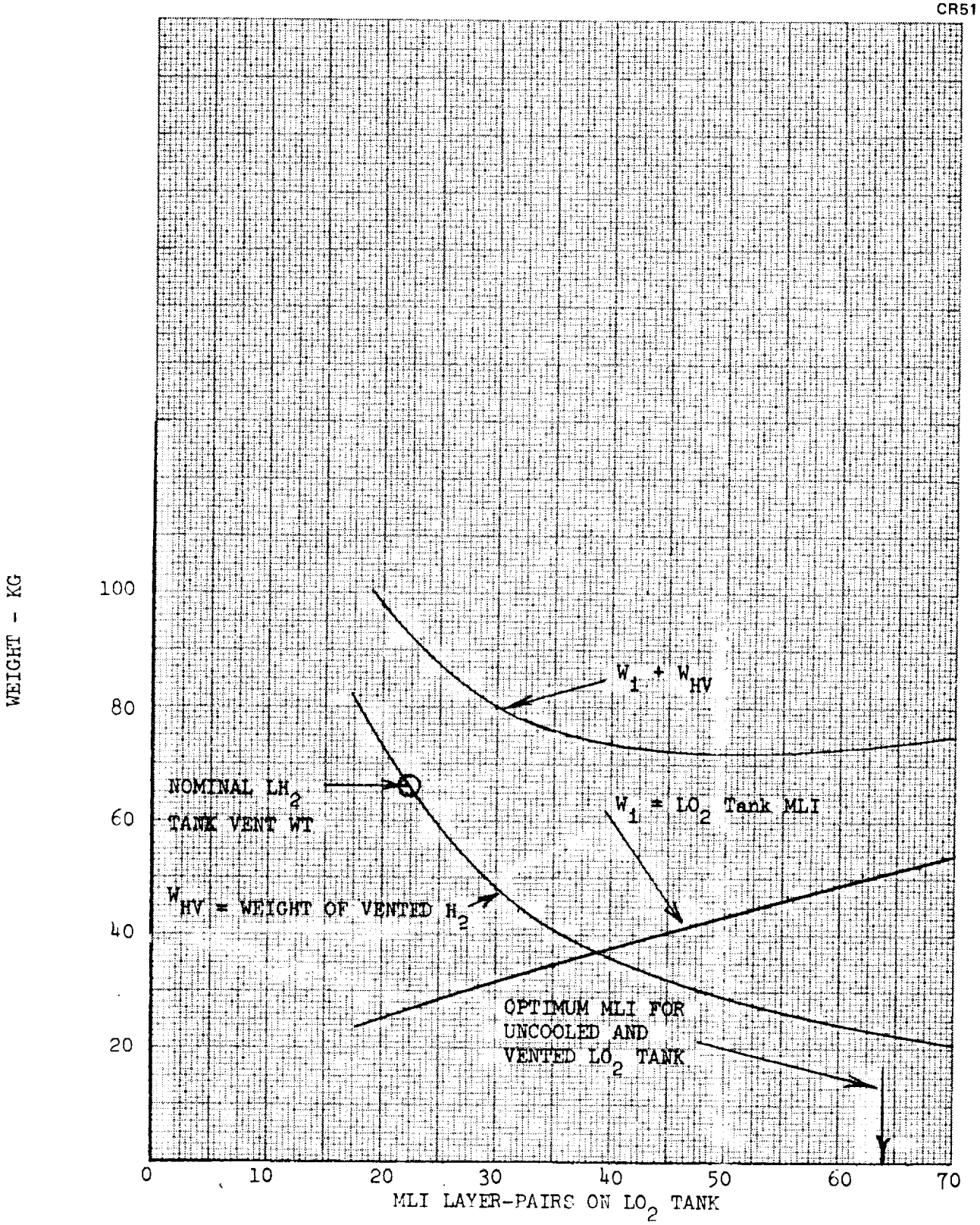

Figure 5. LO_2 Tank MLI Requirements

3.1.1.2 In-Atmosphere Insulation - Distributed Channel Acquisition System Most of the analysis work relative to the in-atmosphere insulation system was reported in Reference 2. The analysis has been checked and expanded in certain areas. The final results are presented in Table 1 and include a complete vacuum jacketed (dewar) system in addition to the purged systems discussed in Reference 2. The results are presented considering missions where subcooled cryogen must be stored through: (1) boost only, (2) boost and entry, and (3) for a complete mission including landing. The vacuum jacket weight was obtained by using the data reported in Reference 3. The appropriate curve from this report is shown in Figure 6. This applies to a 56.6 m^3 (2,000 ft^3) LH_2 tank with a jacket clearance of 11.4 cm. Based on surface area alone, the reported jacket weight would have to be increased by a factor of 1.27 for our 69.2 m^3 and cylindrical L/D = 1.14 baseline LH_2 tank. The 517 kg shown in Table 1 corresponds to a jacket structure using 5056 aluminum honeycomb flex core with boron/epoxy and titanium face sheets. This was the lightest reported design. Other vacuum jacket designs are possible, some of which may involve lower weight than that shown here; however, it is unlikely that these will be closely competitive in terms of total weight with the other insulation concepts identified in Table 1, even for a full mission storage requirement.

Other conclusions that can be drawn from the results summarized in Table 1, include the following:

A. Internal foam provides no weight advantage relative to simple helium-purged MLI although the foam would permit use of GN_2 ground purging.

B. The external foam results in minimum weight except for the case of storage only through boost where it is 7 kg heavier than the simple helium-purged MLI. However, being able to use GN_2 rather than helium is probably worth the 7 kg of added weight.

In the case of simple helium-purged MLI for LH_2 storage over the entire mission, the MLI thickness is increased over that required for space to yield the optimum-purged MLI. This in turn improves the space performances of the system by reducing the in-space boiloff by 32 kg. Thus, the

TAKEN FROM BOEING REPORT REFERENCE 3

A GLASS/EPOXY - ALUMINUM
B GLASS/EPOXY - TITANIUM
C GLASS/POLYRIDE - TITANIUM
D BORON/EPOXY - TITANIUM

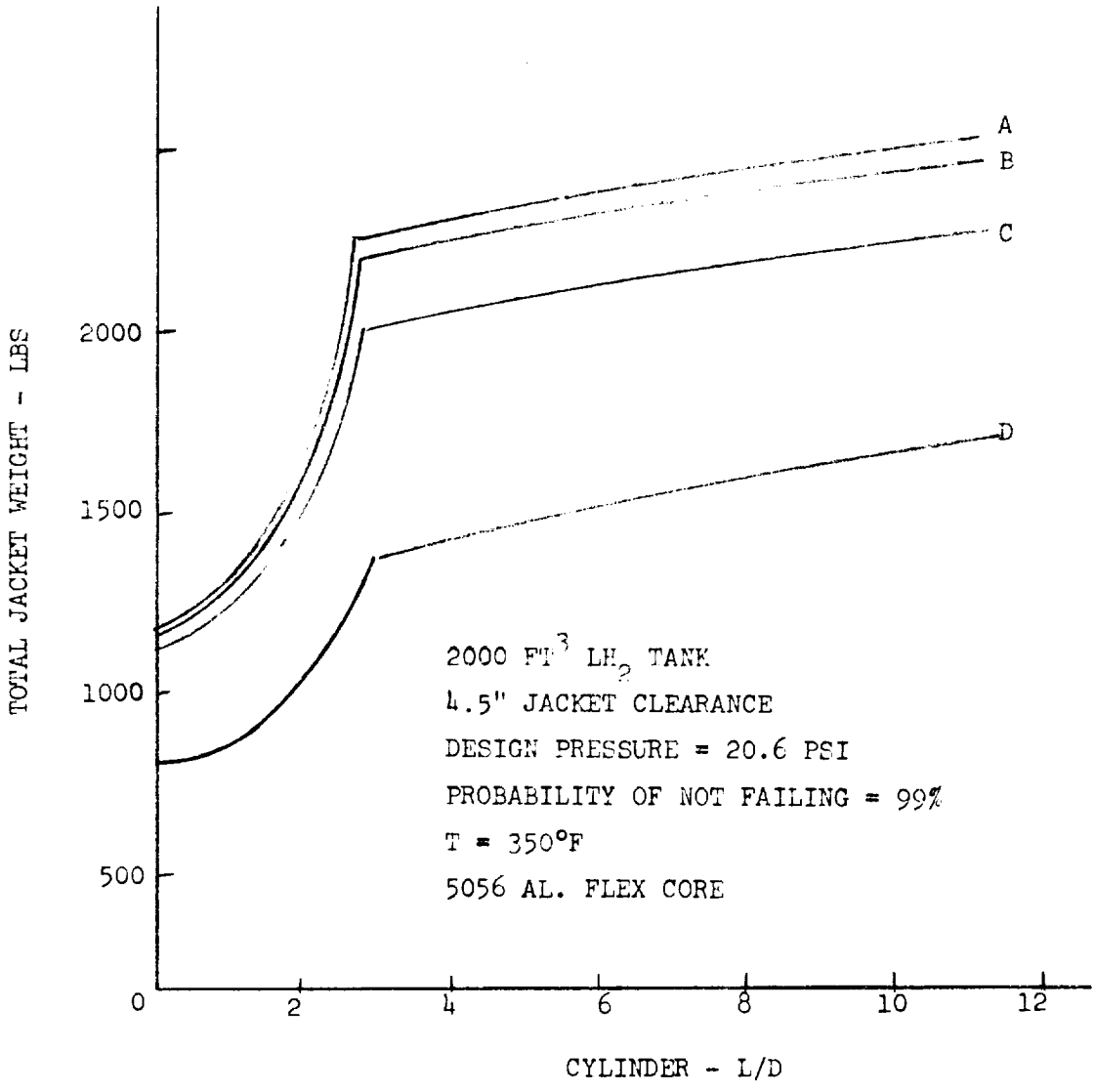

Figure 6. Vacuum Jacket Weight—Honeycomb Structure

effective weight penalty is actually 235 -32 = 203 kg as indicated. In no other case does the in-atmosphere storage provision have a significant influence on in-orbit behavior. However, the helium-purged MLI is still not as light as the optimum external foam. Therefore, the external foam insulation with a GN_2 purge, augmented with helium for the initial reentry purge, is the selected system. This represents some advancement in the state of the art but the concept should be feasible. It is expected that more backup data for the external foam system will be available prior to the conclusion of Phase II of this study.

For the LO_2 system, a simple GN_2 purge is quite adequate for efficient in-atmosphere operation.

3.1.1.3 In-Atmosphere Insulation - Start Tank Acquisition System

The start-tank acquisition concept can be sized so that all propellant for operation during reentry and landing (high heat input periods) can be contained within the spherical start tank. This reduces the effective heat transfer area and could thus potentially save weight in the thermal storage subsystem relative to the baseline distributed channel system with a simple helium-purged MLI of purged MLI/foam composite insulation systems. To evaluate this possible savings, a detailed thermal analysis of a start-tank system was conducted using the recently developed MDAC transient thermal analysis computer code. The following assumptions were made:

A. A 21.9 m^3 (773 ft^3) start tank was assumed (this is the maximum size start tank with no refills, other than those occurring during vehicle acceleration.)

B. A conventional S-IVB type foam insulation with a density of 0.832 x 10^2 kg/m^3 (5.2 lb/ft^3) was used on the start tank.

C. A helium-purged MLI optimized for space operation alone was used on the main tank.

D. The external environment used in the previous insulation system analysis was used and it was assumed that the LH_2 had to be stored through reentry and landing.

E. During reentry, the main tank was assumed to be vented to 1 atmosphere.

For these conditions, the integrated heat load for the total mission up to reentry is about 44 x 10^6 Joules (41, 700 Btu) for 1. 27 cm of MLI. For the entry and landing period, the integrated heat load into the reentry propellant contained in the start tank, with no foam insulation on the start tank, is about 46. 6 x 10^6 Joules (44, 500 Btu) as compared to 86. 4 x 10^6 Joules (82, 000 Btu) to the reentry propellant contained within the main tank with 1. 27 cm of MLI. The total weight penalty of the basic thermal storage system for the start-tank system is shown in Figure 7 as a function of start-tank foam thickness. The weight penalty includes the total usable boiloff, including in-orbit losses from both the main tank and the start tank, and the foam weight. The computed values shown in Figure 7, indicate an optimum start-tank foam insulation of 0. 635 cm (0. 25 in.), yielding a total weight penalty of 263 kg broken down as shown in Table 2. Also shown in Figure 7 and Table 2 are weights for non-start-tank systems, including one using an optimum thermal protection system consisting of a composite external foam/MLI and another using a simple helium purged MLI.

The start tank does result in a minimum thermal storage system weight penalty but has about the same weight as the non-start-tank system. There is a savings of about 83 kg over a non-start-tank system using a simple helium-purged MLI.

From this analysis it is concluded that there probably is no significant advantage, in terms of thermal storage improvement, in the start tank concept unless the selected MLI/external foam composite cannot achieve the expected performance. However, use of a smaller start tank may also result in more thermal improvement, and a decrease in overall hardware weight. This concept will be investigated further.

3. 1. 1. 4 Total Baseline Tankage Insulation System Selection

Based on the preceding analysis, the selected insulation for the baseline distributed channel LH_2 tank will consist of 1. 27 cm of external foam insulation bonded to the tank wall, 48 layer-pairs or 1. 36 cm of MLI (Double Goldized Kapton with Dacron B4A net separators) and a Kapton purge bag. This system is sized to store

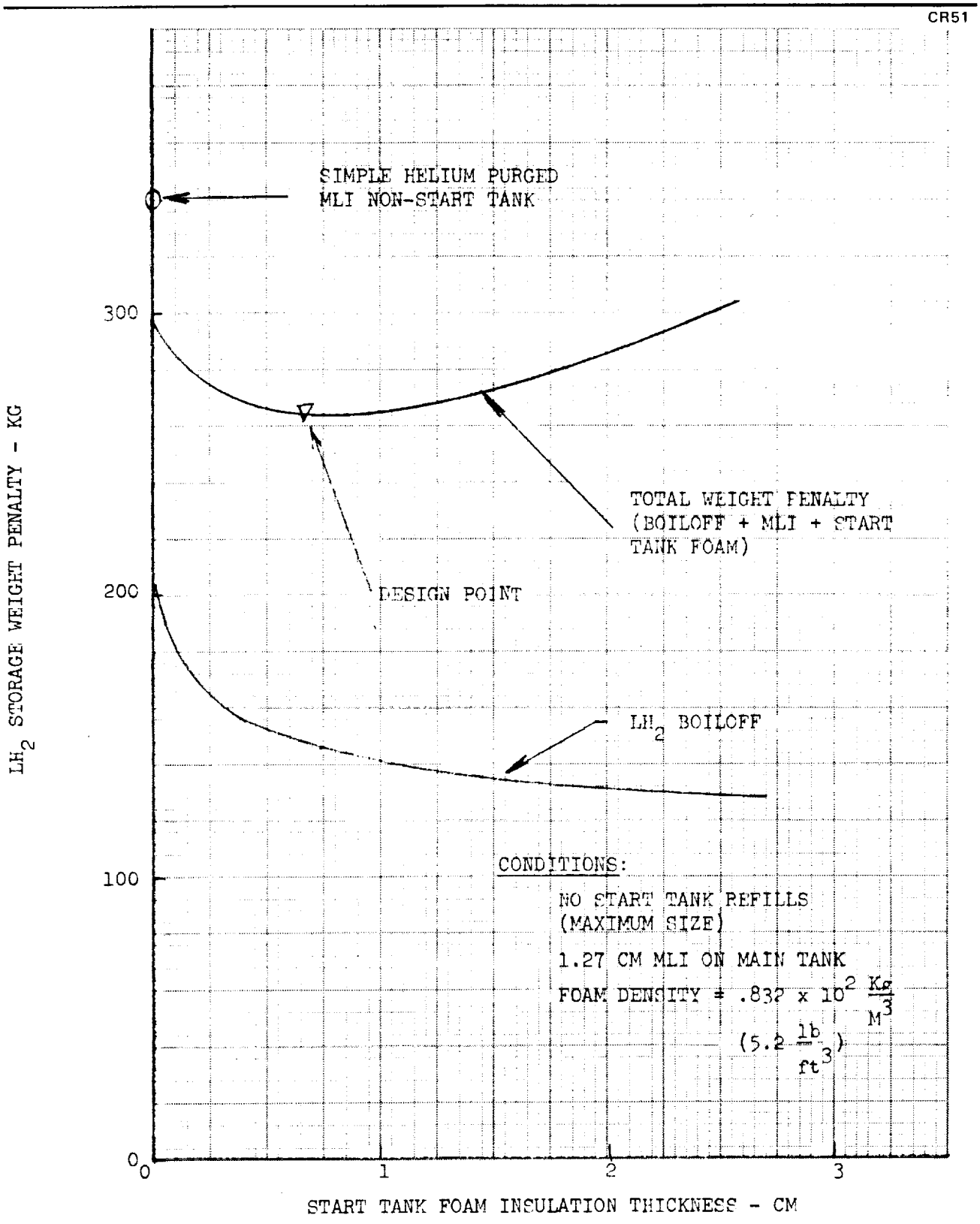

Figure 7. LH_2 Storage Characteristics with Integrated Start Tank

Table 2

LH_2 THERMAL STORAGE WEIGHT PENALTY BREAKDOWN

	Maximum Start Tank Size with Optimum Foam Insulation Thickness (kg)	Distributed Channel Baseline	
		Optimum* (kg)	Simple Helium-Purged MLI (kg)
Main tank total LH_2 boiloff	100	112	170
Start tank boiloff	43	0	0
MLI	99	99	176
Start tank foam	21	0	0
Main tank foam	0	57	0
Total weight penalty	263	268	346

*1.27 cm external foam with 1.27 cm of MLI on main tank.

subcooled LH_2 for the complete mission including landing. The insulation system installation is illustrated in Figure 8 along with weight and performance values. The installation is made in two blankets, which are attached with rigid, low-conductivity, teflon studs at the top and bottom of the tank. The blankets are held together with small plastic buttons placed one foot on centers and small tabs along the edges of the outer layers which are laced together. Joint overlapping is used to minimize joint thermal degradation. Nitrogen purging is used for ground hold and is allowed to excape from the MLI during boost. The system is repressurized with helium to just above atmospheric pressure during reentry. Selected temperature profiles are shown in Figure 9, at critical points in the flight as determined by the MDAC transient heating computer code.

CR51

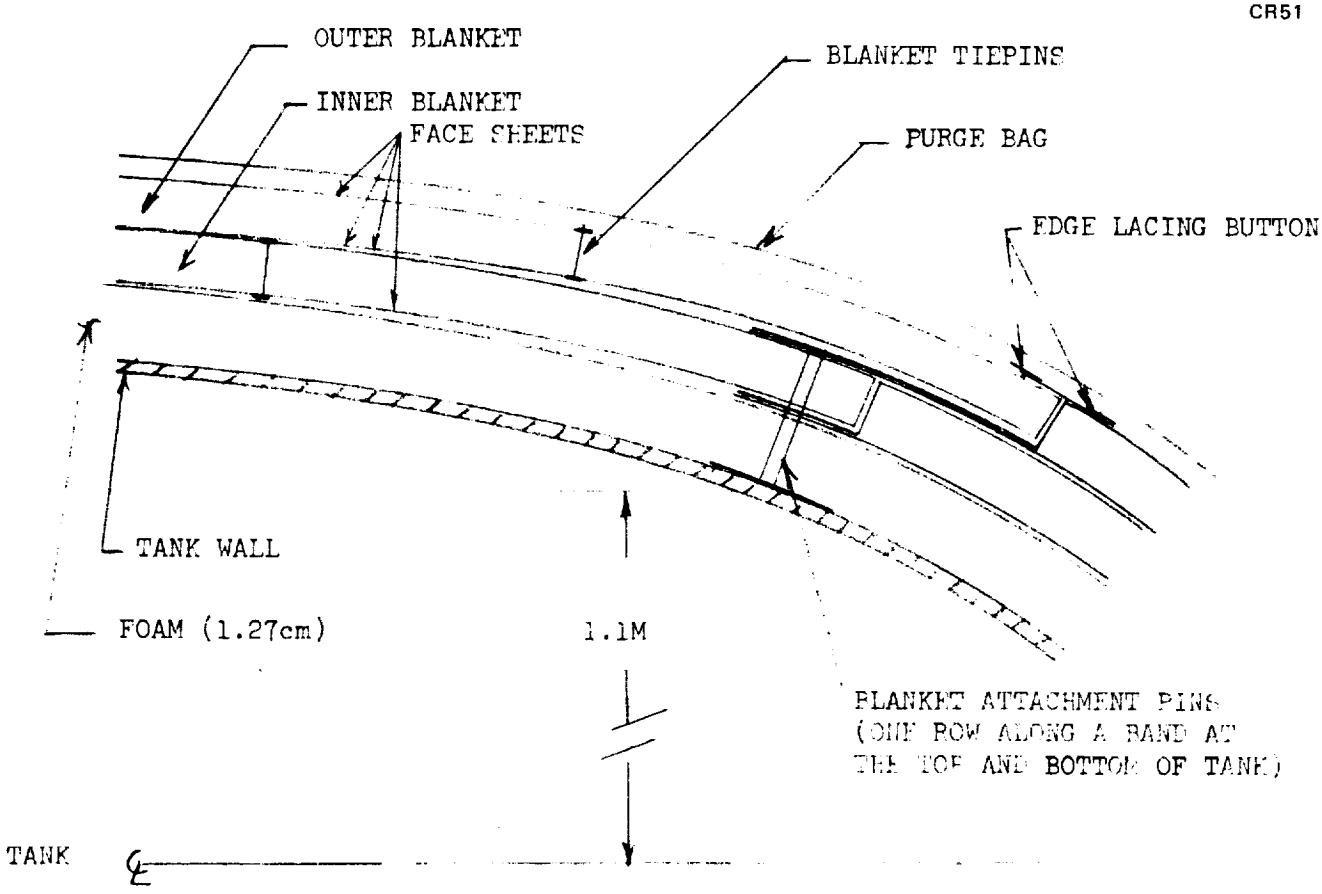

WEIGHT SUMMARY (90 M^2 TANK AREA)

PURGE BAG	26.4 Kg
FACE SHEETS (4)	35.2
MLI (48 LAYER-PAIRS) =	53.7
ATTACHMENTS	1.1
TAPE AND THREAD	2.6
FOAM	58.0
	177.0 Kg

PERFORMANCE

IN-ORBIT HEAT INPUT = 48.8 WATTS (166 BTU/HR)

LH_2 LOSS

THROUGH BOOST =	11 Kg
IN-ORBIT	67
REENTRY	20
LANDING	14
	112 Kg

Figure 8. Recommended Insulation Installation and Performance (LH_2 Tank)

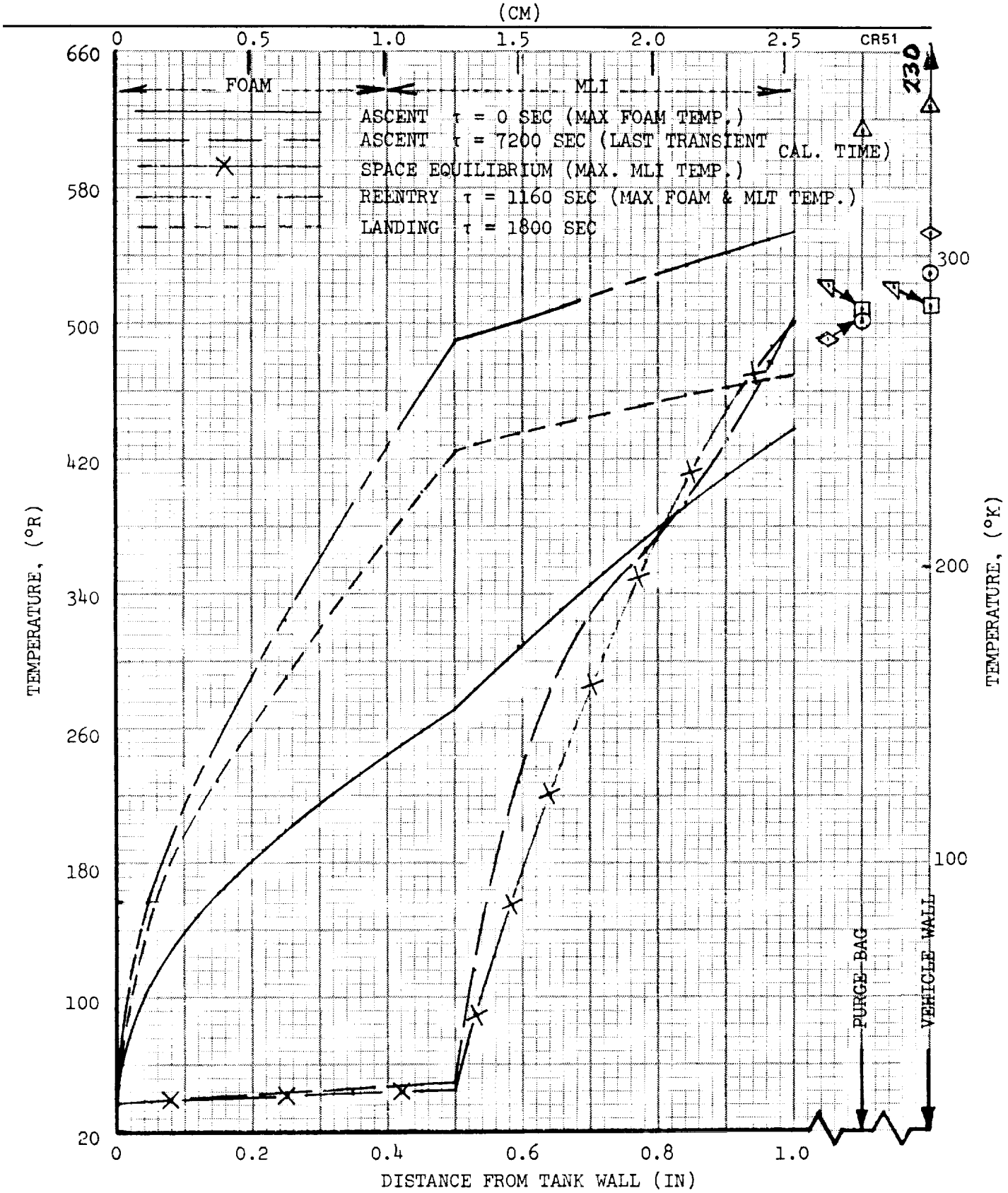

Figure 9. Representative Temperature Profiles for Selected LH_2 Insulation System

3.1.2 Pressurization System Design

Work was continued on defining the pressurization system weight and establishing the effects of design variables on system weight.

3.1.2.1 Parametric Design Data

A parametric study was conducted to determine the pressurization requirements for the baseline distributed channel LH_2 tank as a function of the design NPSP value. A baseline expulsion duty cycle, consisting of 18 identical expulsion steps equally distributed over the seven day mission, was analyzed using the MDAC H431 pressurization computer program. Figure 10 shows the requirements, in terms of total ullage mass at the end of expulsion, for autogenous pressurization. This analysis was based on a constant pressurant inlet temperature of 200°R which was found to be about optimum in terms of pressurant minimization in a previous analysis (Figure 14, Reference 1). Both fixed pressure and true NPSP tank pressure control were investigated. Figure 10 shows that for any appreciable design NPSP, the true NPSP control logic results in minimum pressurant mass. The less efficient constant tank pressure control approach causes increased propellant heating and results in increased tank pressure to satisfy a specific NPSP, thus resulting in higher pressurant weight.

Similar data are presented in Figure 11 for cold (45°R) helium pressurization. Although a different NPSP range was computed for each control logic, it is clear that about the same ullage mass results with the two control logics. (The final tank pressures are also comparable.) This result follows from the fact that with cold helium negligible heat transfer occurs. However, to assure design NPSP properly during all mission burns, it is recommended that the true NPSP control logic also be used with this cold helium pressurization system on the basis of control implementation rather than minimum system weight.

The results from Figures 10 and 11 are plotted together along with the corresponding final tank pressures in Figure 12. It can be seen that for a given design NPSP, total ullage mass with cold helium pressurization is slightly less than that with autogenous pressurization. This results because, as a

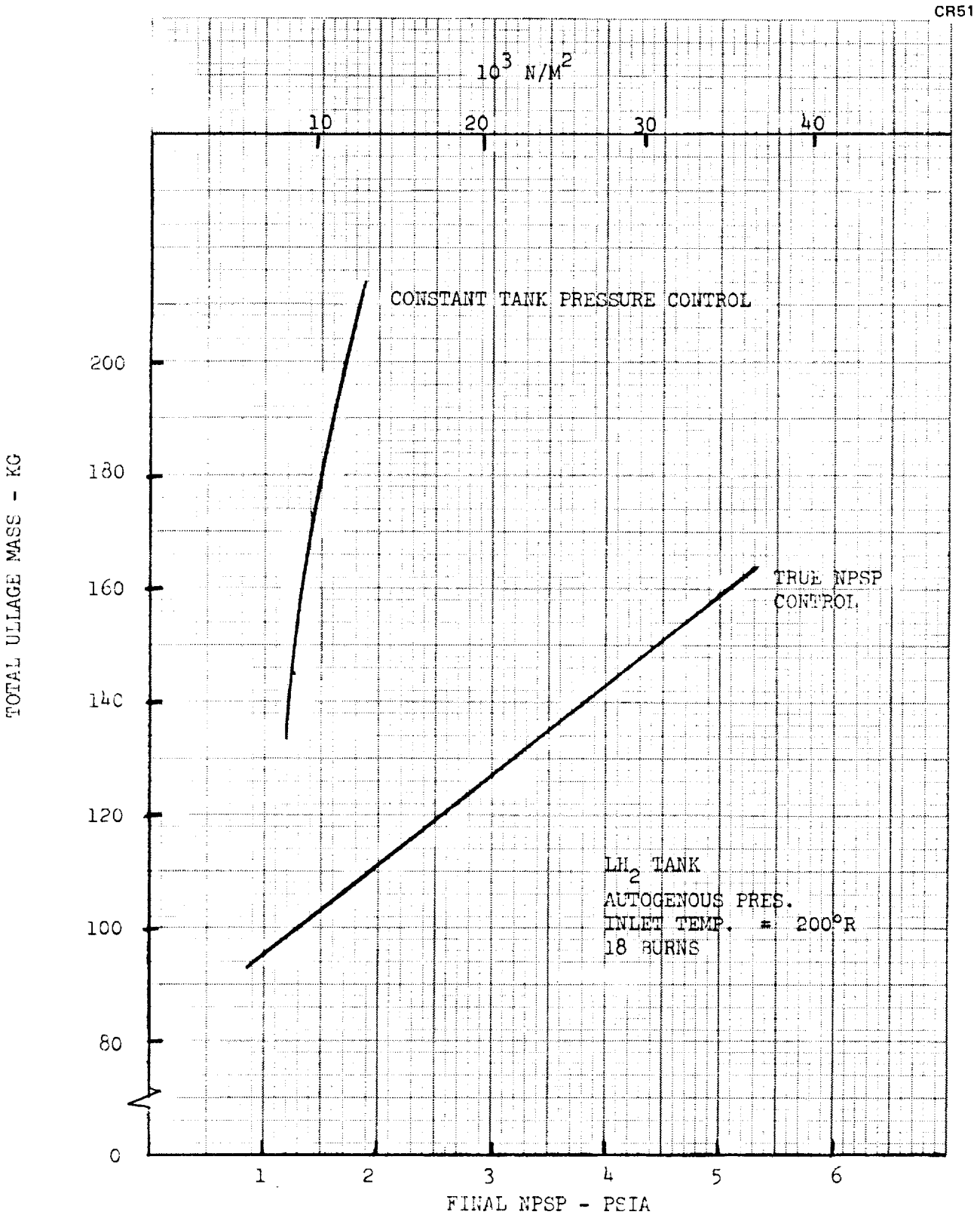

Figure 10. Influence of Control Logic on LH_2 Tank Pressurant Mass (Autogenous Pressurization)

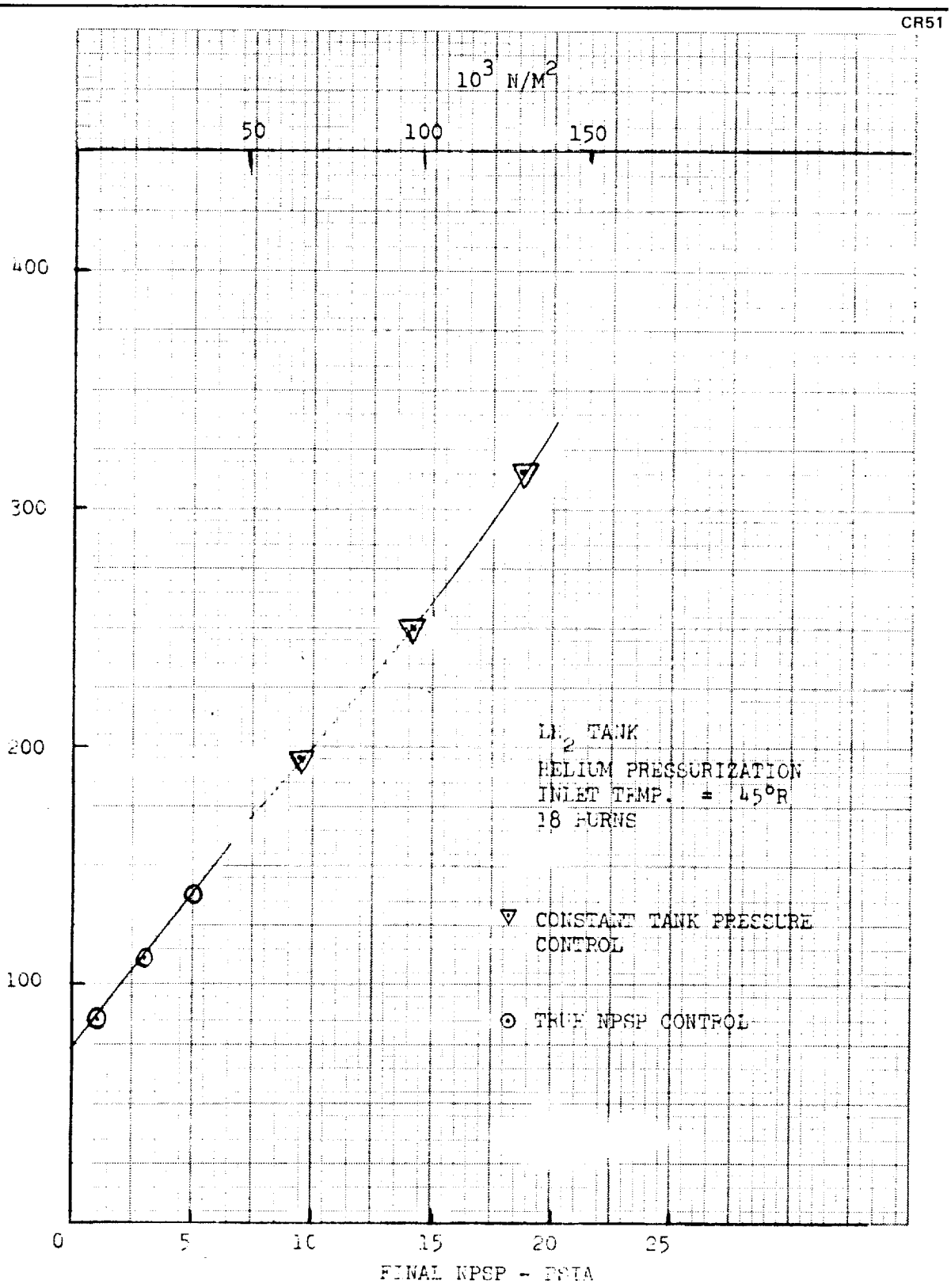

Figure 11. Influence of Control Logic on LH_2 Tank Pressurant Mass (Cold Helium Pressurization)

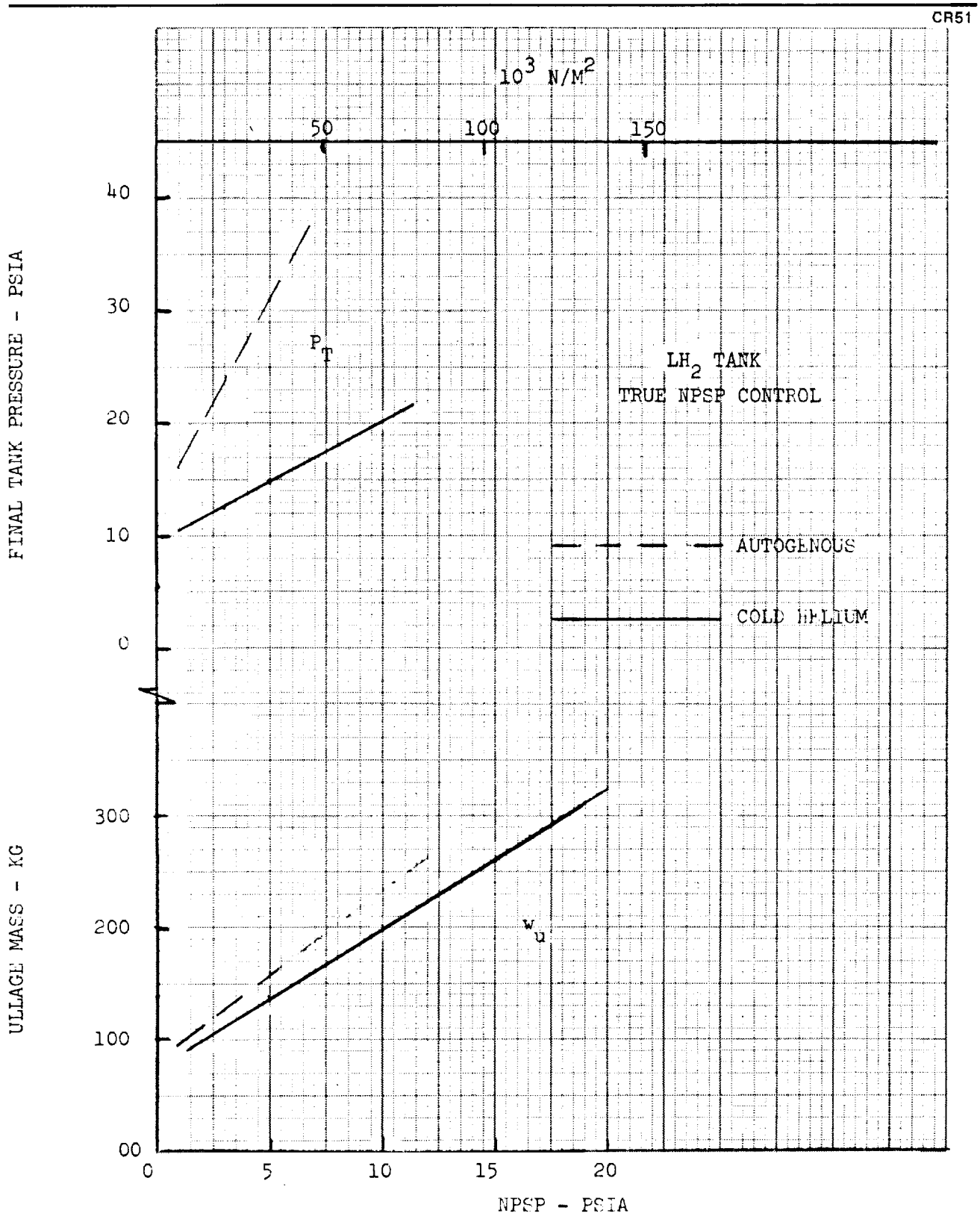

Figure 12. LH_2 Tank Pressurant Mass Requirements and Comparison

consequence of heat transfer, the final tank pressure with autogenous pressurization (even with true NPSP control) is greater than that with cold helium. The total system weight for a cold-helium system is greater than that of an autogenous system at the same design NPSP because of the helium storage bottle. This is illustrated in Figure 13 where the system weight includes the ullage-gas, helium-storage bottle and increases in LH_2 tank weight to accommodate the extra propellant that is vaporized for pressurization and the helium bottle storage. The indicated weights do not include any weight penalty for conditioning (heating or cooling) the pressurant. The noteworthy fact from Figure 13 is the relatively small weight difference between the two systems: about 70 kg at 34.5×10^3 N/m^2 (5 psia) NPSP. As discussed in previous progress reports, such a small savings by using warm GH_2 could be easily erased by even a limited acquisition cooling system for the distributed channels. The weight savings may, however, be retained with the start-tank system. Another significant observation is the high penalty incurred by increasing NPSP (about 30 kg per psi of NPSP). Thus, the minimum design NPSP should be used. From a control standpoint, based on MDAC design studies under contract NAS3-13310 (Reference 4), control should be possible at $\Delta P = 13.8 \times 10^3$ N/m^2 (2 psia).

3.1.2.2 Effects of Duty Cycle Variation on Pressurization System Design

All of the pressurization system analyses up to this point have been conducted on the assumption that the expulsion duty cycle could be adequately represented by a series of identical expulsion steps (same flowrate and expulsion time) equally spaced throughout the mission (equal coast time between expulsion steps). This was a completely arbitrary assumption, and a limited-scope parametric study has been performed to assess the variation in pressurization system design resulting from duty-cycle differences. As pointed out in Reference 1, the duty cycle for a space propulsion module generally involves the consumption of a large quantity of cryogen during the first and last hours of the mission with a series of small expulsion steps distributed over the coast operational period. Table 4 of Reference 1 also shows that there is always a rather large initial ullage (12 to 35 percent) for the baseline missions. To define the impact on the system design, the pressurization requirements were evaluated for a range of conditions for near-optimum LH_2 pressurization using heated (200°R) GH_2 and cold-helium pressurants.

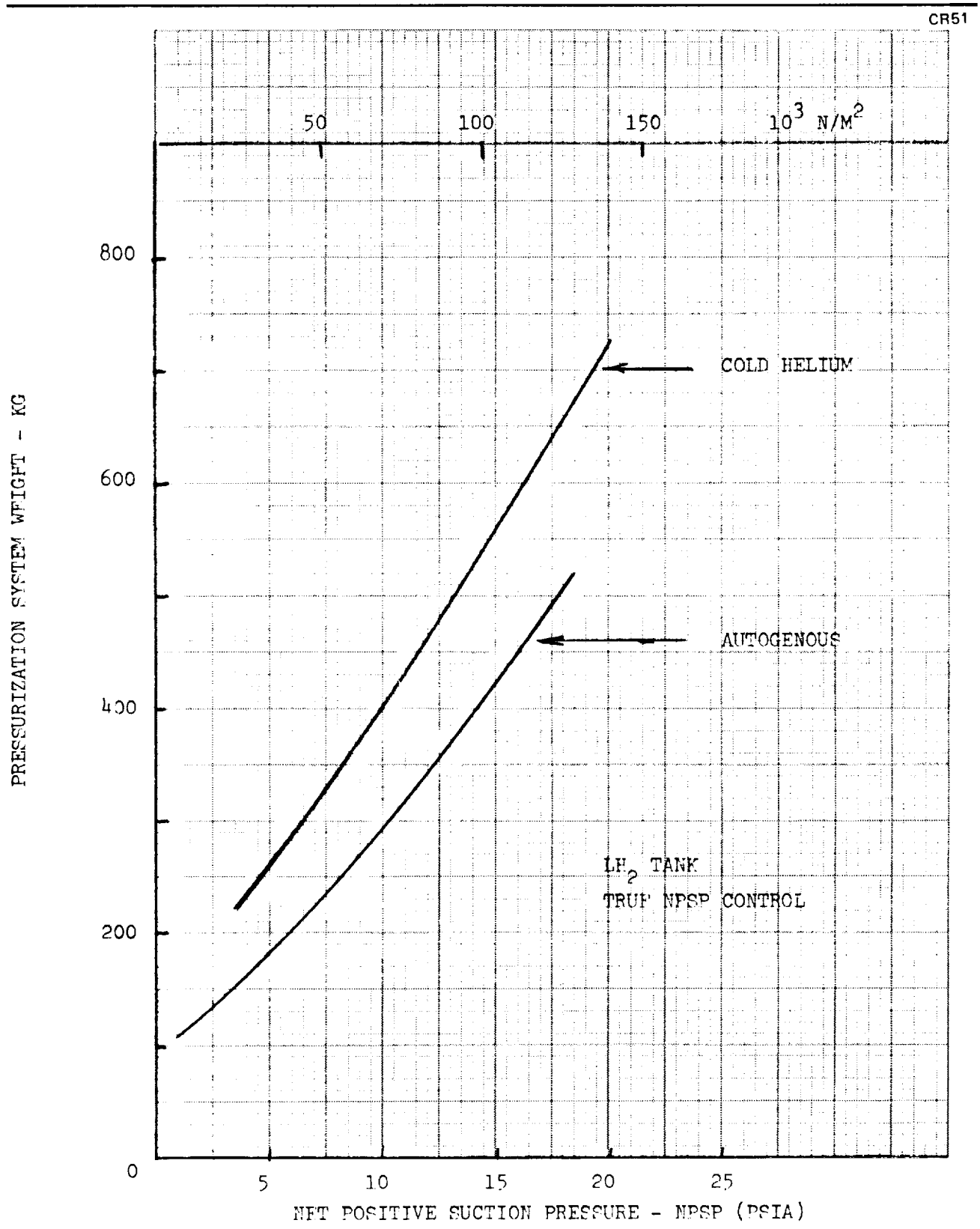

Figure 13. Comparison of Autogenous and Cold Helium Pressurization

Results with GH_2 are shown in Table 3, while results with cold helium are shown in Table 4. As can be seen from Tables 3 and 4, combinations of two expulsion duty cycles and initial ullage values were studied. The duty cycles included the baseline, consisting of equivalent expulsion steps equally distributed over the seven-day mission, and a weighted cycle in which it was assumed that 40 percent of the loaded cryogen was consumed both at the very beginning and end of the mission with 20 percent of the cryogen being expelled in equivalent steps equally distributed over the seven-day mission. The combination of weighted distribution and 30-percent ullage would most clearly approach our representative Shuttle APS as shown in Table 4 of Reference 1. By studying various combinations for both 18 and 6 expulsion steps, a relatively clear picture of the impact can be seen. In the case of GH_2 pressurization, the combination of the equal distribution expulsion steps and 30-percent ullage, Cases B and B', results in the heaviest pressurization system. However, this is not a very realistic combination. On the other-hand, Cases A and A', which have been the baseline throughout the study, represent a conservative design condition relative to the most likely operating conditions (Cases D and D').

This same trend does not carry over into the cold helium system. In this instance, the weighted expulsion duty cycle with large ullage produces the heaviest pressurization system (about 20 percent greater than the assumed baseline, Cases A and A'. In summary, for an LH_2 autogenous pressurization system, the system should be sized for a minimum (5 percent)ullage and a duty cycle consisting of 18 identical expulsion steps equally distributed over the seven-day mission. This will result in a slight over capacity of 10 percent for a representative mission. For a LH_2 pressurization system using cold helium, sizing should be based on a maximum ullage (30 percent) with a weighted burn distribution. The pressurization system weights were computed, based on these design points. Other assumptions included: (1) true NPSP control logic with a 34.5×10^3 N/m^2 (5 psi) ΔP, (2) 18 expulsion steps, (3) inlet temperatures of 111°K and 22.2°K for GH_2 helium respectively.

Table 3

INFLUENCE OF DUTY CYCLE ON PRESSURANT REQUIREMENTS
(LH_2 PRESSURIZATION WITH GH_2 AND TRUE NPSP CONTROL)

Case	Number of Expulsion Steps	Expulsion Step Distribution	Initial Ullage (Percent)	Final Ullage Mass (kg)	Final Tank Pressure (10^3 N/m^2)
A	18	Equal*	5	160	214
B		Equal	30	190	248
C		Weighted**	5	110	203
D		Weighted	30	145	240
A'	6	Equal	5	100	150
B'		Equal	30	110	157
C'		Weighted	5	80	150
D'		Weighted	30	95	160

*Assumes all steps to be equal in total expulsion and equally spaced during the mission.

**Assumes that first expulsion consumes 40 percent of liquid and occurs at beginning of mission consuming 40 percent of the initial volume and that the rest of the steps are equal and equally distributed during the seven-day coast.

Table 4

INFLUENCE OF DUTY CYCLE ON PRESSURANT REQUIREMENTS (LH_2 PRESSURIZATION WITH HELIUM AND TRUE NPSP CONTROL)

Case	Number of Expulsion Steps	Expulsion Step Distribution	Initial Ullage (Percent)	Final Ullage Mass (kg)†	Final Tank Pressure (10^3 N/m^2)
A	18	Equal*	5	75 + 59 = 134	100
B		Equal	30	73 + 67 = 140	106
C		Weighted**	5	134 + 50 = 184	117
D		Weighted	30	102 + 60 + 162	121
A'	6	Equal	5	96 + 58 = 154	104
B'		Equal	30	88 + 66 = 154	108
C'		Weighted	5	130 + 50 = 180	116
D'		Weighted	30	109 + 60 = 169	120

*Assumes all steps to be equal in total expulsion and equally spaced during the mission.

**Assumes that first expulsion consumes 40 percent of liquid and occurs at beginning of mission consuming 40 percent of the initial volume and that the rest of the steps are equal and equally distributed during the seven-day coast.

†Given as helium mass + vaporized H_2 mass = total.

Total LH_2 pressurization system weight (W_{pst}) is given by

W_{pst} = helium + propellant vapor + helium bottle + bottle tank weight penalty + propellant tank weight penalty + insulation/vent system penalty

$$= W_{HE} + W_{PV} + W_{HB} + \Delta W_{TB} + \Delta W_{TV} + \Delta W_i \quad (1)$$

As discussed in Reference 1, for helium bottle conditions of 13.79×10^6 N/m^2 (2,000 psi), design working stress of 6.2×10^8 N/m^2 (90,000 psi), final bottle pressure of 6.9×10^5 N/m^2 (100 psi) and final temperature of 11.1°K.

$$W_{HB} = \frac{W_{HE}}{7.7}(11.05) = 1.44\, W_{HE} \quad (2)$$

$$\Delta W_{TB} = \frac{dW_T}{dL}\Delta LB$$

$$\Delta L_B = \frac{\Delta V_B}{A_T} = \frac{V_B}{A_T} = \frac{W_{HE}}{870} = 0.064\, W_{HE} \quad (3)$$

$$\Delta W_{TV} = \frac{dW_T}{dL}\Delta L_V$$

$$\Delta L_V = \frac{W_{PV}/\rho L}{A_T} = 0.113\, W_{PV} \quad (4)$$

$$\Delta W_i = \frac{dW_i}{dL}\Delta L = \frac{W_{HE}}{870} + \frac{W_{PV}}{500}15 = 0.173\, W_{HE} + 0.03\, W_{PV} \quad (5)$$

Thus

$$W_{pst} = W_{HE} + W_{PV} + 1.44W_{HE} + 0.64W_{HE} + 0.113W_{PV} + (0.0173W_{HE} + 0.03\, W_{PV}) \quad (6)$$

For Autogenous LH_2 Pressurization

	(kg)	(lb)	
W_{pst} =	0	(353)	Helium
	160	(353)	Vapor
	0		Bottle
	0		Bottle penalty
	18	(40)	Propellant tank penalty
	5	(11)	Insulation penalty
	183	(404)	

For Cold Helium

	(kg)	(lb)	
W_{pst} =	109	(240)	Helium
	60	(132)	Vapor
	155	(342)	Bottle
	7	(15)	Bottle penalty
	7	(15)	Tank penalty
	4	(8)	Insulation penalty
	342	(752)	

Therefore, considering only the pressurization system with no pressurant temperature conditioning and with no interactions from other feed-system subsystems, the autogenous system is 159 kg (350 lb) lighter than the cold-helium system. Estimates reported in Reference 1 indicate that a cooled and foam-insulated channel to accommodate the heating brought about with 111°K inlet gas autogenous pressurization would weigh 200 to 500 kg, thus exceeding the savings achieved with autogenous pressurization. A study is now underway to determine if a lightweight cooled channel with a weight penalty significantly less than 159 kg is feasible and practical.

3.1.3 Vent Subsystem Design

The analysis of the internal tank pump mixer/heat exchanger TVS was conducted in greater detail than reported in Reference 2. Two design accelerations were considered: (a) 10^{-4} g which corresponds to steady-state, in-orbit operation, and (b) 10^{-2} g which is representative of attitude control accelerations. The low 10^{-4} g level should be an adequate design criteria for the TVS, from simply a venting standpoint.

Basic equations for sizing the mixer pump for a TVS of this type are given in Reference 5. From this reference, the velocity at the liquid-gas interface required to penetrate the interface and to thus mix the propellant is given by:

$$V_i = \frac{0.057}{b^2}\left\{\frac{\beta\Delta T_{MAX} P}{\left[1 - \left(\frac{V_{MAX}}{V'_{MAX}}\right)^2\right](P+1)(P+3)}\right\}^{1/2} a^{1/2} Z^{1/2} \qquad (7)$$

where

$b = 0.25$

$V_{MAX}/V'_{MAX} = 0.9$

$P = 1.0$

a = acceleration

Z = distance to the interface (tank length)

Also the product of the jet exit diameter (D_o) and velocity (V_o) is given by

$$V_o D_o = \frac{1}{2}\left\{\frac{\beta\Delta T_{MAX} Z^3 aP}{\left[1 - \left(\frac{V_{MAX}}{V'_{MAX}}\right)^2\right](P+1)(P+3)}\right\}^{1/2} \qquad (8)$$

The mixer volumetric and weight flow are given respectively by

$$\dot{V}_o = AV_o = \frac{\pi D_o^2}{4} V_o = \frac{\pi}{4} D_o (V_o D_o) \tag{9}$$

$$\dot{w}_o = \dot{V}_o \rho \tag{10}$$

The required time to mix the tank contents, θ, is given by

$$\theta = \frac{N D_t^2}{0.456\ V_o D_o} \tag{11}$$

where $N = 6.0$, and D_t = tank diameter.

The theoretical pump head is approximated by $H = V_o^2/2g$, which gives

$$\dot{V}_o = \frac{(V_o D_o)^2 \pi}{4\sqrt{2gH}} \cdot \tag{12}$$

Pump power input = $\dot{P}_{IN}$:

$$\dot{P}_{IN} = \frac{H \dot{V}_o \rho}{\eta} \tag{13}$$

Small axial pump/motors have efficiencies, η, as shown in Figure 14 from Reference 6. Part A of Table 5 summarizes the sizing parameters for the two design accelerations based on the above equations.

Considering the internal thermodynamics of the tank, the rate of pressure change, dP/dt is

$$\frac{dP}{dt} = \frac{dP}{dT} \frac{dT}{dt} \tag{14}$$

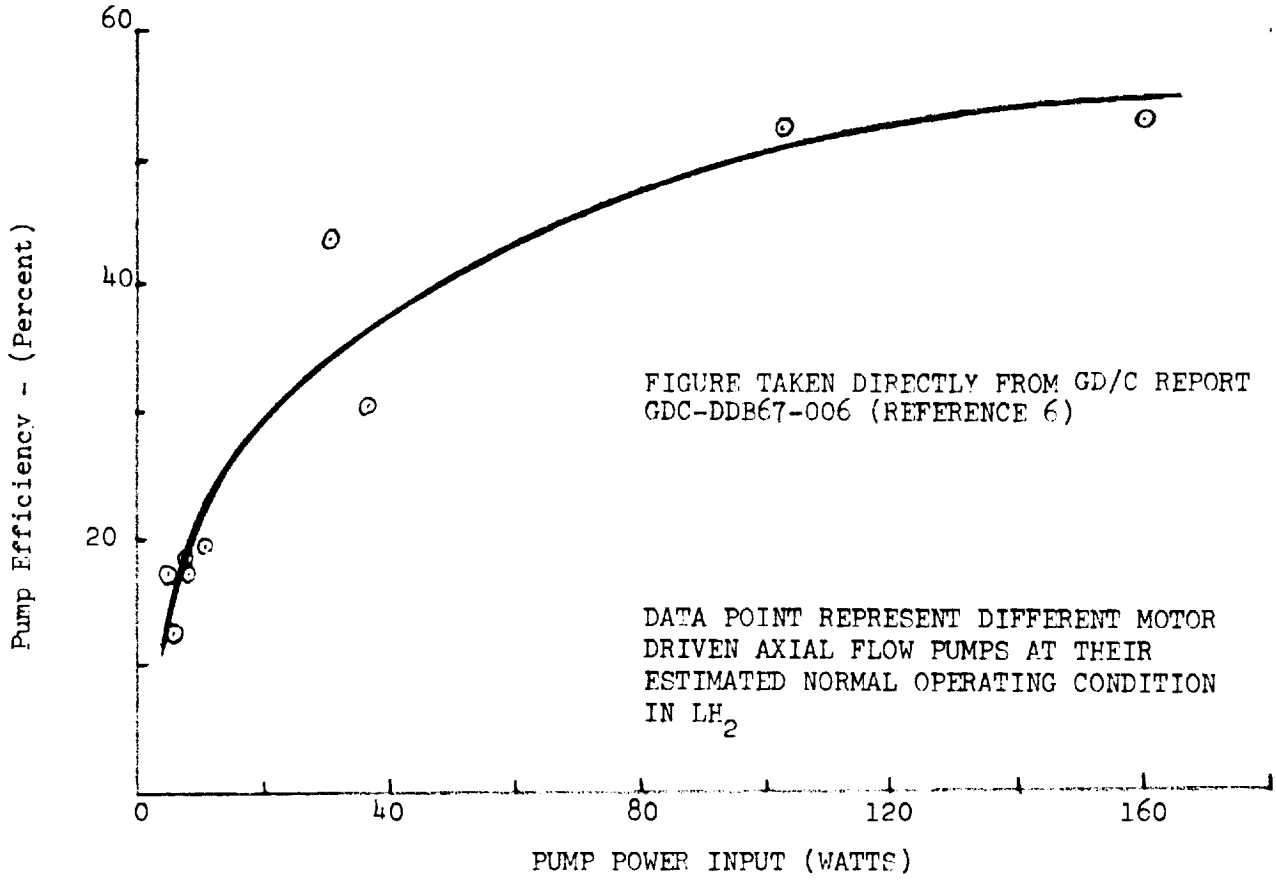

Figure 14. Influence of Power on Effiency for Small LH_2 Pumps

Table 5

PUMP-MIXER/HEAT EXCHANGER TVS SIZING PARAMETERS

A-Pump/Mixer Sizing Factors	Design Acceleration		
	10^{-2} g's		10^{-4} g's
Required interface velocity	0.061 (0.2)	m/sec ft/sec	0.0061 (0.02)
Mixing time	0.2	hr	2.0
Exit diameter x velocity	25.5×10^{-2} (2.74)	m^2/sec ft^2/sec	2.55×10^{-2} (0.274)
Pump outlet diameter	5.1 (2.0)	cm in.	2.54 (1.0)
Volumetric flow	1.02×10^{-2} (21.6)	m^3/sec ft^3/min	0.05×10^{-2} (1.07)
Weight flowrate	0.72 (1.58)	kg/sec lb/sec	0.035 (0.08)
Pump outlet velocity	5.0 (16.4)	m/sec ft/sec	1.0 (3.3)
Pump head	1.28 (4.18)	m ft	0.052 (0.17)
Pump fluid power	8.9	watts	0.018
Pump efficiency	33	%	2.3*
Pump input power	27	watts	0.78*
Estimated pump weight	0.57	kg	0.27
LH_2 loss from pump heat input per cycle	0.044	kg	0.0127
B-Vent Cycle Factors			
Vent time per cycle	0.5	hr/cycle	5.0
Vent flowrate	18.2 (40)	kg/hr lb/hr	2.6 (5.7)
Vent cycles	8	-	7

*Minimum practical pump/mixer size is 5 watts at 12-percent efficiency which would require resizing of the mixer and vent system characteristics

The rate of temperature change, for mixed tank contents, is

$$\frac{dT}{dt} = \frac{\frac{dQ_{net}}{dt}}{W_P C_P} = \frac{\dot{w}_v H_v - (\dot{Q} + \dot{P})}{W_P C_P} \tag{15}$$

where H_v is heat of vaporization, $\dot{Q}$ is heat input, $\dot{P}$ is power in, and W_P = propellant weight.

$$\therefore \quad \frac{dP}{dt} = \left(\frac{dP}{dT}\right) \frac{\dot{w}_v H_v - (\dot{Q} + \dot{P})}{W_P C_P} \tag{16}$$

The term dP/dT is evaluated from the Clapeyron equation

$$\frac{dP}{dT} = \frac{\Delta H_{fg}}{\Delta V_{fg} T} \tag{17}$$

where ΔH_{fg} is the enthalpy change for vaporization, and ΔV_{fg} is the specific volume change during vaporization.

The number of vent cycles, N_v is

$$N_v = \frac{\frac{\dot{Q}_{in} t_t}{H_v}}{\dot{w}_v t_v - \frac{\dot{P} t_v}{H_v}} = \frac{\dot{Q}_{in} t_t}{(\dot{w}_v H_v - \dot{P})\, t_v} \tag{18}$$

where t_t = total mission time, $\dot{w}_v$ = venting flow rate, and t_v = total venting time.

Figure 15 shows the vent time per cycle and vent cycles for a 0.5-psi pressure change. For a practical design, propellant mixing should occur well within the duration of the venting cycle. For 10^{-4} g design acceleration, propellant mixing requires about 20 hr (see Table 5). This is

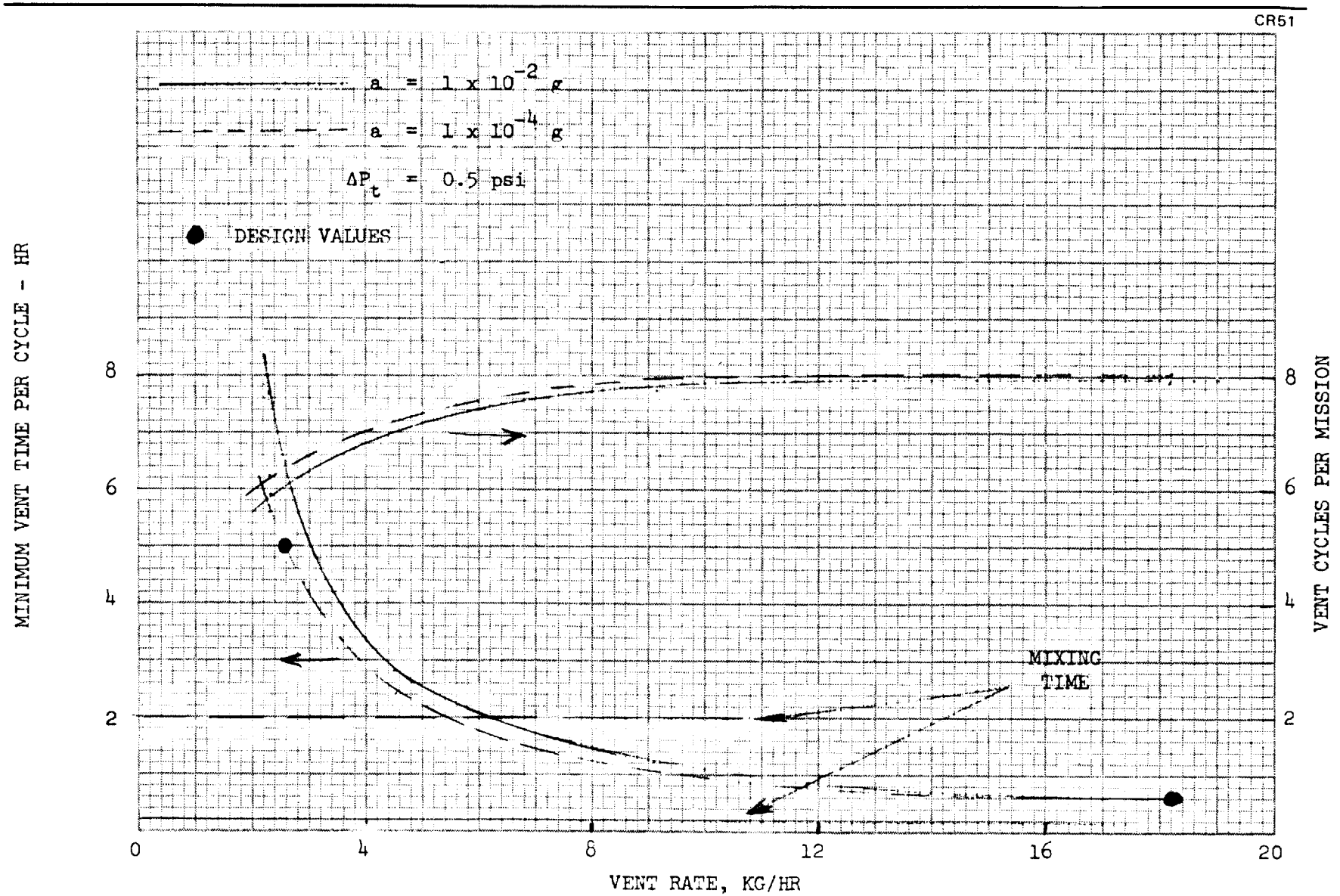

Figure 15. LH_2 Tank Venting Parameters with Pump Mixer TVS

noted on Figure 15. To permit adequate margins, it has been assumed that venting time must be 2.5 times the mixing time. Thus, for 10^{-4}g acceleration, a venting time of 5.0 hr with a vent flow of 2.7 kg/hr is required. These and corresponding values for 10^{-2} g are summarized in Part B of Table 5.

Compact counterflow heat exchangers were designed, based on the design data of Reference 7 and the requirements of Table 6. Because of helium pressurization of the tank, the critical design requirement for the heat exchanger is to transfer sufficient heat when flowing helium on the hot side, since the heat transfer coefficient with helium is much less than for liquid hydrogen. The design of the heat exchanger is also based on expansion across the throttle valve (cold side) from 17 psia to 3.4 psia (heat exchanger cold side pressure), to ensure staying above the triple point. The heat exchanger effectiveness was assumed to be 0.9 which strikes the proper balance between pumping power and heat exchanger size. The heat exchanger core weight (based on stainless steel) and size are shown parametrically in Figures 16 and 17. The helium and LH_2 pressure drop (hot side) are shown in Figures 18 and 19. Table 6 summarizes the pertinent design characteristics of the heat exchangers designed for 10^{-2} and 10^{-4}g's. The weights shown assume aluminum heat exchangers with a 25 percent factor added for manifolds.

The general heat exchanger/pump package configuration and location in the tank is shown in Figure 20. The unit is situated in the main tank so that the bulk of the propellant is available for cooling.

This system will be further detailed and compared with the cooled-shroud TVS in the coming months. As a part of this work, care will be taken to integrate the TVS with the overall acquisition system for functions such as pump cooling and bypass management control.

3.1.4 Propellant Acquisition Subsystem Design

In general, the more detailed design and evaluation of the acquisition subsystem is awaiting completion of some of the more fundamental bench tests being conducted under Task B (see Section 3.2). However, work in several distinct areas is in progress, particularly bypass management control and zero-g refill of the start tank.

Table 6

TVS COMPACT HEAT EXCHANGE PARAMETERS

	Design Acceleration		
	10^{-2}	g's	10^{-4}
Vent flow	18.2	kg/hr	2.6
	(40)	lb/hr	(5.7)
Heat transfer rate	2, 290	watts	325
	(7, 800)	Btu/hr	(1, 110)
Weight (Aluminum)	9.4	kg	1.35
	(20.7)	lb	(3.0)
Size (frontal area)	0.152 x 0.152	m x m	0.076 x 0.076
	(6 x 6)	in. x in.	(3 x 3)
Length	0.435	m	0.254
	(17.5)	in.	(10)
Helium ΔP (warm side)	4.73×10^3	N/m^2	4.73×10^3
	(0.685)	psi	(0.685)
LH_2 ΔP (warm side)	57.2	N/m^2	57.2
	(0.0083)	psi	(0.0083)
H_2 ΔP (cold side)	1.27×10^{-4}	N/m^2	2.35×10^3
	(1.84)	psi	(0.34)

3.1.4.1 Pump Bypass Flow Management

In Reference 2, the problems of transient pump operation and its impact on the feed system were discussed. It was concluded that some level of pump bypass flow during startup and shutdown would have to be accommodated either by dumping the flow directly overboard or passing the flow back to the propellant tank.

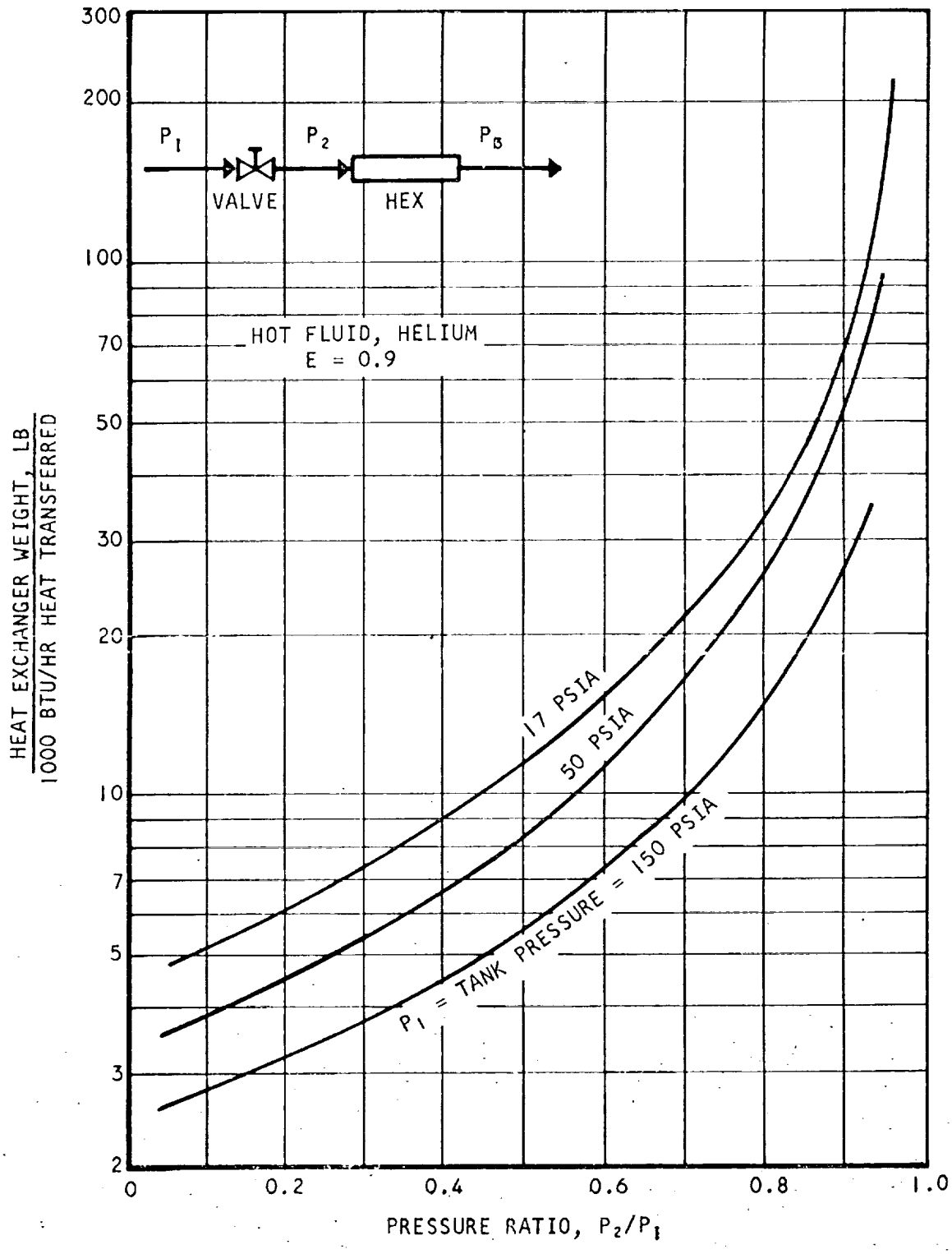

Figure 16. Heat Exchanger Weight

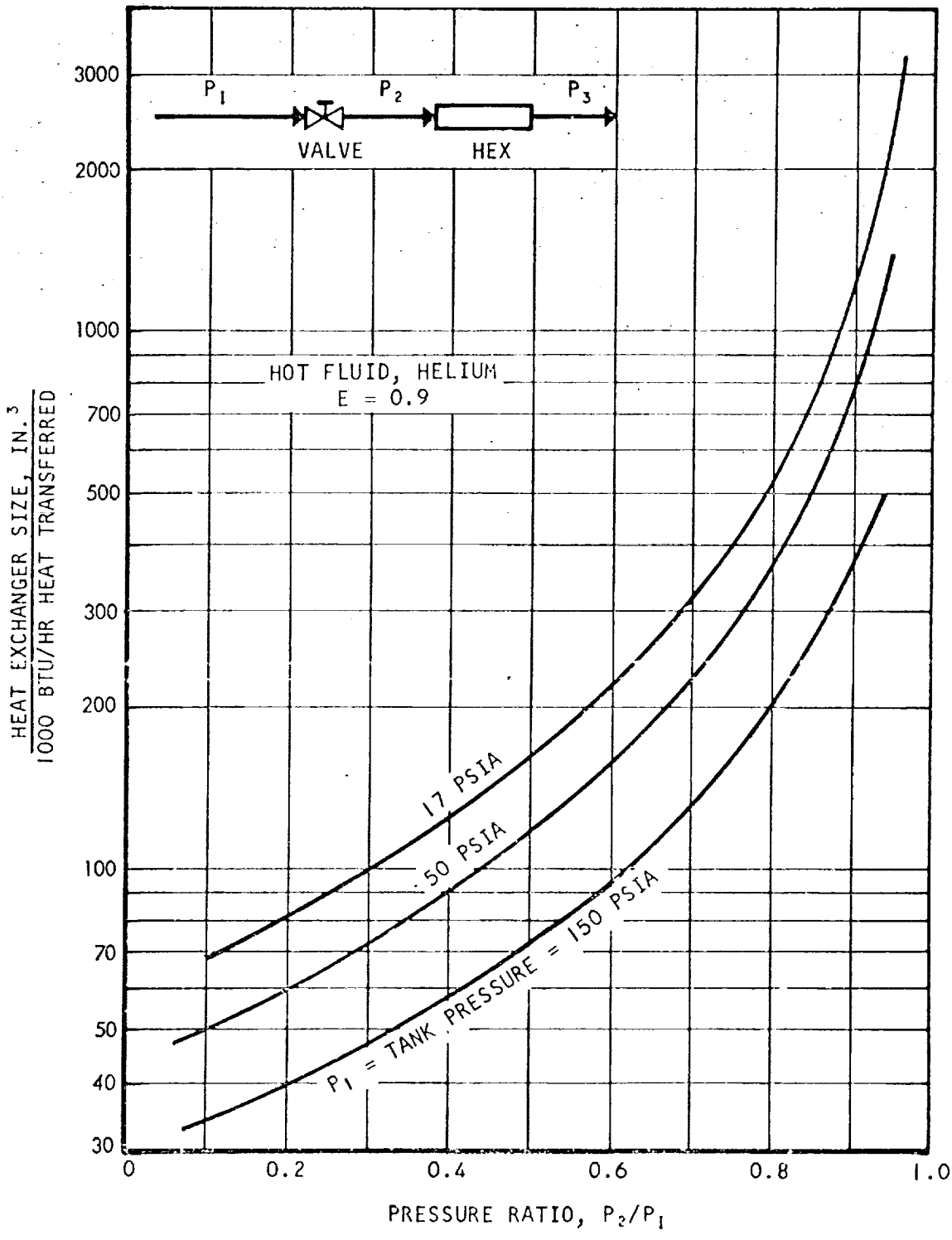

Figure 17. Heat Exchanger Size

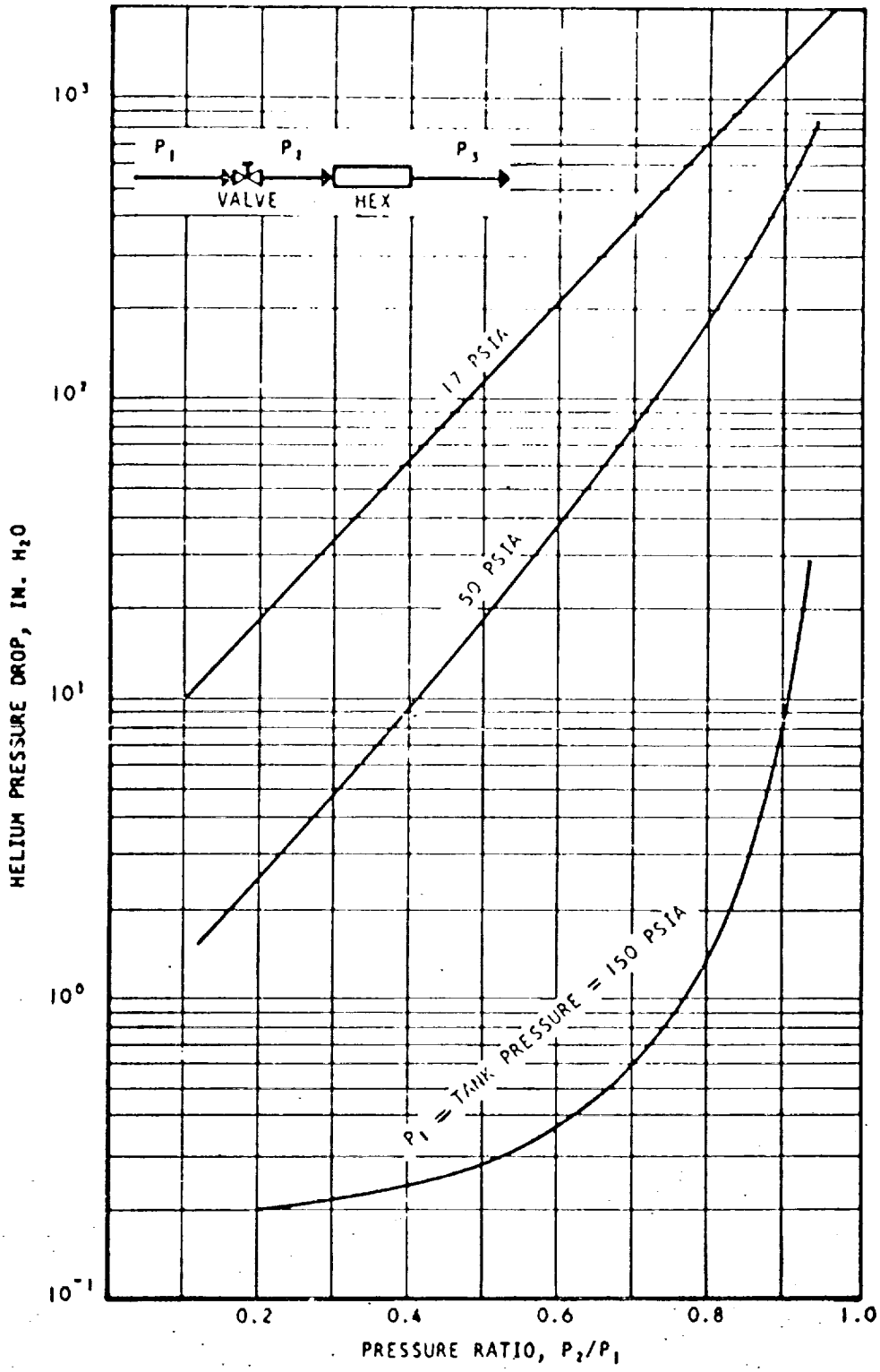

Figure 18. Heat Exchanger Hot Side Pressure Drop with Helium

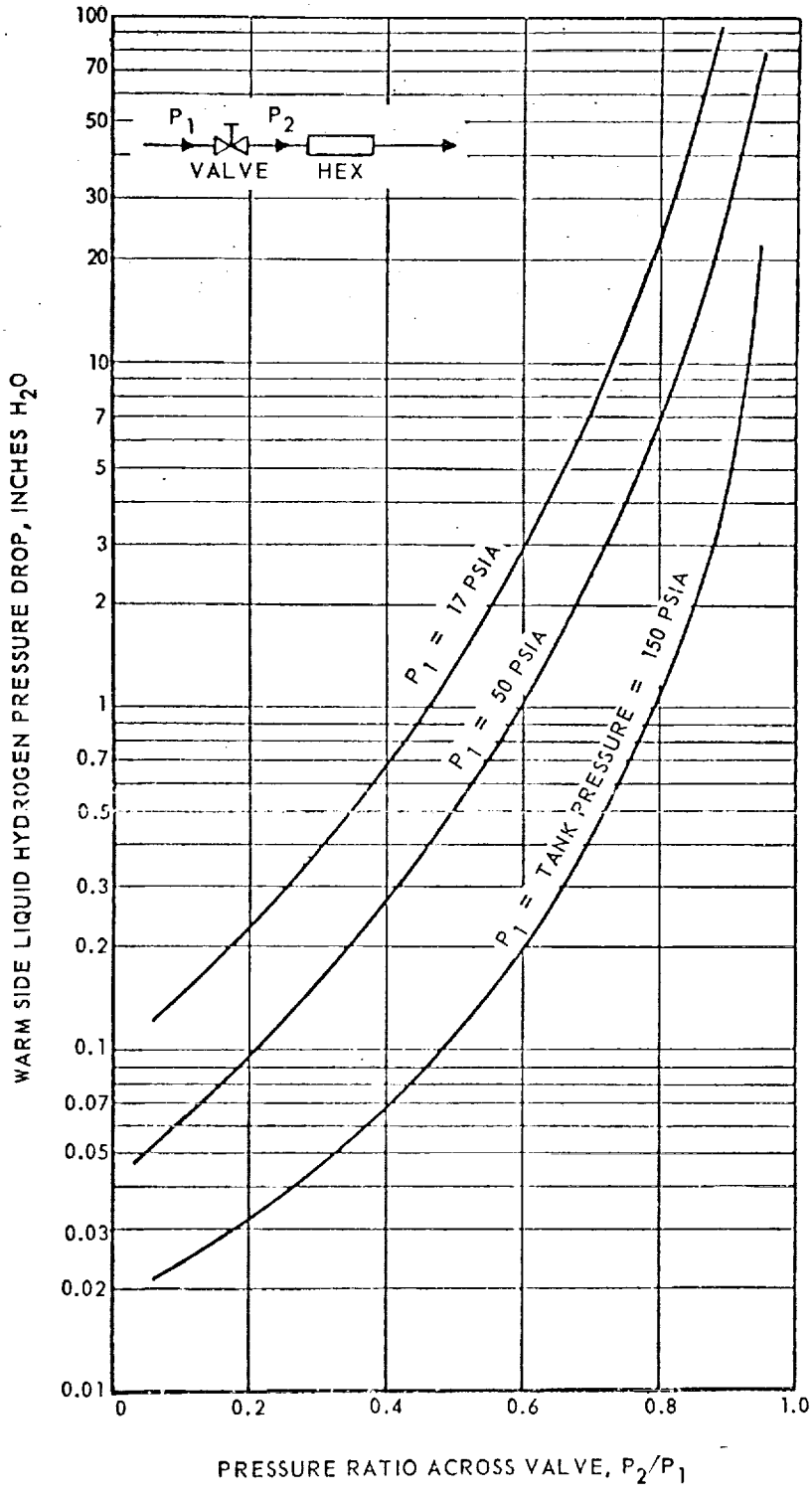

Figure 19. Heat Exchanger Warm Side Pressure Drop with LH_2

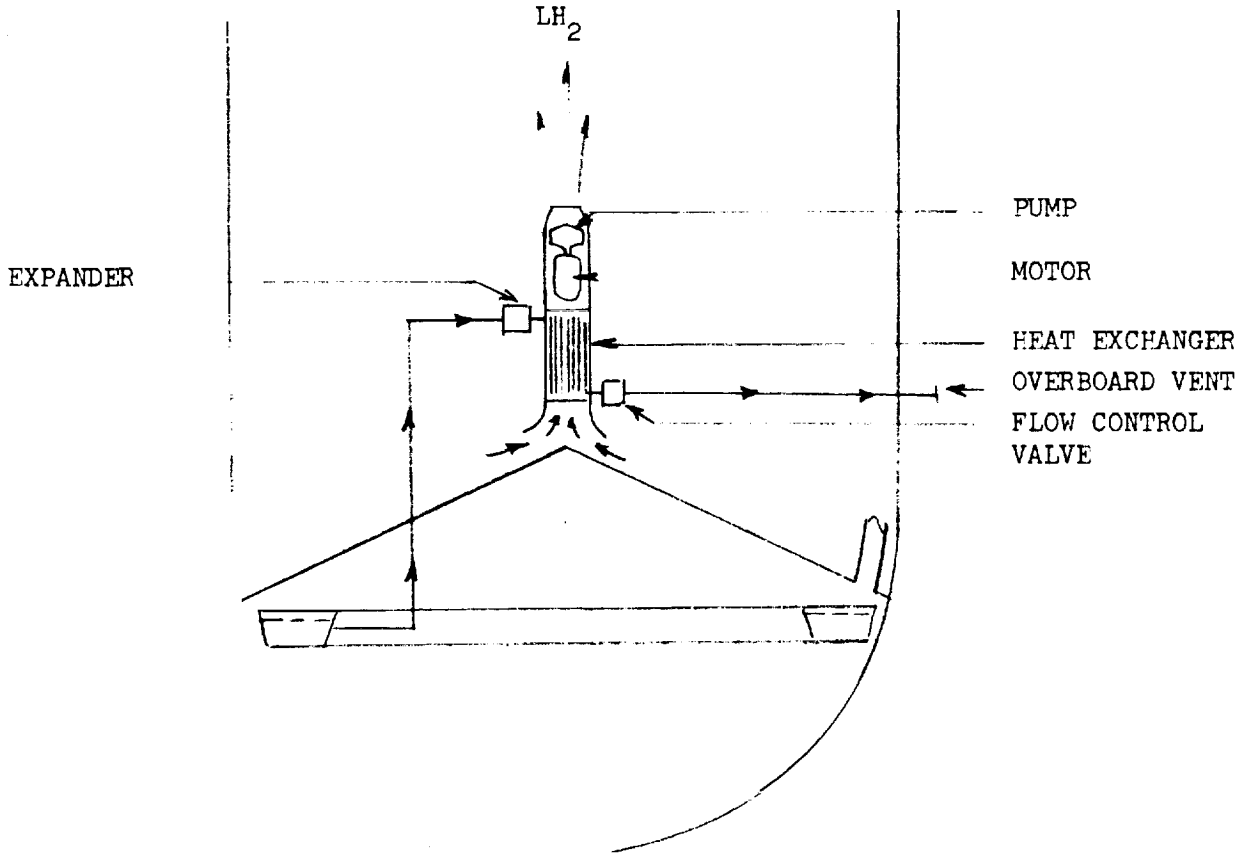

Figure 20. Internal Tank Pump/Mixer TVS Concept

It was further concluded that thermodynamically, the preferred technique for managing this pump bypass flow in the baseline system would be to recirculate the bypass back to the propellant tank and to absorb the resulting feed-system heat addition by boiling off and venting tanked cryogen. However, this must be accomplished in a controllable and predictable manner. One possible method for achieving this energy exchange is illustrated in Figure 21. As shown, the warm bypass flow is passed through a heat exchanger mounted within the cryogen tank. In the heat exchanger, the warm bypass flow is directed adjacent to passages conveying lower temperature cryogen. This coolant, which is subcooled propellant, is throttled and dumped overboard through the vent system after absorbing the heat from the bypass flow. The coolant pump may or may not be required depending upon heat exchanger ΔP requirements. The coolant must have sufficient cooling capacity and the heat exchanger must be large enough to cool the bypass flow back down to tank temperature conditions. The bypass flow conditions, taken from Reference 8, are summarized in Figure 22 for 100-percent bypass flow. The heat exchanger must be sized for the maximum local $\dot{Q}$ conditions.

Preliminary calculations indicated that such a system was weight competitive and might be integrated with the internal tank pump/heat exchanger TVS concept. However, more detailed and realistic heat exchanger calculations indicated very large and heavy heat exchangers would be required and that this type of concept may not be practical. This study is still in progress and will be completed in the next quarter.

3.1.4.2 Start-Tank Refill Concepts

It was shown in Reference 2 that use of additional vehicle acceleration, as provided by dedicated APS firing, to affect start-tank refill incurred a high weight penalty, primarily as a result of propellant consumption which was not sufficiently balanced by lower weight of a reduced capacity start tank. Another candidate concept for providing independent refill of the start tank uses a zero-gravity vacuum refill procedure for which feasibility has been demonstrated during MDAC IRAD activities.

With this design concept, the start-tank size is at least large enough to contain sufficient propellant to satisfy reentry requirements. This has been

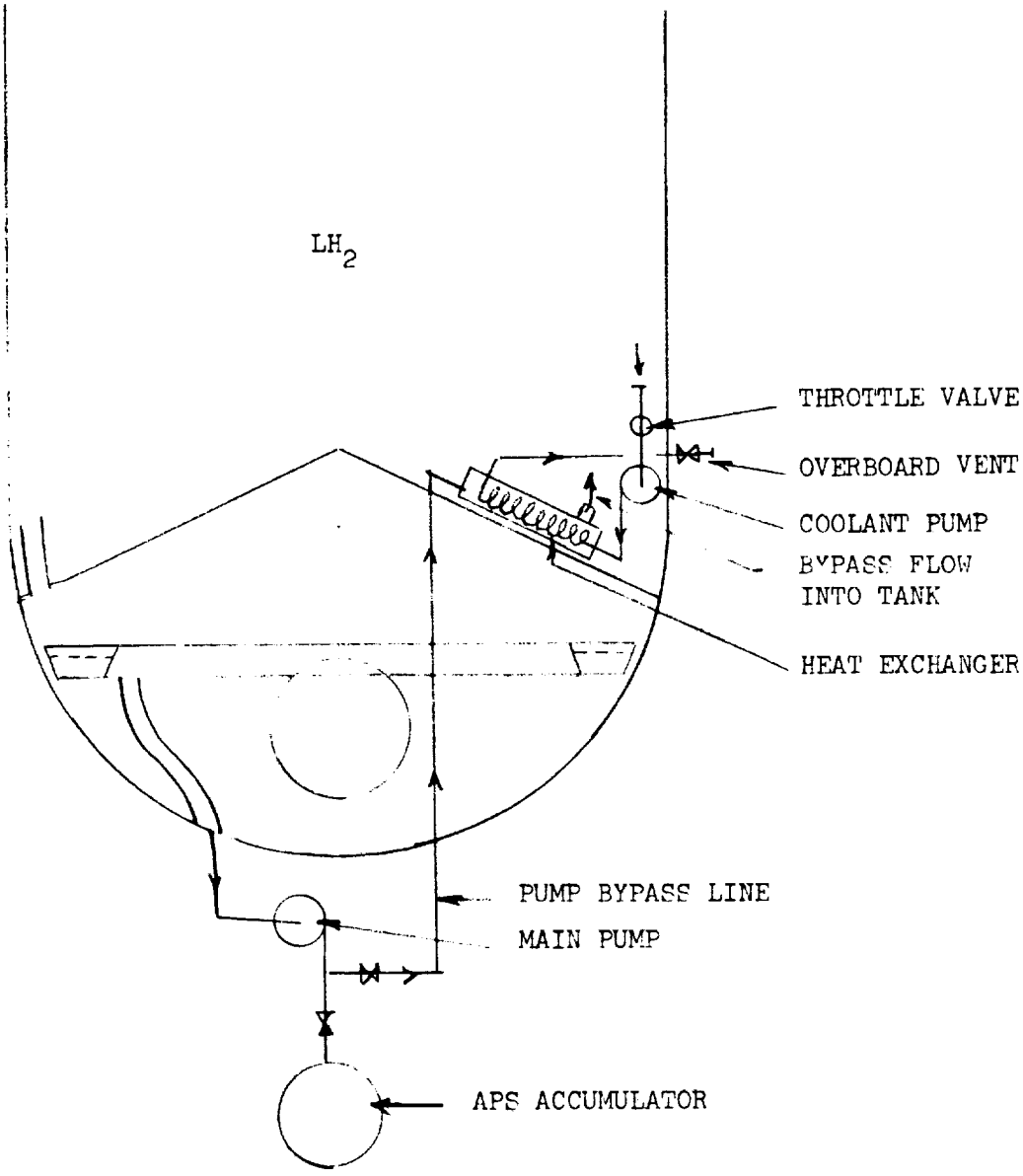

Figure 21. Thermal Pump Bypass Management Concept

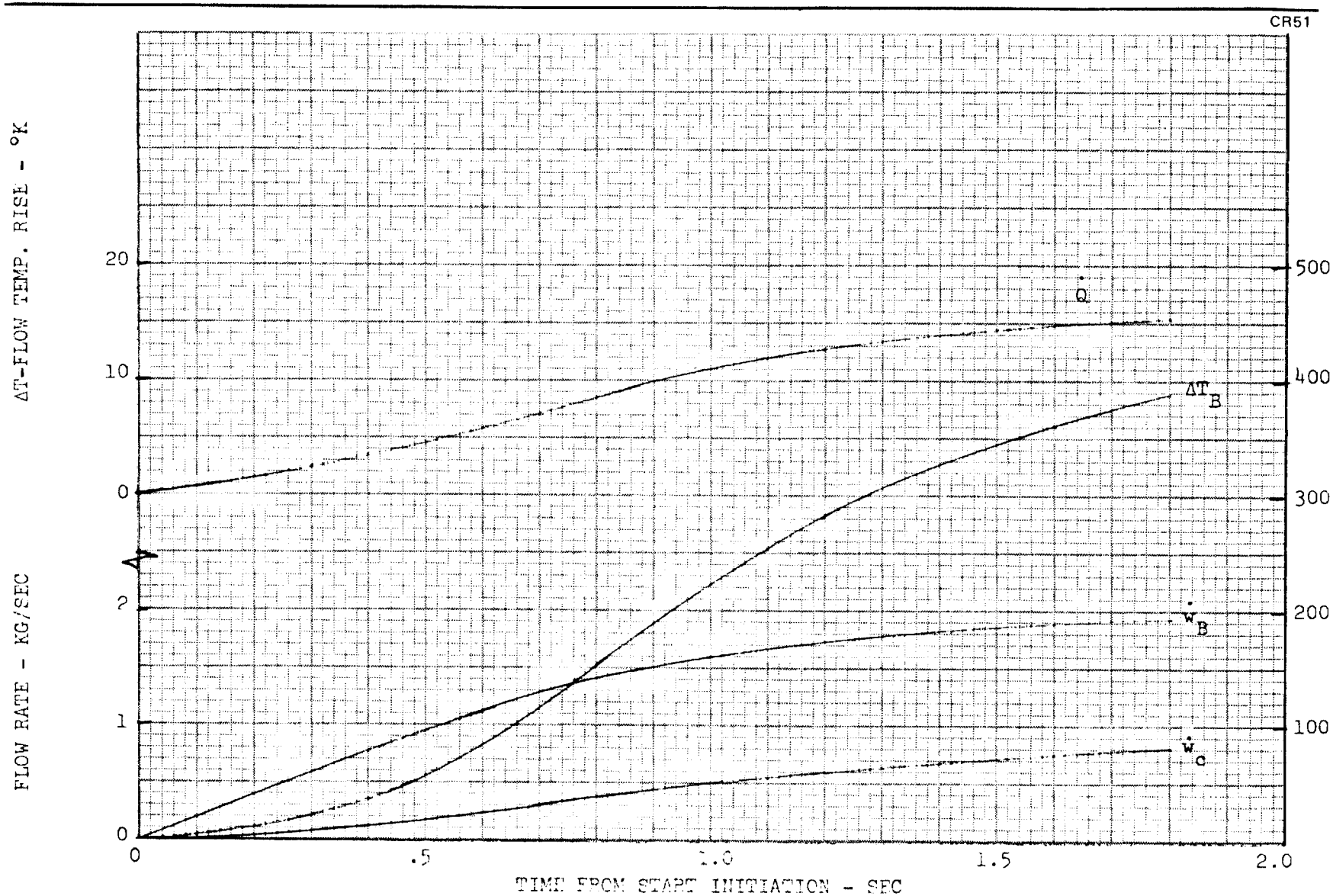

Figure 22. Pump Startup Flow Conditions

shown to diminish boiloff losses and provide propellant control during the reentry maneuvers. To illustrate operation, assume that the start tank has been partially emptied by various low-g propellant demands, and that it is necessary to initiate refill in preparation for low-g propellant expulsion, such as APS accumulator refill. (If engine restart were required, refill would be accomplished during the engine burn, which is the normal start-tank refill mode and imposes no weight penalty). The start-tank pressure is first increased 1 to 2 psi above the main-tank pressure, and the small bypass valve between the start-tank feedline and the main tank is opened. Propellant thus flows out of the start tank into the main tank until surface tension breakdown occurs in the screen acquisition device, assumed to be a screened channel. The total residual liquid remaining in the start tank at this point is the liquid in the channels plus the liquid on the walls of the start tank. This liquid, as well as the helium and hydrogen vapor pressurant, is then vented overboard. After a sufficiently low start-tank pressure is reached (0 to 5 psia), the start-tank vent valve is closed. The refill valve, which is connected to a redundant screen device (e.g., a ring channel contained in the ring baffle and trap region) is then opened and liquid propellant flows into the start tank. This process involves essentially reversible evaporation and condensation, and has been shown during MDAC IRAD tests (Reference 9), to result in complete refill even with minimum start-tank pressures as high as 6 psia.

Prior to vacuum venting of the start tank, the total liquid volume remaining is equal to the volume of the liquid in the channels, V_c, plus the residual volume, V_r, of liquid which was not communicated to the channels during the transfer operation from the start tank.

The mass of fluid vented, $M_{\text{vent refill}}$, is composed of the helium and propellant vapor in the ullage, and the liquid remaining in the tank at the initiation of venting.

$$M_{\text{vent refill}} = \rho \frac{P_{He}}{P_{total}} \left(V_{st} - \left[V_c + V_r\right]\right) + \rho_{vapor} \frac{P_{vapor}}{P_{total}} \left(V_{st} - \left[V_c + V_r\right]\right) + \rho_{prop} \left(V_c + V_r\right) \tag{19}$$

The terms ρ_{He}, ρ_{vapor}, and ρ_{prop} are the densities of the helium, vapor, and liquid propellant. The terms P_{He}, P_{vapor}, and P_{total} are the pressures of the helium and vapor, and the total start-tank pressure. V_{st} is the start-tank volume. The mass of potentially usable propellant, $M_{use,\,st}$, in the full start tank is

$$M_{use,\,st} = \rho_{prop}\left(V_{st} - \left[V_c + V_r\right]\right) \tag{20}$$

The total mass of usable propellant, M_{prop}, equals the number of refills times the amount of potentially usable propellant available after each refill plus the propellant which flows through the start tank during engine burns, M_{engine}. Thus, for any mission the minimum number of refills, N*, is

$$N = \frac{\dfrac{M_{prop\ reqd} - M_{engine}}{V_{st}}}{\rho_{prop}\left(1 - \dfrac{V_c + V_r}{V_{st}}\right)} \tag{21}$$

The total mass of propellant and pressurant vented overboard, is

$$M_{vent\ total} = N \cdot M_{vent\ refill} \tag{22}$$

Thus, from Equations (20) and (21)

$$M_{vent\ total} = \frac{M_{prop\ reqd} - M_{engine}}{\rho_{prop}\left(1 - \dfrac{V_c + V_r}{V_{st}}\right)} \left\{\rho_{He}\,\frac{P_{He}}{P_{total}}\left[1 - \frac{(V_c + V_r)}{V_{st}}\right]\right. \tag{23}$$

$$\left. + \rho_{vapor}\,\frac{P_{vapor}}{P_{total}}\left[1 - \frac{V_c + V_r)}{V_{st}}\right] + \rho_{prop}\,\frac{(V_c + V_r)}{V_{st}}\right\}$$

*N would be rounded off to the nearest whole number greater than the N calculated.

The fractional weight penalty is therefore

$$\frac{M_{\text{vent total}}}{M_{\text{prop reqd}}} = \left\{ \left[\frac{\rho_{He} P_{He}}{\rho_{prop} P_{total}} + \frac{\rho_{vapor} P_{vapor}}{\rho_{prop} P_{total}} \right] + \frac{\frac{V_c + V_r}{V_{st}}}{1 - \frac{V_c + V_r}{V_{st}}} \right\}$$

$$\times \left[1 - \frac{M_{\text{engine}}}{M_{\text{prop reqd}}} \right] \tag{24}$$

Equation (24) shows the necessity for reducing the ratio $(V_c + V_r)/V_{st}$ to as low a value as possible to minimize the weight penalty. However, even if this ratio approaches zero, the term $(\rho_{He} P_{He})/(\rho_{prop} P_{total}) + (\rho_{vapor} P_{vapor})/(\rho_{prop} P_{total})$ leads to a weight penalty. The total weight penalty is also reduced as the amount of propellant used directly by the engines increases, corresponding to a decrease in the amount of propellant which must be transferred to the start tank by vacuum refill.

Consider the case of a total start-tank pressure of 207×10^3 N/m^2 (30 psia) for both the hydrogen and oxygen tanks. Assume the helium partial pressure is 69×10^3 N/m^2 (10 psia) so that the hydrogen and oxygen partial pressure is 138×10^3 N/m^2 (20 psia). Thus, for hydrogen

$$\left.\frac{M_{\text{vent total}}}{M_{\text{prop reqd}}}\right|_{\text{Hydrogen}} = 0.023 + \frac{\frac{V_c + V_r}{V_{st}}}{1 - \frac{V_c + V_r}{V_{st}}} \tag{25}$$

and for oxygen

$$\left.\frac{M_{\text{vent total}}}{M_{\text{prop reqd}}}\right|_{\text{Oxygen}} = 0.00364 + \frac{\frac{V_c + V_r}{V_{st}}}{1 - \frac{V_c + V_r}{V_{st}}} \tag{26}$$

Preliminary estimates to determine the feasibility of vacuum refill are given below. As a first approximation, assume that $(V_c + V_r)/(V_{st})$ is much less than 0.023 for hydrogen, and much less than 0.00364 for oxygen. In this idealized case, the maximum weight penalty is estimated from the total propellant weights as given in Reference 1. For the case of 4,750 kg (10,444 lb) of LH_2 and 17,950 kg (39,536 lb) of LO_2, with all propellant being transferred to the start tank by vacuum refill, the total weight penalty associated with vacuum refill is 110 kg (240 lb) for LH_2 and 65 kg (145 lb) for LO_2, for a total minimum weight penalty of 175 kg (385 lb). The optimum number of refills has not yet been determined, but for the case of only six refills, the system weight was estimated to be 2,094 kg, without propellant settling (Table 11, Reference 2). This weight includes 75 kg of pump bypass weight which is probably conservative. Assume that at least 50 kg of pump bypass can be saved by employing the start-tank system which permits pump bypass to be expelled into the main tank, except for very small ullage volumes. In this case, the total system weight is 2,044 kg, to which is added the start-tank vacuum refill penalty of 175 kg, for a total of 2,219 kg. This weight compares with the 2,189 kg of the distributed channel baseline system as given in Table 11 of Reference 2. The above example is overly conservative since none of the start-tank refills are assumed to occur as a consequence of engine operation; with typical missions, the refill penalty should be less than half the above estimate. This concept will be further investigated in the coming months.

The vacuum refill technique also offers a unique means of correcting an unforeseen surface tension breakdown. Assume that the screen device in the start tank fails with the liquid level relatively low. In this case, liquid can not unconditionally be transferred into the main tank since the breakdown may have resulted in screen drying. As a conservative estimate, assume that the propellant volume is 10 percent of the start-tank volume when failure occurs and that the start tank size is maximum, associated with no refills other than occur during engine operation and vehicle acceleration. The hydrogen start-tank volume for the "no-unscheduled-refill" case is 21.9 m^3 (773 ft^3) and for oxygen, 2.6 m^3 (92 ft^3). Thus, the hydrogen vented overboard will be 154 kg (340 lb) and the oxygen vented overboard would be

293 kg (650 lb). Designing the "no-unscheduled-refill" system for the total additional propellant weight of 447 kg (990 lb), therefore provides a redundant method for correcting screen breakdown and ensuring completion of the mission. The percentage increase in propellant is approximately two percent.

3.2 PHASE II, TASK B—BENCH TESTING

The design of an integrated cryogen feed system for advanced space applications involves by necessity moving into areas of advanced technology. This is particularly true in the case of the cryogenic propellant acquisition system where relatively little experimental research has been conducted. Thus, in order to establish a firm basis for the feed system preliminary design, a series of bench tests have been developed, evaluated, and planned. This test list, in its present point of evolution, is shown in Table 7. This listing includes a designation letter, description and purpose statements, criticality rating, applicability rating, remarks, and a disposition statement.

The criticality ratings are as denoted below:

A. Required to show feasibility of design concept.
B. Required to establish preliminary design and overall performance.
C. Required for detailed design.
D. General technology base expansion.
E. Potentially useful design data.

Currently, 17 tests have been suggested and of these, 4 have been dropped from further consideration because of low criticality, poor cost effectiveness, or questionable feasibility. The LOX bubble-point tests were dropped since there does not seem to be a major problem here. Ten tests have been definitely selected for implementation while the remaining two are still being detailed and evaluated. Other tests may be added but the 10 selected tests represent about 80 percent of the budgeted funds. The selected tests either provide basic information on the fluid dynamic or heat transfer characteristics (such as bubble point with vibration and heat transfer) or checkout design/fabrication concepts (such as screen joining). All the tests will have a strong impact on the remaining tasks of this program.

Table 7

CANDIDATE BENCH TESTS (Page 1 of 2)

Designation	Description	Purpose	Test Criticality	Practicality	Concept Applicability	Remarks	Disposition	
							Action	Status
A	Liquid flow tests using subscale ducting models.	To establish and/or evaluate analytical techniques for designing low ΔP ducting.	E	Partial	Dist. Channel start tank (with channel)	Would not be possible to simulate full-scale system but basic analysis could be checked out with model testing. Poor cost effectiveness.	Drop	-
B	Basic screen bubble-point test in LH_2 with simulated warm gas heating (also possible liquid heating).	To demonstrate if a typical screen can in fact maintain retention with heat transfer occurring across the screen.	A	Yes	All	Similar tests have been conducted with LH_2 with favorable results but it may be dangerous to extrapolated to LH_2.	Proceed	In set-up at LH_2 Lab
C	Attach screen material coupons to backup and support structure by various techniques.	To evaluate fabrication techniques for joining screen materials.	C	Yes	All	Low criticality for design but could minimize problems during Phase III of the program.	Proceed	50% complete in MMRE Welding Lab.
D	Bubble-point test in LOX with long-term exposure.	To evaluate any long-term exposure effects on LOX bubble point with typical screens.	B	Yes	All	There does not appear to be a problem.	Drop	
E	Large size channel segment fabrication and bubble-point and pressure tests.	To establish reasonable assurance that a large size channel can be built to satisfy design requirements.	B	Yes	Dist. Channel and spin off for other concepts	This should uncover many potential problems that could arise during Phase III.	Proceed	No action to date.
F	Bubble-point test with LH_2 for selected screen mesh.	To clear up uncertainty in bubble-point measurements.	B	Yes	All	There appears to be discrepancies in MDAC data and data between MDAC and LMSC.	Proceed	Planning complete.
G	Cleaning experiments	To assess the adequacy of various cleaning techniques.	D	Yes	All	Difficult to accomplish and could take on detailed development aspects.	Drop	-
H	Flow loss tests with composite screen/backup structure.	To provide ΔP data to assess interactions of screen and backup materials.	B	Yes	All	Would permit more realistic design margins.	Proceed	70% complete.
I	Bubble-point test with representative screen with vibration present.	To establish if there is retention degradation within due to vehicle vibration	B	Partial	All	Difficult to simulate vehicle conditions.	Proceed	Build-up in progress.
J	Bubble-point tests with controlled screen deflection and distortion.	To establish structurel design criteria for screen rigidity requirements.	C	Partial	All	Difficulty in simulating true situation.	Proceed	Build-up complete.
K	Screen material basic strength.	To establish limit conditions for structural design.	C	Yes	All	Low criticality at this time.	Drop	-
L	To determine the bubble-point performance of pleated screens.	To explore potential problems and benefits of pleating.	D	Yes	All	May have good potential for advanced applications.	Proceed	Build-up complete.
M	Wicking.	To assess wicking characteristics in practical design concepts.	D	?		Our present designs are based on minimization of reliance on wicking. Practicality is in question.	Develop more details	No action to date.

Table 7

CANDIDATE BENCH TESTS (Page 2 of 2)

Designation	Description	Purpose	Test Criticality	Practicality	Concept Applicability	Remarks	Disposition	
							Action	Status
N	Screen support heat transfer experiment.	To establish thermal design criteria and limits for screen support elements.	C	-	Open Screen	Would appear to be sufficient data to design around this problem if it is real.	Drop	-
O	Screen patching techniques.	To establish techniques for patching screen with cryogens.	C	Yes	All	Could help Phase III activity.	Proceed Integrate with C	No action.
P	TVC heat transfer experiment for a cooled finned tube.	To evaluate basic heat process in a cooled wall element.	B	Yes	All		Develop details	No action.
Q	Channel duct fabrication test.	To evaluate rivet joining for duct sections.	B	Yes	Channel	Strong impact on Phase III.	Proceed	No action.

The tests that currently are in progress include: (B) screen heating with LH_2, (C) screen/backup plate joining techniques, (H) screen/backup structure flow tests, and (L) screen bubble-point tests with vibration. In most cases, progress has involved coordinating plans, obtaining materials, building up test hardware and, in some cases, initiating the testing. Detailed progress in each area is discussed below:

3.2.1 Test B—Heat Transfer Effects on LH_2 Bubble Point Tests

The presence of a warm ullage within the propellant tank may adversely affect the retention capability of a fine-mesh screen. If evaporation from the screen exceeds the rate at which liquid can be resupplied from that contained by the screen system then drying will result with a loss in retention.

The apparatus sketched in Figure 23 is available to conduct bubble-point tests in LH_2 with a controlled rate of heat addition to the liquid from a warm pressurizing gas (GH_2). This equipment has been used to conduct identical tests in LN_2 as part of an MDAC IRAD Program. The results of LN_2 tests are reported in Reference 10. No change in bubble point was observed during tests using six different fine-mesh screen samples with heat transfer rates up to 3,000 Btu/hr-ft^2.

The test apparatus includes a resistance heater and electric fan positioned directly above the screen. The evaporating liquid is heated and directed down against the screen to further the evaporation process. Gas is bled from the foam-insulated cylinder at a sufficient rate to hold the ΔP across the screen at the desired level. Net heat transfer to the screen is computed, based on the net mass flow from the cylinder and the latent heat of vaporization. Pressure across the screen is gradually increased until failure is observed through a dewar window.

Installation of the apparatus within the test dewar is complete and this unit is being plumbed into the facility LH_2 supply and disposal system. TV monitoring of the screen will be used to permit remote operation. Two screen specimens (250 x 1,370, and 200 x 1,400, see Figure 24) have been prepared by attaching them to sample plates which in turn will be attached to the lower end of the foam insulation cylinder during separate tests.

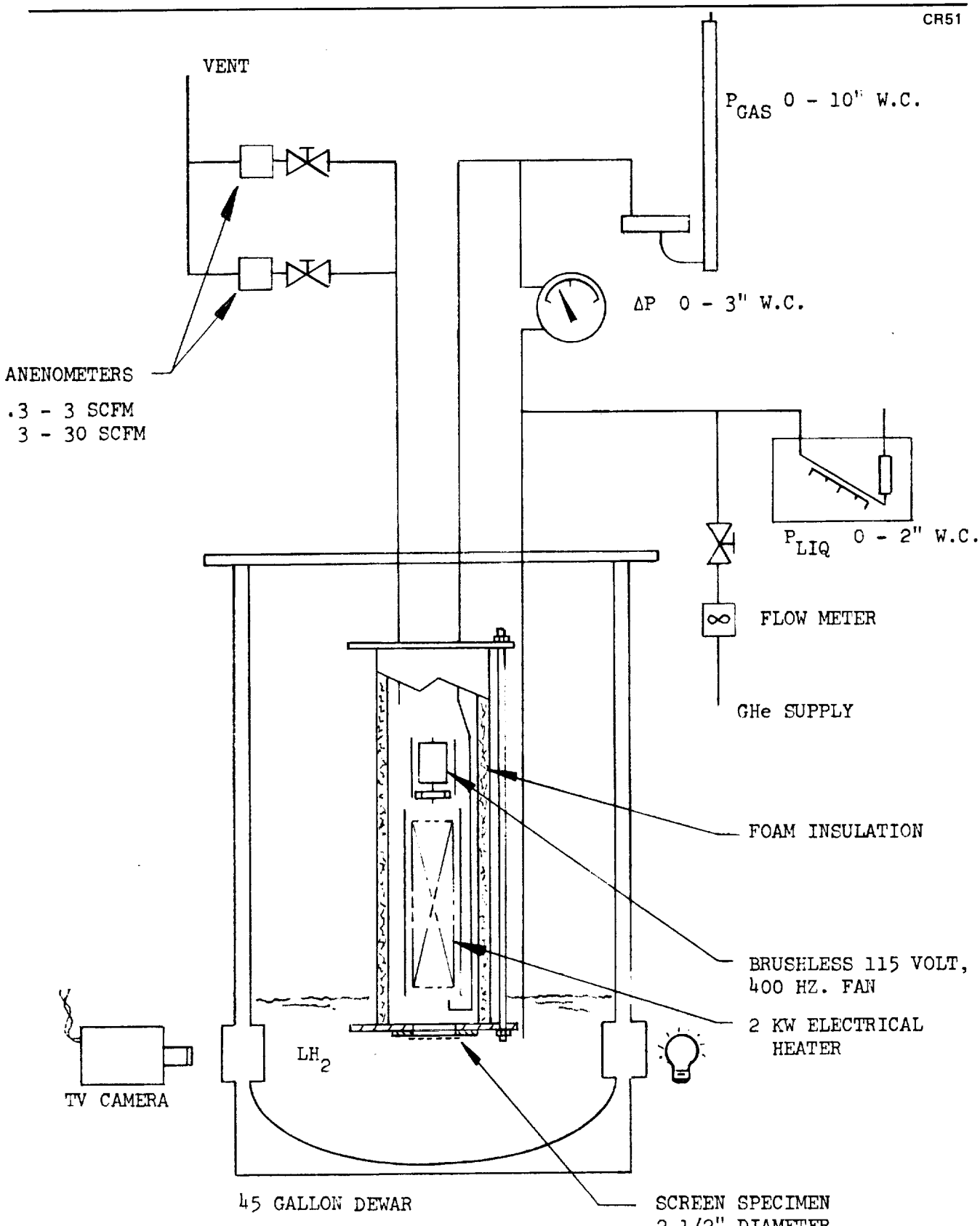

Figure 23. Screen Heating Apparatus

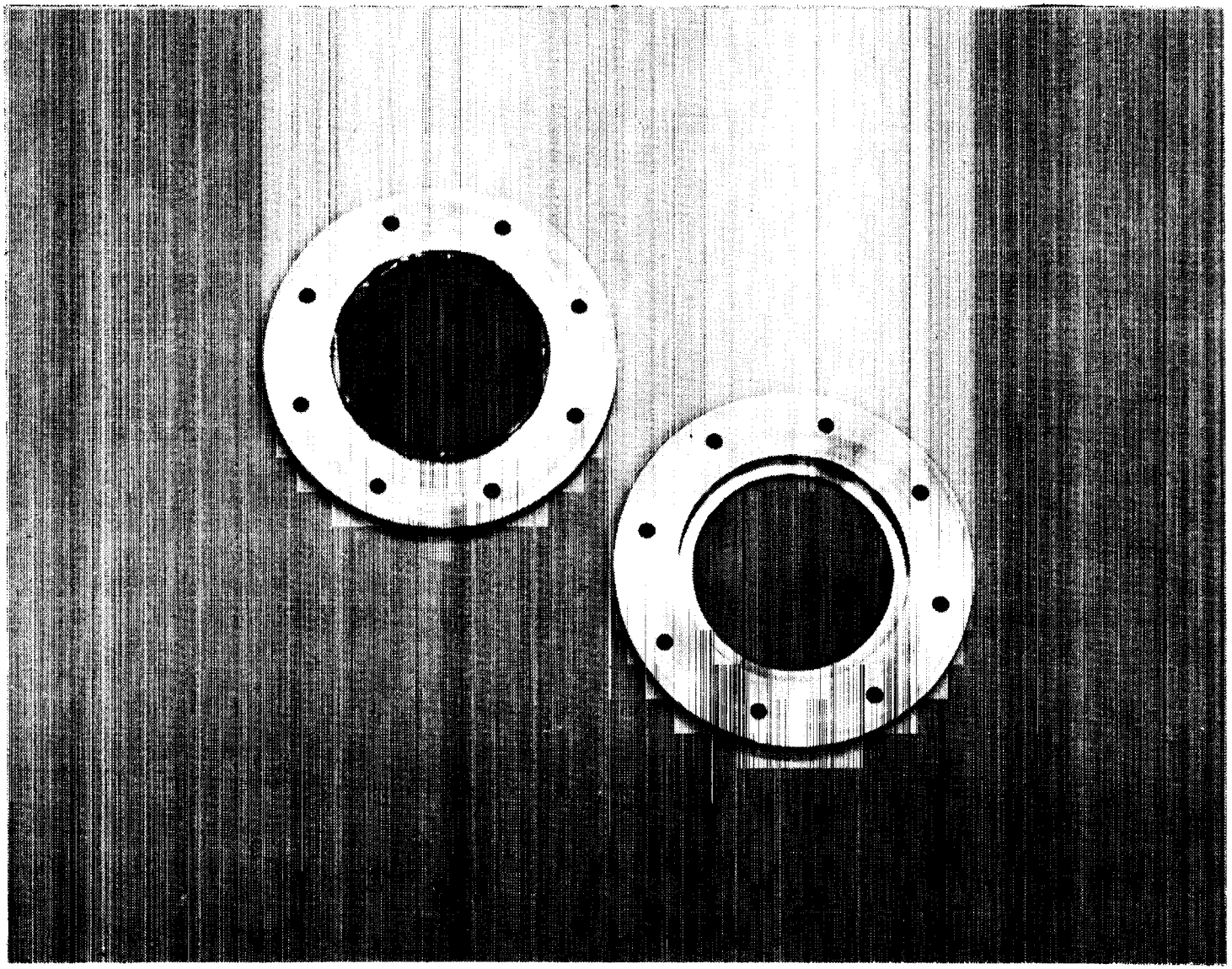

Figure 24. Heat Transfer Test Screen Samples and Holders

3.2.2 Test C—Screen Attachment Techniques Evaluation

After a survey of possible fabrication procedures that could be used to attach the screens to the supporting members within the acquisition device, two techniques were selected for experimental evaluation. The objective is to develop and demonstrate simple attachments that will form a leak-tight joint with a minimum of preparation and tooling. The two selected processes are the GTA fusion weld (gas tungsten arc) and roll spot welding (with spot welding as a subcategory). Welding is preferred over various mechanical techniques because it is inherently more permanent and eliminates the need for the seal common to mechanical attachment. The problems to be overcome in the welding process are primarily concerned with controlling heat addition to prevent burning of fine wires within the screen and to prevent excessive distortion.

To facilitate attachment of the screen within the channels, it has been proposed that the screen be used in a flat state. In addition, it has been recommended that it be joined to a flat stainless-steel sheet (the screen will most probably be stainless steel to minimize difficulties brought about by differential thermal contraction which potentially can degrade the screen bubble point). This sheet in turn is mechanically attached to the channel itself after the channels have been positioned within the propellant tank.

Two gauges of stainless steel sheet have been selected for use during the welding tests: 0.020 and 0.032 inches. Preliminary tests used 200 x 1,400 stainless steel screen. The screen was sandwiched between two pieces of the same gauge sheet and the three layers were fused together. The weld bead area is as sketched in Figure 25.

The roll spot-welding process involves a series of overlapping spot welds created at the interface or interfaces of lap surfaces. The weld is created by the resistance to welding current across the interface and the simultaneous application of pressure by means of slowly rotating copper wheels. The primary welding variables include welding current (high amperage, short duration) contact pressure, and travel speed. Figure 26 shows several of the preliminary roll spot-welded specimens. Peel tests and section cuts

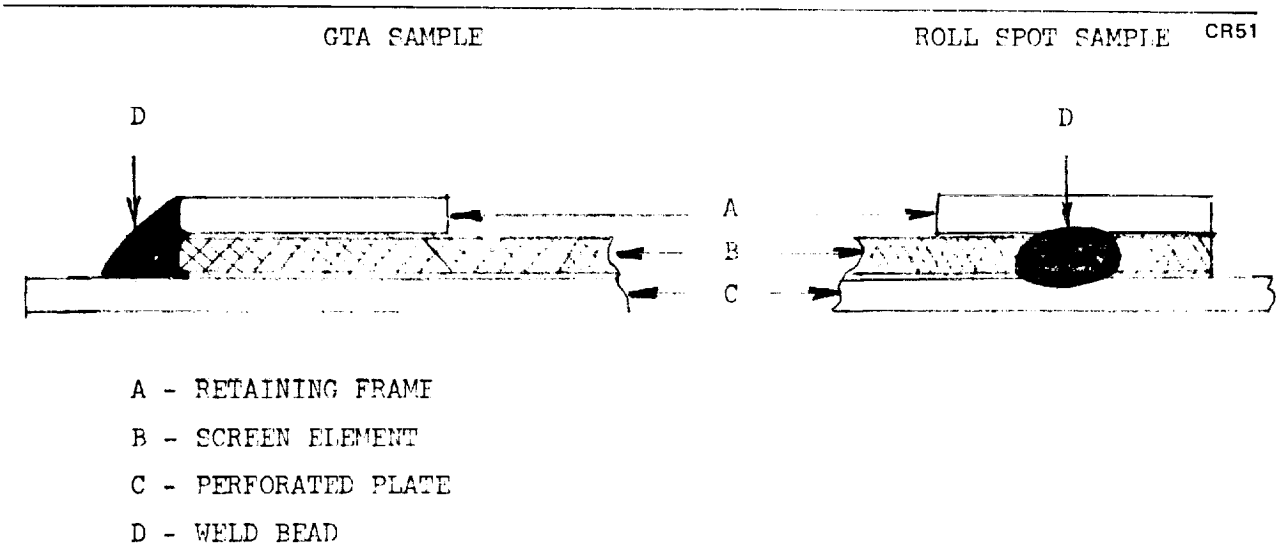

Figure 25. Selected Screen Attachment Weld Samples

made perpendicular to the weld indicated that fusion was satisfactory. To avoid skewing and misalignment, several spot welds were used to secure the two layers of stainless steel sheet and screen.

Preliminary GTA welding tests also used both gauges of stainless steel sheet in a lap-joint configuration. The welds were made by clamping the small assemblies in a vice between two pieces of 1/2-inch-thick copper plates to serve as chill and control distortion. Figure 26 shows several of the weld specimens. Note that distortion is significantly less with GTA specimens than that evident in the roll spot specimens. Sections made through the weld indicate good fusion in both gauges of material. Attempts to form a lap joint between a screen and single piece of sheet were unsuccessful. The latter configuration resulted in several holes burned in the screen. Preliminary tests with configuration in which the screen edge is welded directly to the base plate and using the sandwich of two sheets of stainless steel and screen indicated that this technique could be used if necessary.

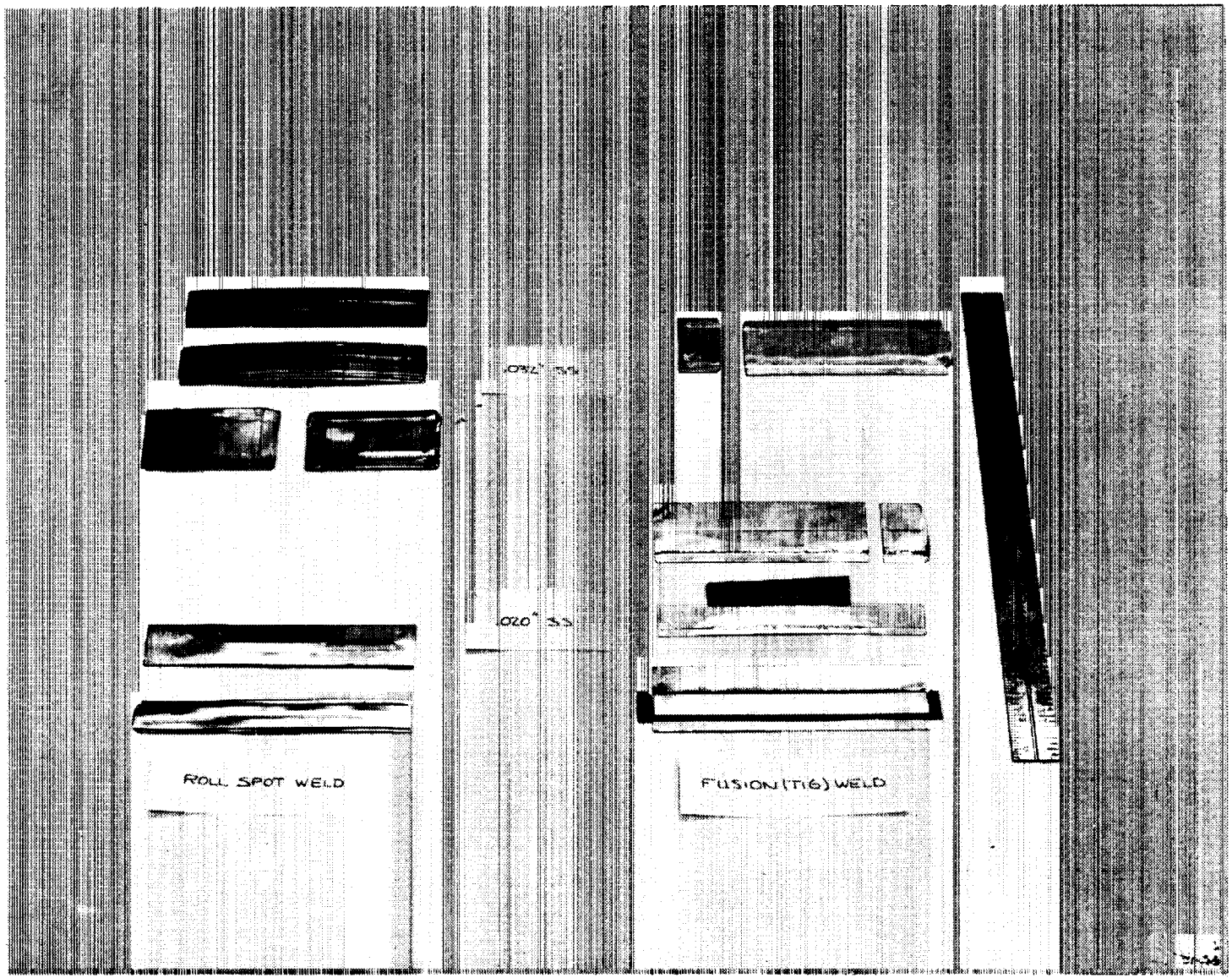

Figure 26. Preliminary Weld Samples

The next step in the welding bench tests will be to make up a number of 5-inch-square panels consisting of a screen sandwiched between a perforated backup sheet and narrow frame that follows the perimeter of the screen. A test fixture is available (see Figure 27) to run bubble-point tests on the square weld specimens, and thus check out the acceptability of the welds from an acquisition performance standpoint.

3.2.3 Test E—Channel Segment Fabrication Test

This test will not be initiated until completion of most of the more basic tests and further evaluation of the preliminary design.

3.2.4 Test F—LH_2 Bubble-Point Testing

The LH_2 bubble-point tests of the fine-mesh screen specimens described in Reference 11 resulted in test results that have not been completely explained. During those tests where GH_2 was used as a pressurizing media, the test data were repeatable and in agreement with predictions based on isopropyl alcohol bubble-point tests with the same screen samples. However, the results with GHe were erratic and not adequately predictable. A set of bench tests has been initiated to delve into this peculiarity with GHe which is critical because helium is our primary candidate pressurant.

The referenced tests with GHe provided no means to control or measure the GHe partial pressure behind each of the screen samples. It is hypothesized that the data scatter is related to the uncontrolled scatter in GHe partial pressure. The apparatus shown schematically in Figure 28 has been designed to provide a controlled and known GHe partial pressure. A second modification in the test apparatus is to mount the screen in a position where it can be viewed directly through the dewar window. Close observation of the screen is felt to be needed to detect the point of initial pore failure as opposed to gross (multipore) failure detected in the referenced tests.

Each of six screen samples will be bubble tested in turn, using the same procedure. The dewar will be filled with LH_2, completely submerging the samples and bank of one-inch tubes that serve as individual accumulators behind each screen (see Figure 28). The dewar will be vented to atmosphere. Liquid level is to be monitored with a carbon resistor point level

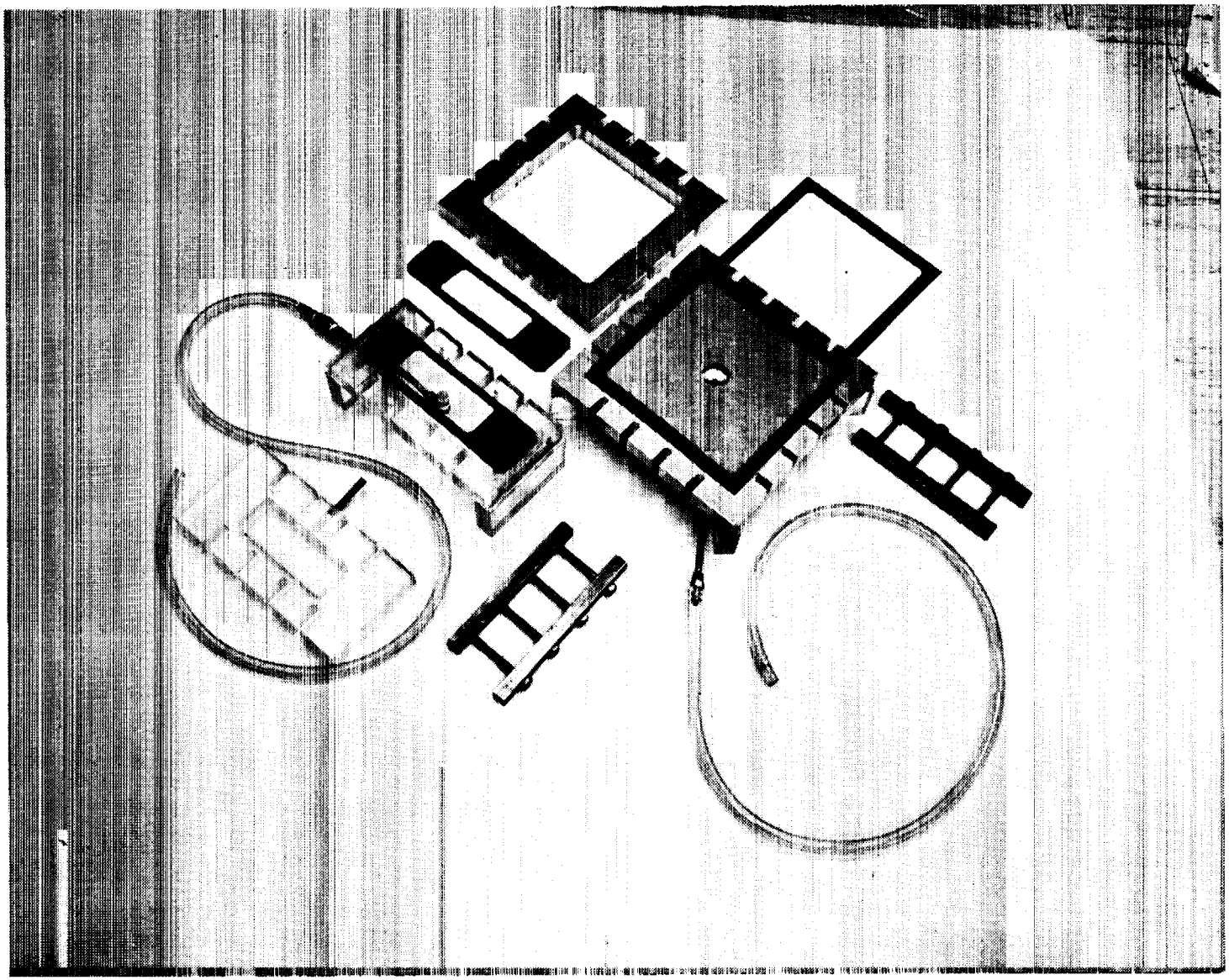

Figure 27. Screen Sample Bubble-Point Test Apparatus

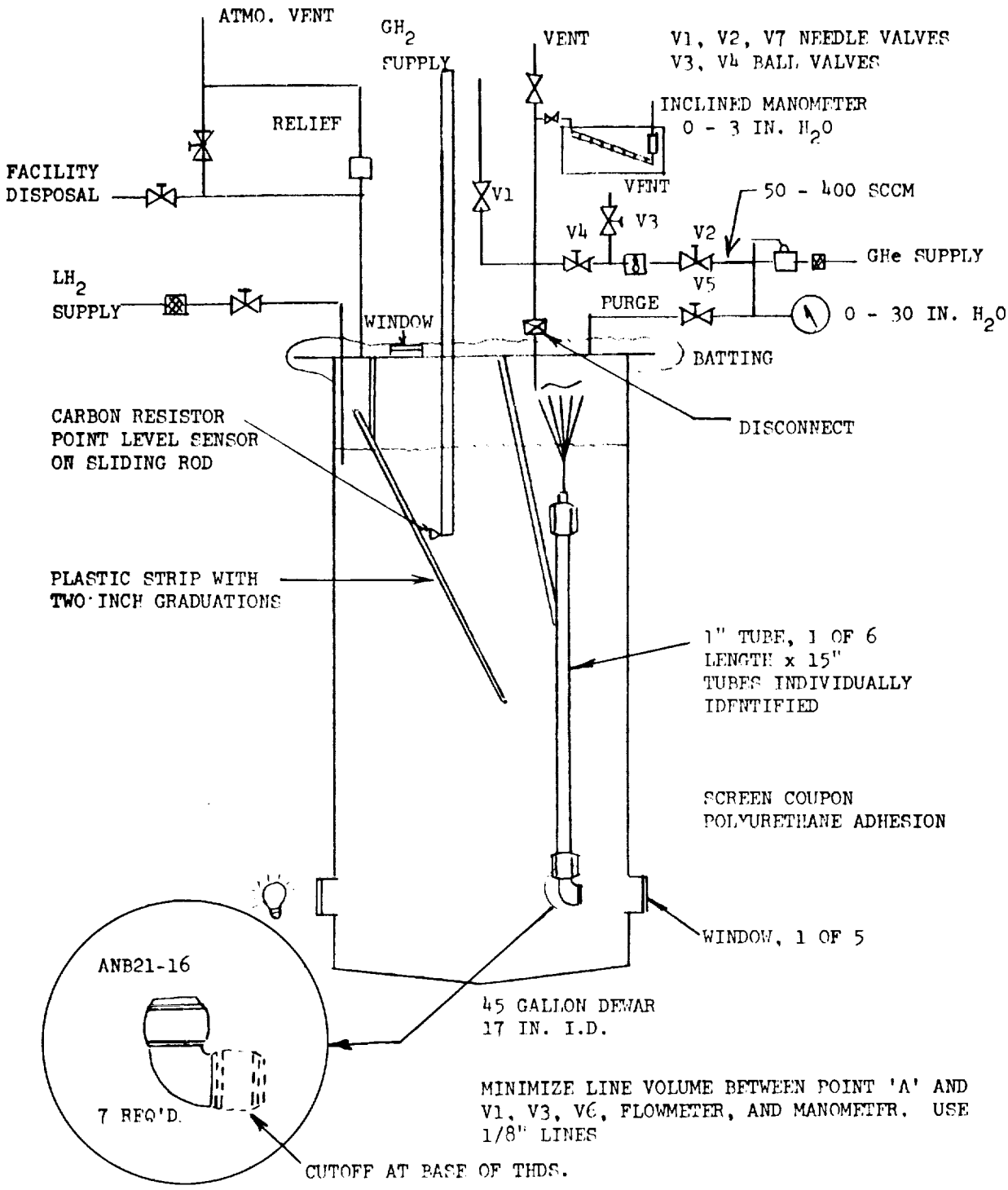

Figure 28. Bubble-Point Test Apparatus

sensor with a graduated plastic strip serving as a redundant level detector. The one-inch tube connected to the screen of interest will be filled with LH_2 by venting through valve V6. GHe will then be used to displace this liquid through the screen at a rate measured by a flowmeter. In this fashion the tube will be charged with a known amount of GHe at which point continued pressurization will take place slowly with GH_2 through V1. At the point of screen failure, the ΔP across the screen will be indicated at the manometer at the point of screen failure. This pressure and the accumulator volume when combined with the amount of GHe present will yield the total amount of gas present at breakdown. It is a simple matter then to compute the GHe partial pressure.

Each screen will be tested without requiring that the dewar be opened. To switch from one screen to the next requires that a single disconnect be made at the dewar lid. The screens will also be bubble-point tested using GH_2 alone.

The screen samples required for this test have been prepared and attached to the modified fluid fittings as they will be used in LH_2. Preliminary isopropyl alcohol bubble-point tests will be conducted with each. It is planned that the LH_2 testing will take place following the heat transfer tests described in Section 3.2.1 which uses the same dewar.

3.2.5 Test H—Flow Loss Experiments

The expulsion capability of simple surface-tension devices are limited for large cryogenic systems that experience significant destabilizing accelerations, such as during APS maneuvers. Surface tension devices made from fine-mesh screen materials have been found to provide improved head retention and expulsion capabilities because of the relatively high surface-tension pressure that can be supported across the small effective pore size of the screen. The retention performance of these screen materials is expressed by a bubble-point property which is the pressure differential across the screen at which gas breaks through the wetted screen and enters the liquid.

The screen channels and collection ducts of a retention subsystem must be sized so that viscous, dynamic, and hydrostatic losses within the passage

are minimized. The sum of these losses must not exceed the bubble-point pressure for the basic screen used on the channels at any point to ensure that pressurant does not enter the suction line. Therefore, the basic screens must offer minimal resistance to flow.

An MDAC numerical program (acquisition channel sizing code) is available for analyzing specific retention-system configurations. The program uses correlation equations devised by Armour and Cannon (Reference 12) to calculate the pressure loss accompanying flow through the screen into the screen channel but does not consider losses through screen backup materials and any interaction effects. Since backup perforated sheet is being considered to support the more flexible basic screen material, flow losses associated with these configurations are being determined in the series of tests described herein.

The objectives of this test program are to determine the pressure drops through representative dutch-twill screens for a wide range of Reynolds numbers, to determine the effects of backup perforated sheet behind these same screens, and to determine means to minimize these effects. Three sizes of screen and nine different backup configurations were tested using both gaseous nitrogen (GN_2) and helium (He) as the working fluid.

Test Setup

The basic components in the test setup are a flow tube designed to contain the test element, a pressurized gas supply, a gas filter, a manometer to measure the pressure drop across the test element, a vertical open-end water manometer to measure the static pressure immediately upstream of the test element, a variable area flowmeter calibrated for both GN_2 and He, and associated lines and valves. The apparatus was fabricated in the Propulsion Subsystem Laboratory at Huntington Beach, California, and is shown in Figures 29 and 30.

The setup is shown schematically in Figure 31. The flow tube consists of two identical halves which are bolted together at their flanged ends. Each flange contains a soft gasket which seals the test element between the bolted flanges for testing.

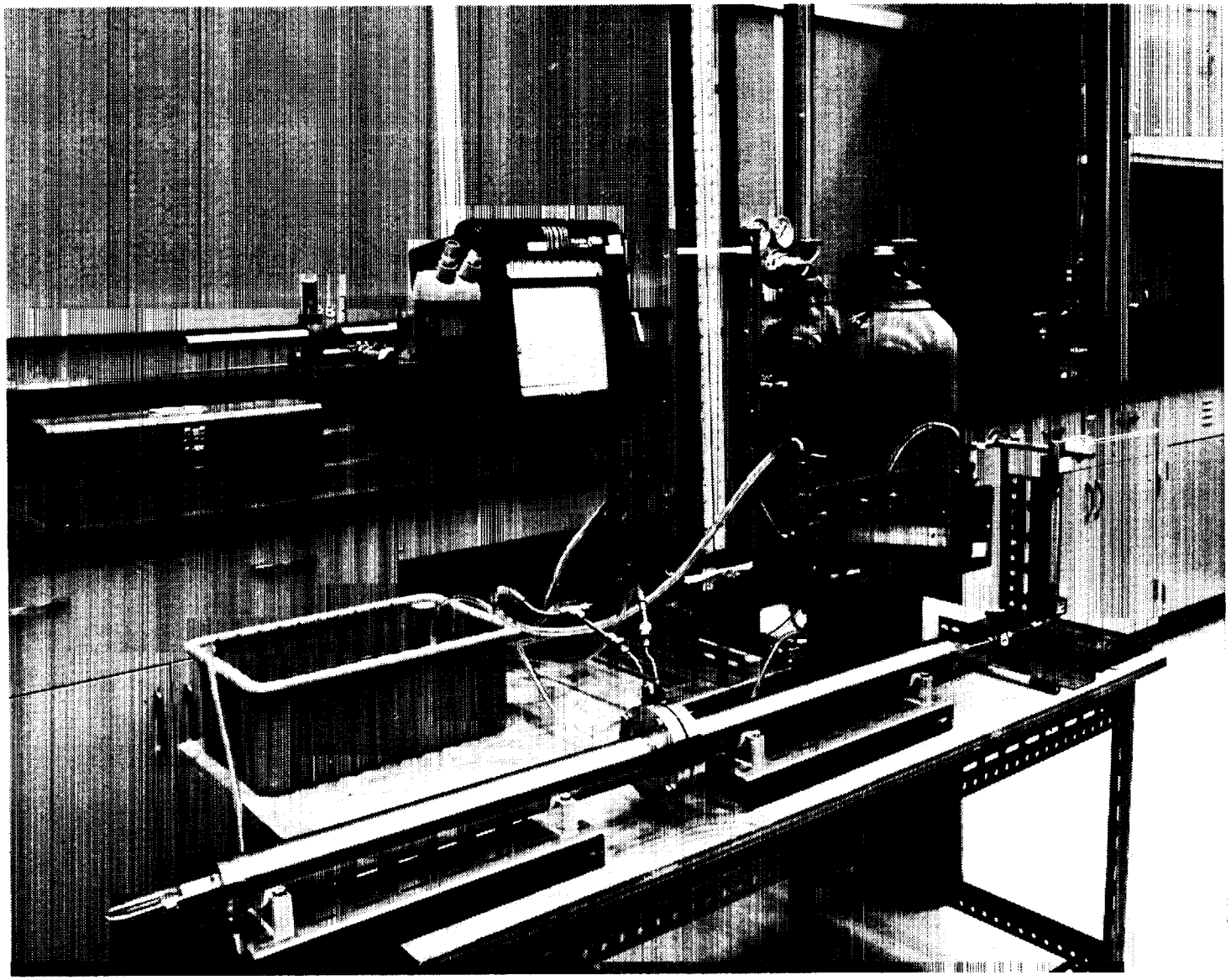

Figure 29. Flow Loss Test Setup

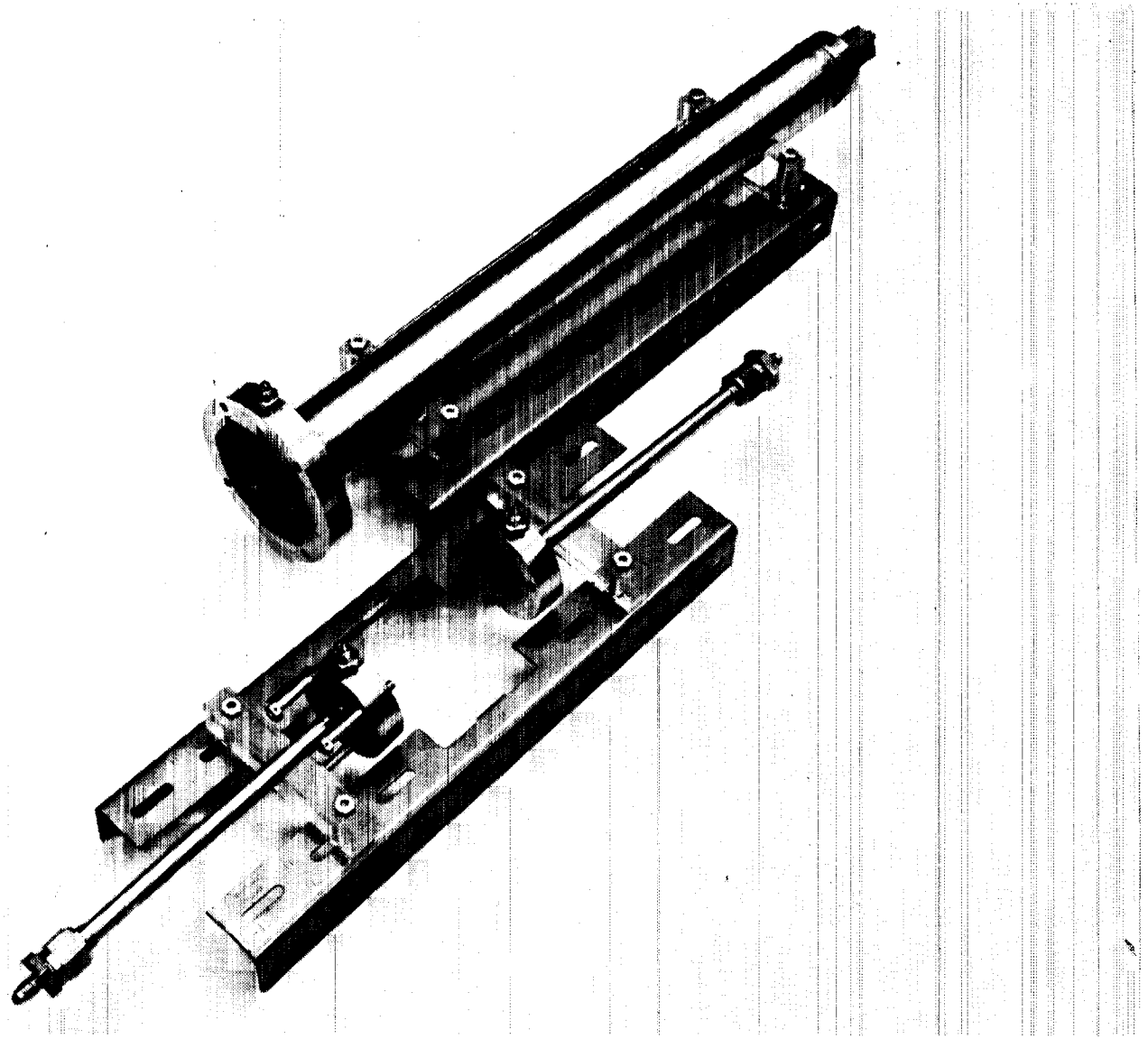

Figure 30. Flow Loss Test Device

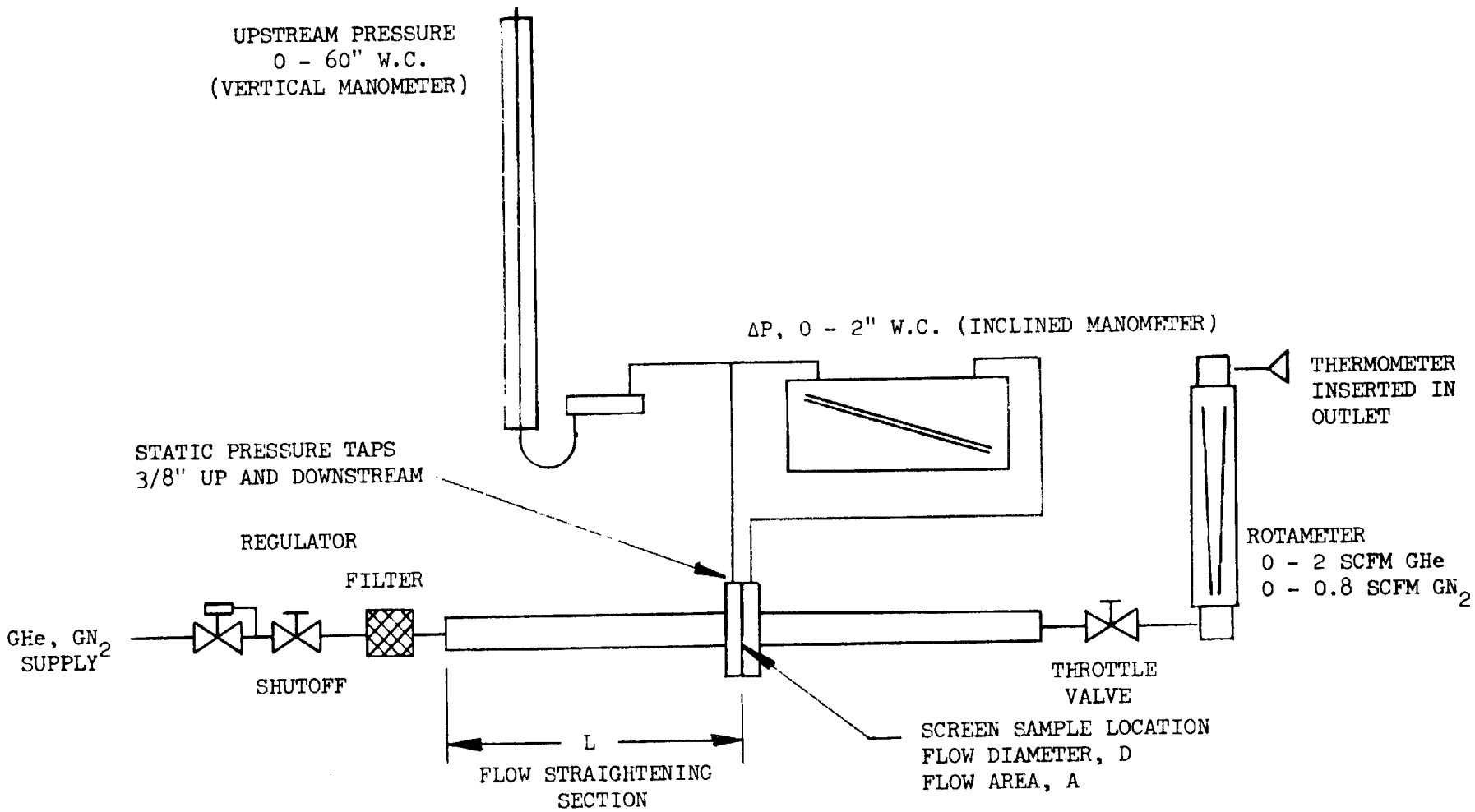

	L(IN)	D(IN)	A(IN^2)
LARGE FLOW UNIT	20	1.90	2.83
SMALL FLOW UNIT	8	0.42	0.15

Figure 31. Screen/Backup Pressure Drop Test Apparatus

Pressure taps are drilled through each flange so that static pressures may be measured 3/8-inch upstream and downstream of the element. Two flow-unit tube sizes (see Figure 30) are available to allow for a greater range of flow velocities within the limits of the flowmeter. Pressurized supplies of both GN_2 and He are on hand to provide a wider range of Reynolds numbers. An inclined manometer is used to measure pressure drops of less than 2 inches of water, whereas a 40-inch vertical manometer is used to measure those greater than 2 inches of water.

Summary and Results

The characteristics of the three types of stainless-steel, dutch-twill screens and of the nine perforated sheets (see Figure 32) which were used as screen backup materials are summarized in Tables 8 and 9, respectively. More than 20 data prints were recorded for each of the three basic screens to represent the full range of Reynolds numbers possible with the available combinations of two inert gases and two flow areas. The effects of the perforated sheets as screen backup material were determined using the larger flow tube according to the schedule shown in Table 10.

The basic screen data are plotted in terms of a flow friction factor in Figure 33 as suggested by Armour and Cannon (Reference 12), and in terms of a dimensionless pressure loss (Poiseuille number, P_o) in Figure 34. The data points are uniformly lower than the Armour and Cannon correlation curve in Figure 33, which indicates that the correlation equation is conservative by a factor greater than 2. Note, however, that the correlation is successful in aligning the data points for the three screens. It was further noted that the flow losses associated with gaseous helium were slightly less than those for gaseous nitrogen.

The Poiseuille number, P_o, is a convenient parameter for comparing pressure losses because it remains nearly constant for a specific screen in the laminar flow regime (see Figure 34). The laminar flow regime extended to a Reynolds number of approximately 1.0. The results of the GDC study (Reference 13) were presented in this manner for a number of screens which included the 200 x 1,400 mesh size. The GDC values of D and B (defined in Table 8) were adjusted so that their data can be compared with those from

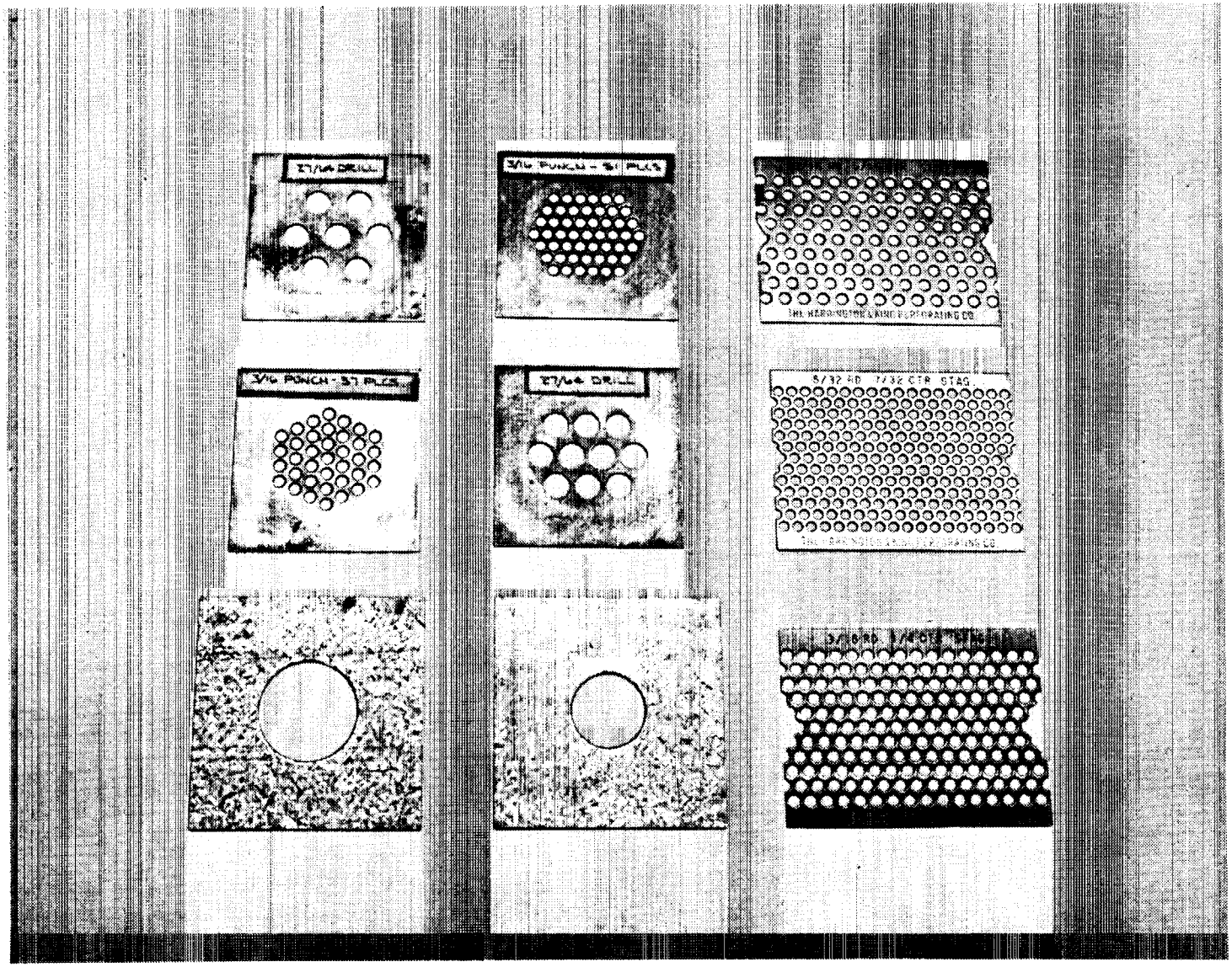

Figure 32. Perforated Plate Test Samples

Table 8

CHARACTERISTICS OF STAINLESS STEEL DUTCH TWILL SCREENS TESTED

Mesh (wires/in.)	200 x 1,400	250 x 1,370	325 x 2,300
Wire diameter (in)	0.0028/0.0016	0.0022/0.0015	0.0015/0.0010
Pore diameter, D(ft)	7.14×10^{-5}	5.67×10^{-5}	4.83×10^{-5}
Screen thickness, B(ft)	5.00×10^{-4}	4.50×10^{-4}	2.92×10^{-4}
Surface area per unit volume, $A(ft^{-1})$	19,930	22,443	33,598
Void fraction, ϵ	0.248	0.204	0.245
Tortuosity factor, Q	1.3	1.3	1.3

Table 9

CHARACTERISTICS OF PERFORATED BACKUP SHEETS

Identifier	Open Area Fraction, F_A	Hole Size (in.)	Description
1	0.623	1-1/2	Single Hole
2	0.510	3/16	1/4 in. Center-to-Center
3	0.496	3/16	51 Holes
4	0.495	27/64	10 Holes
5	0.460	5/32	7/32 in. Center-to-Center
6	0.361	3/16	37 Holes
7	0.350	1-1/8	Single Hole
8	0.345	3/16	7 Holes
9	0.330	27/64	5/16 in. Center-to-Center

Table 10

TEST MATRIX FOR SCREEN/PERFORATED SHEET COMBINATIONS

Screen Mesh	Gas											
	GN_2										GHe	
200 x 1, 400		x								x		
250 x 1, 370	x	x	x	x	x	x	x	x	x	x	x	x
325 x 2, 300		x								x		
	1	2	3	4	5	6	7	8	9	2	3	4

Perforated Sheet Identifier

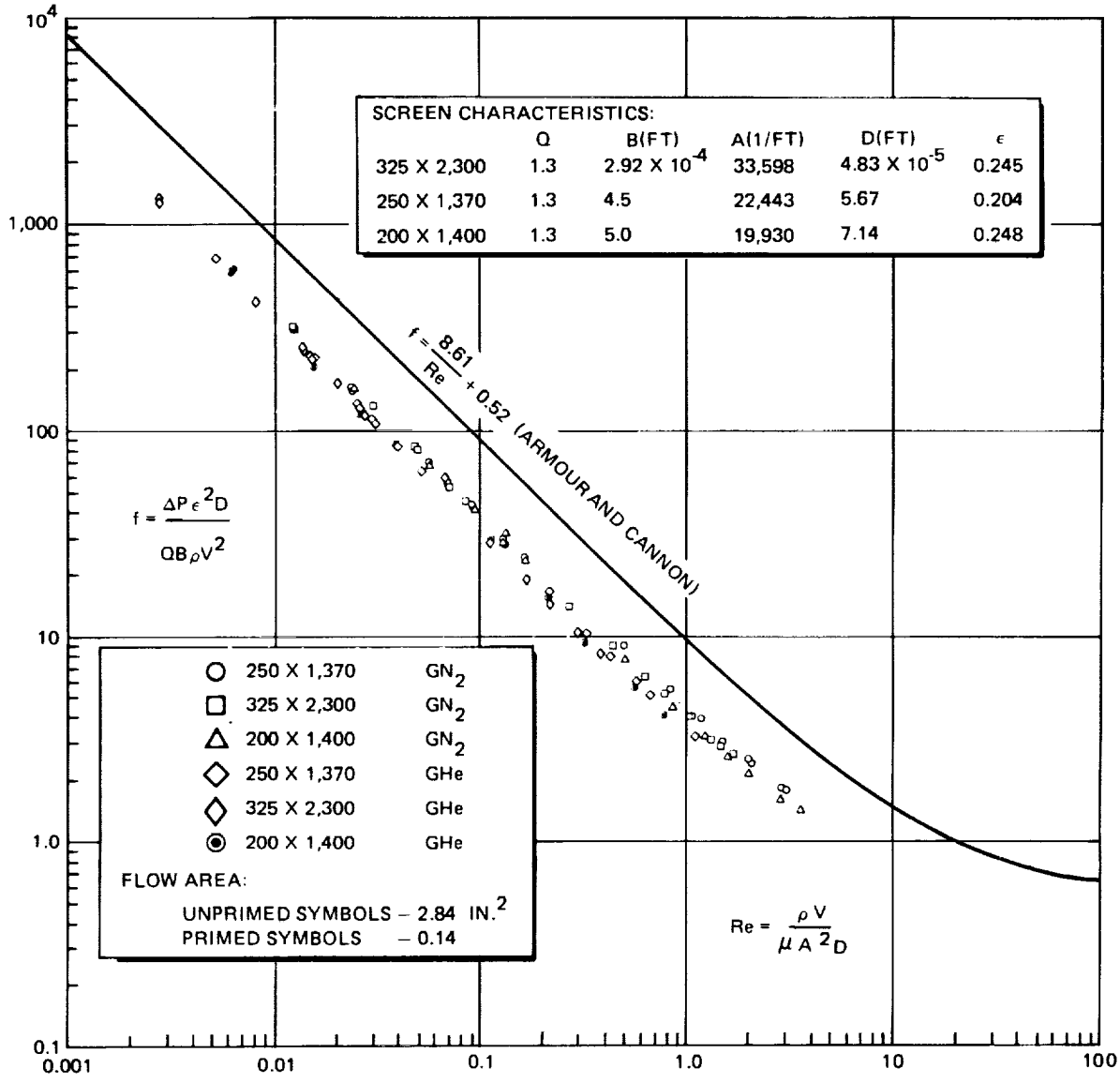

Figure 33. MDAC Flow-Loss Data Correlations for Dutch Twill Screen

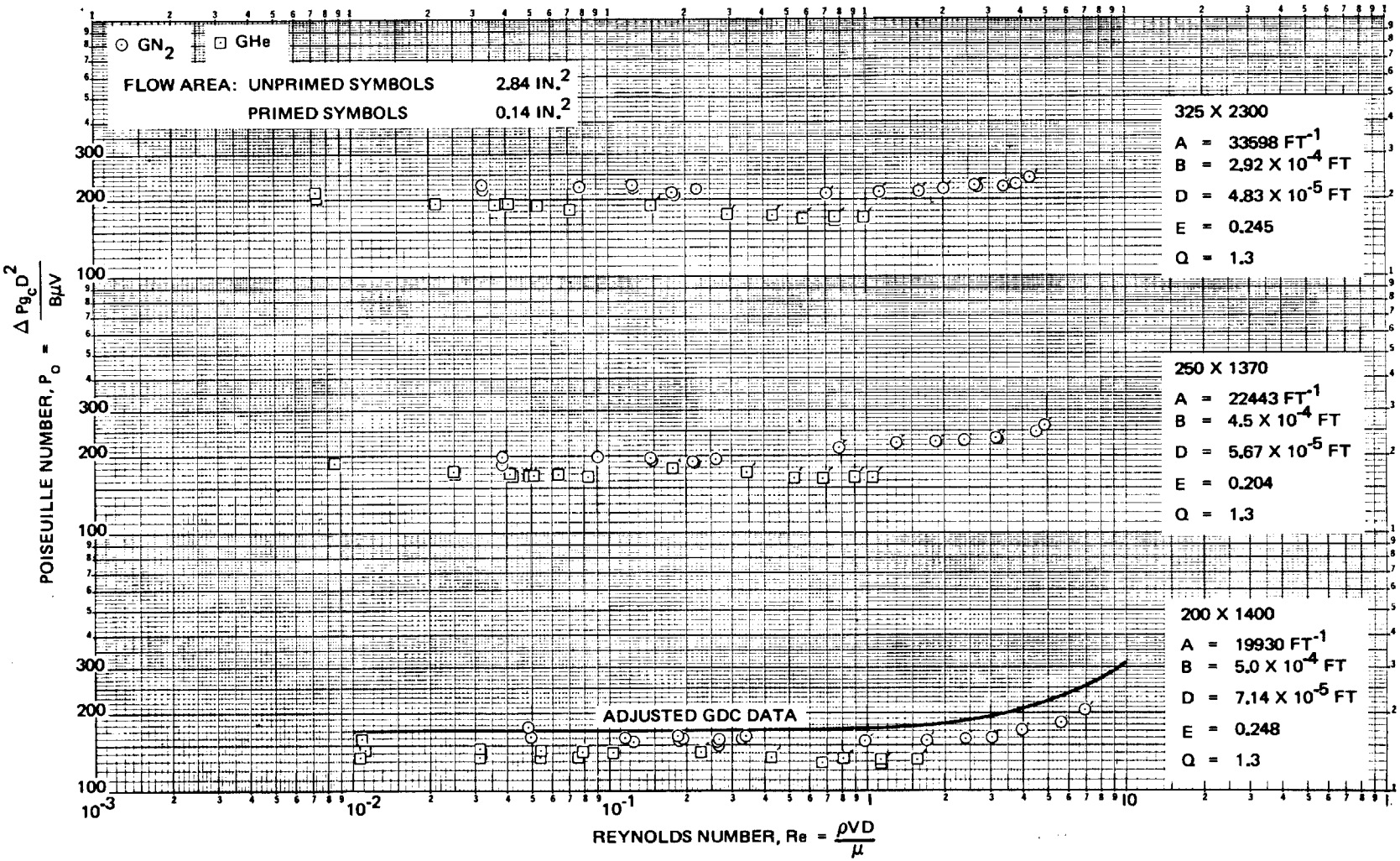

Figure 34. MDAC Flow-Loss Data for Dutch Twill Screen

the MDAC tests. The comparison indicates that GDC experienced pressure losses slightly higher than those of MDAC, as seen in Figure 34.

The pressure drop across a screen/perforated sheet combination is greater than that across the screen alone, as expected. The effects of the nine perforated sheets were compared on the basis of a pressure loss ratio, $\Delta P/\Delta P_o$, where ΔP is the average combined pressure loss (averaged over all data points for a specific screen) and ΔP_o is that for the basic screen alone. This parameter is plotted in Figure 35 against the fractional open area, F_A, of the perforated sheet. The plot indicates that a correlation would involve something more complicated than simply F_A. Pressure losses associated with flow through the perforated sheets alone were not measurable with the instrumentation at hand, which indicates that the loss across a combination is not merely additive, but is strongly affected by the flow paths between and

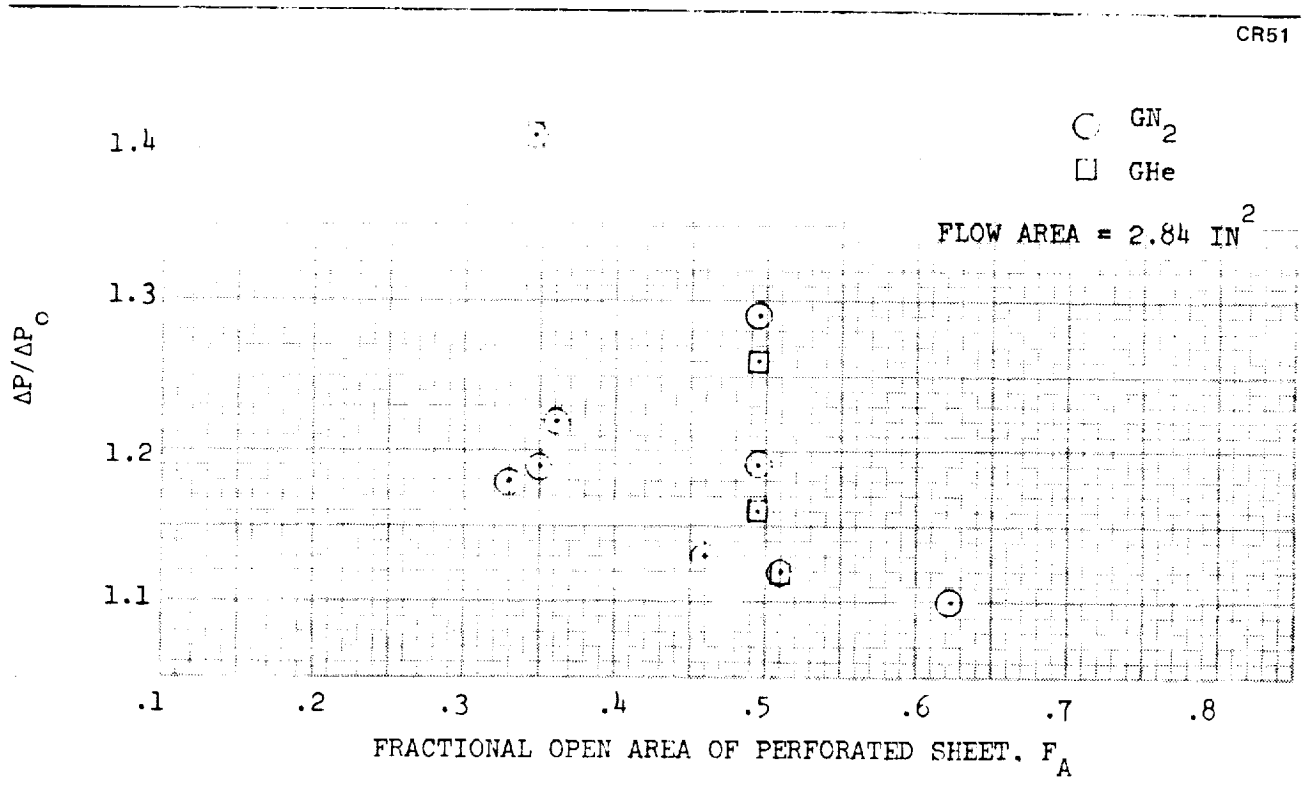

Figure 35. Effects of Perforated Backup Sheets on Screen Pressure Loss

parallel to the screen and sheet. It may be possible to nullify this effect by inserting a lightweight (aluminum) coarse mesh spacer between the two elements to provide less severe flow paths rather than squeezing the elements together, as done in these tests. Various spacers will be evaluated in the test program to determine if such a solution is possible.

The curves presented herein represent the results of tests completed as of the date of this report. Further tests to be conducted in this experimental program include the following:

A. Evaluate the effects of coarse mesh spacers on the pressure losses across screen/perforated sheet combinations.

B. Duplicate some of the above tests using water rather than gas as the working fluid.

C. Determine the bubble-point and flow-loss characteristics for robusta-type screen. This type of weave offers the potential of a lower flow loss compared to dutch-twill screen having the same bubble point.

3.2.6 Test I—Vibration Testing

The operational environment of a surface-tension acquisition device includes oscillatory inputs having their origin in rotating machinery, acoustics, flow instabilities, etc. Figure 36 indicates the possible range in vibration parameters that may be expected on the Space Shuttle. The nature of the response of the liquid/gas interface within a screen to a vibration input has not been clearly defined. Reference 14 summarizes test results related to the change in expulsion capability for a complete pleated-screen tank liner (11-inch diameter) when subject to sine and random vibration. One effect clearly demonstrated was that for low frequency sine vibration ($\omega < 85$ Rad/sec) the oscillations acted to modify the hydrostatic head within the propellant simulant as indicated by $a_v = \omega^2 A$ where a_v is the induced peak acceleration and A the vibration amplitude. These tests were, however, unnecessarily obscured by the complex geometry employed. Overall system behavior was demonstrated but the underlying behavior at the various points on the screen could not be deduced.

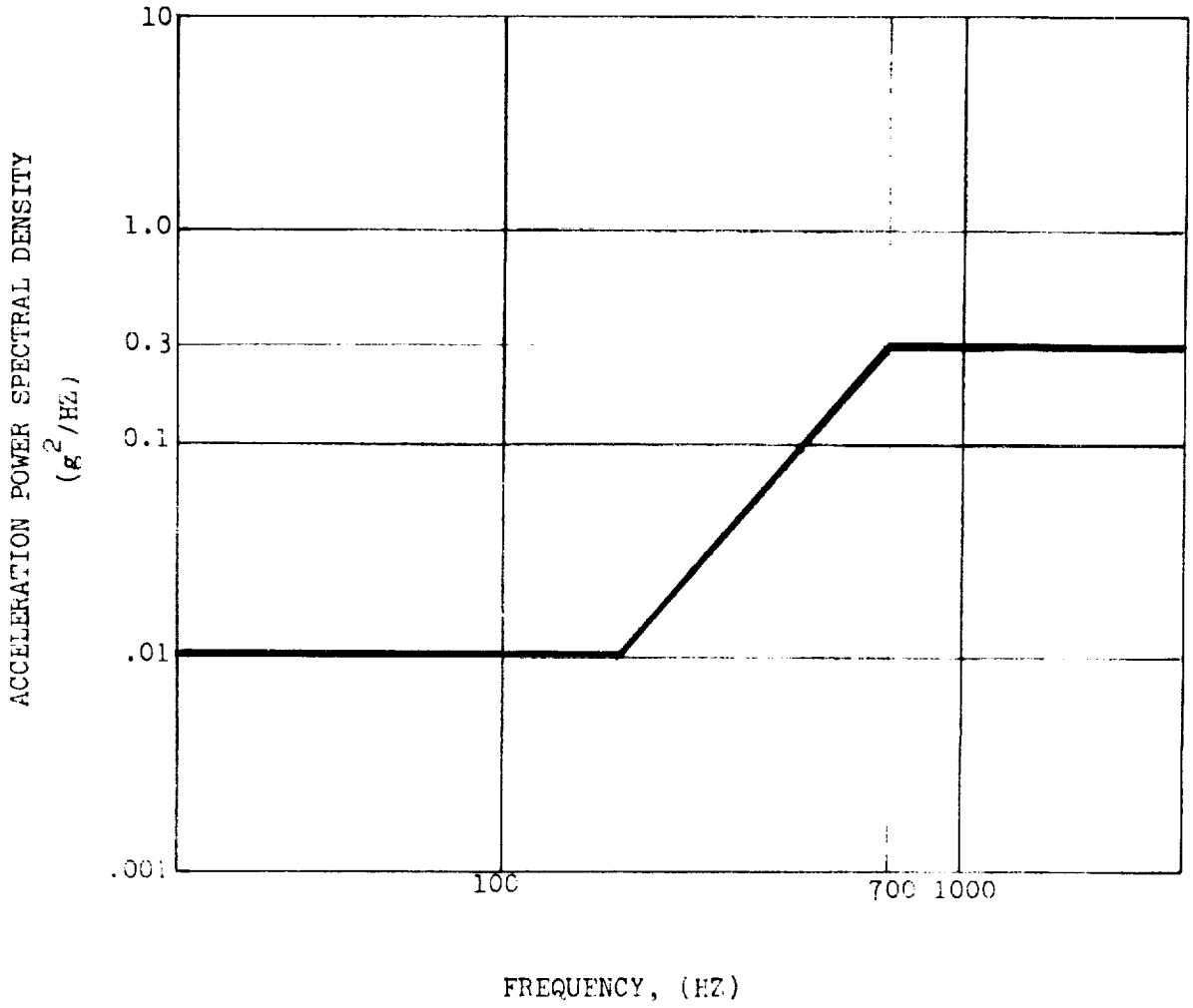

FROM: DESIGN ANALYSIS OF CRYOGENIC TANKAGE CONCEPTS, NAR REPORT SD72-SA-0025, NAS 7-200

Figure 36. Orbitor Engine-Induced Vibration Spectra

Additional insight into vibration related phenomenon in wetted screens is to be gained using the simple apparatus sketched in Figure 37. Four pieces of screen are sandwiched between a metal base plate containing eight pressurization ports (two per screen) and a Plexiglas block containing eight cylindrical holes; two above each piece of screen (diameters 3/8 and 1 inch). The base plate is mounted directly on the shaker platform. The cavities in the Plexiglas block allow a small amount of alcohol to be placed over each screen so that the bubble point can be measured when pressurization with GN_2 takes place through the appropriate port in the base plate. The transparent block permits screen breakdown to be observed directly. If the back pressure of alcohol is to be increased above one inch, an extension piece can be clamped to the top of the Plexiglas block to permit any depth up to 24 inches.

The experimental apparatus has been fabricated and is in the process of being attached to the shaker platform (12,000 LBF unit). Vibration inputs will take place both parallel and perpendicular to the plane of the four screen samples. It is planned that the bubble point for each sample will be measured for specific acceleration levels as the frequency ranges from 5 to 1,000 Hz. The bubble point will also be checked at specific frequencies as the acceleration level is varied. An alcohol depth of one inch or less will be used in both axis and the added depth capability will be used when the axis is perpendicular to the screen.

3.2.7 Test J—Screen Deflection and Fatigue Investigations

Use of a screen within a propellant tank as part of an acquisition device introduces cyclic loading on the screen during periods of outflow and liquid motion. It is not practical to completely restrain the movement of the screen since these restraints customarily prevent flow through localized portions of the screen. Reduced flow area generally results in a reduction in operational safety factor for the acquisition device and is therefore undesirable. The large screen areas that are attractive because they minimize flow losses also tend to aggravate problems that might be caused by screen flexing. The primary detrimental factor that flexing might cause is a

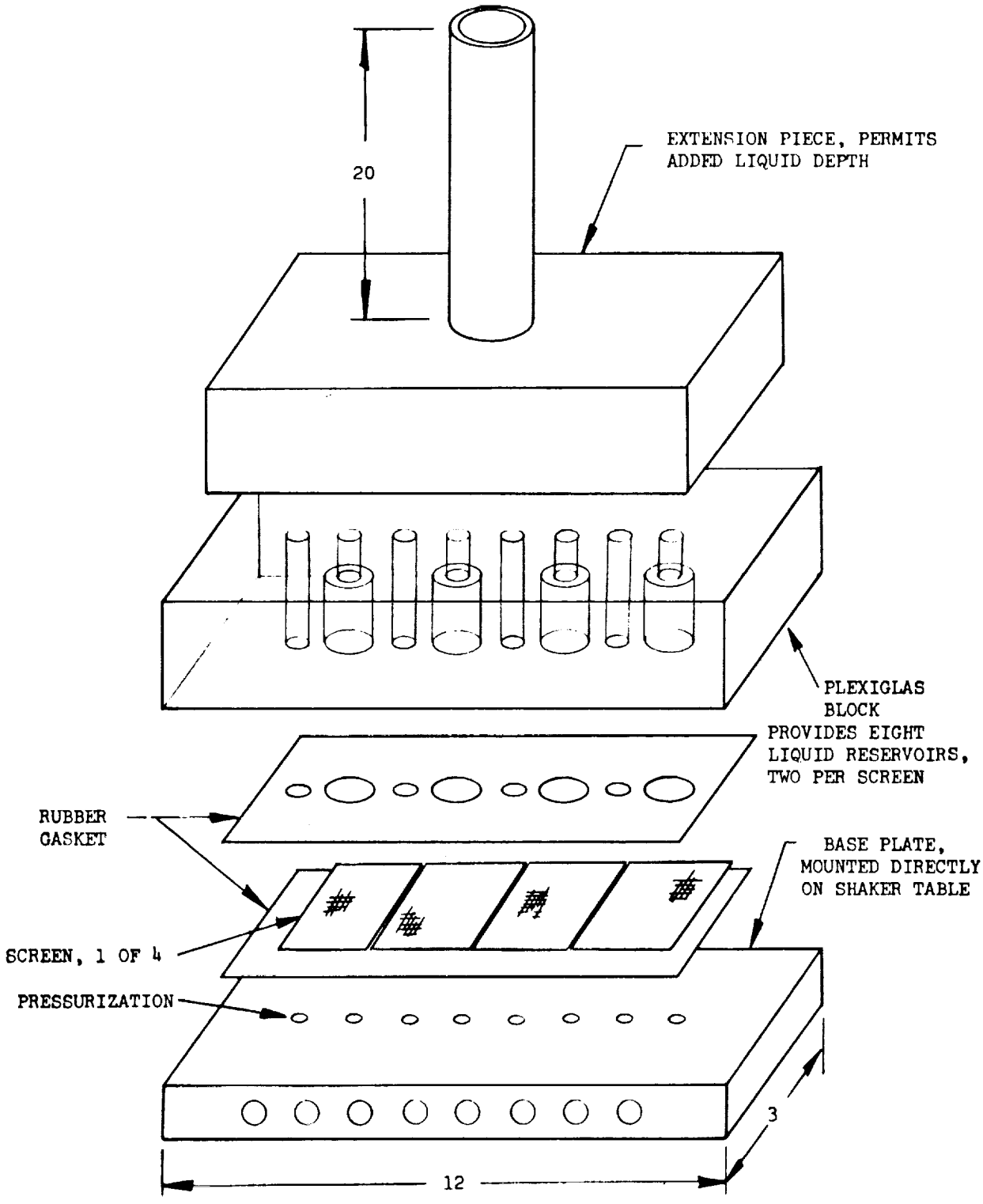

Figure 37. Vibration Test Fixture

reduction in the screen bubble point because of broken wires or movement of wires in the screen, thus causing a change in the effective pore size in a local region.

A set of bench tests has been initiated to investigate the sensitivity of screen bubble-point pressure to cyclic screen deflections. These tests will be carried out using the welded screen assemblies described in Subsection 3.2.2 as well as the bubble-point apparatus designed to accommodate these samples. The apparatus will be modified by the addition of the small electric motor and eccentric drive shown in Figure 38. An attachment will be made to the center of the welded screen assembly as it is clamped in the bubble-point apparatus. The motor and variable speed control will introduce a vertical deflection in the center of the screen having a frequency of approximately 1 Hz. The bubble point of the screen can be checked in isopropyl alcohol while the deflections are taking place. Initially, the deflection amplitude will be quite low (< 0.1 inch). A large number of oscillations (minimum: 1,000) will be input at this amplitude and then checked at regular intervals while noting those new locations when the screen is observed to fail. Both fusion welded and roll spot-welded screen assemblies will be tested.

These tests will be qualitative in nature. If it is shown that significant changes in bubble point occur, then additional studies may be warranted. The two different weld processes may give entirely different results. The fusion-welded assemblies will be more taut and consequently may be more sensitive to the forced deflections.

3.2.8 Test L—Pleated Screen Tests

Pleating of the basic screen in a surface-tension acquisition device offers the potential of increasing the area available for liquid flow by a factor of as much as three or four, with a corresponding dramatic reduction in flow loss through the screen. The reduction in loss is reflected in a higher operational head retention safety factor for the acquisition device. This advantage must be weighed against several detrimental factors brought about by pleating, such as increased screen weight and increased complexity in screen attachment. Another potential disadvantage that offsets the increase in

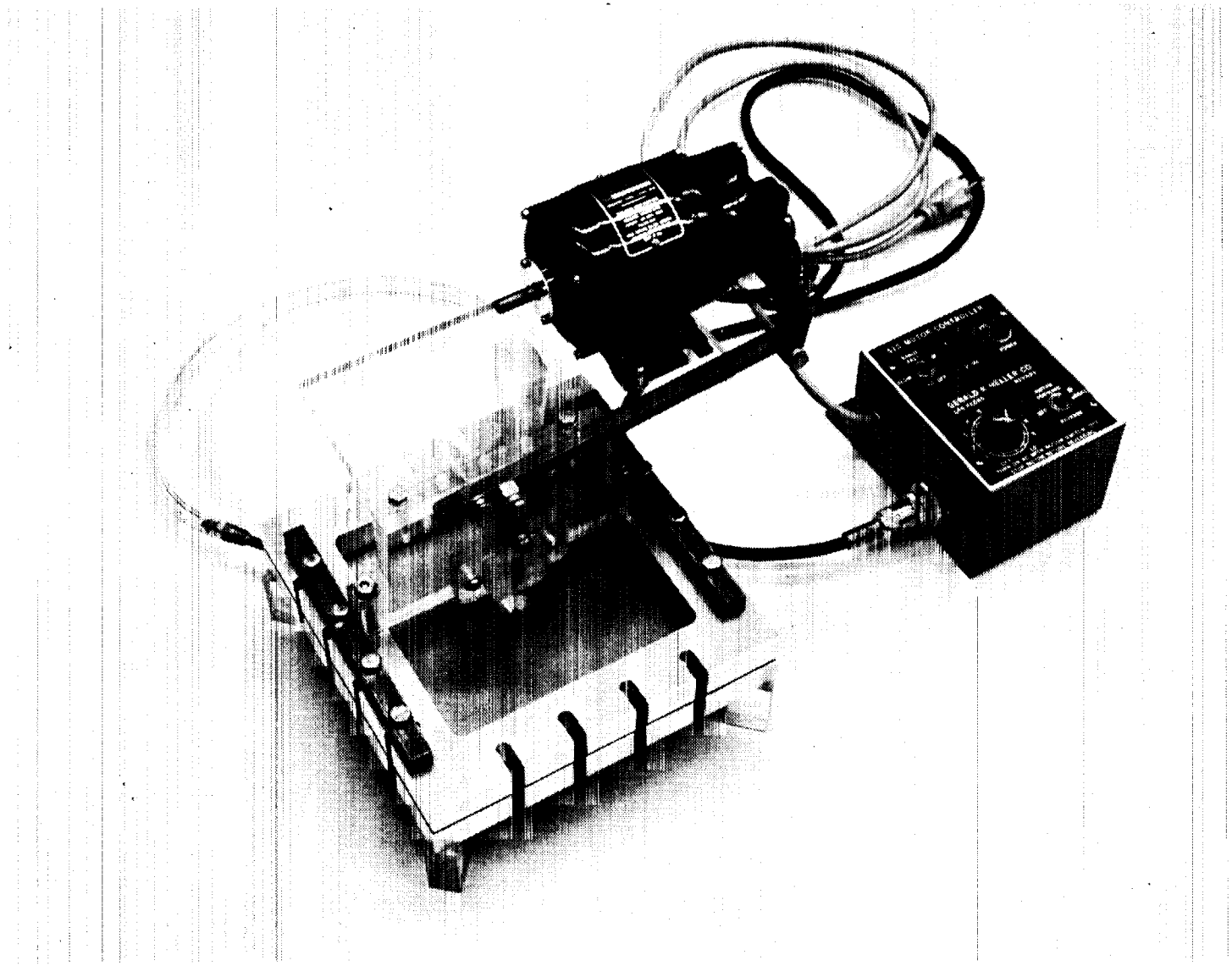

Figure 38. Screen Deflection Test Apparatus

safety factor is a potential reduction in the surface tension capability of the screen because of changes in the pore size distribution brought about solely by the pleating process. Filter industry experience has shown that working the screens through a pleating machine does indeed cause a loss in bubble-point performance.

To quantitatively evaluate this effect, the bubble point will be measured for various pleated-screen elements. Eighteen screen samples have been pleated by a Rabofsky pleating machine to determine what degradation in bubble point occurs. Each 2-in. x 6-in. flat sample was initially bubble-point checked in the apparatus shown in Figure 1, using isopropyl alcohol as a test fluid. Each sample was then pleated using a pleating blade radius of 0.015 in., 3/16 in. pleat height, and pitch of approximately 10 pleats/inch (pitch is a variable dependent upon the wire count and size for a given set of counter weights on the pleater). This type of pleat is representative of that which may be used in an acquisition device. Pleating took place both perpendicular and parallel to the warp direction in the screen. It is expected that bubble-point degradation may be influenced by the anisotropy of the screen. The screen samples (unsintered) are those listed as follows:

		No. Samples	
	Screen Mesh	Pleat Parallel to Warp	Pleat Perpendicular to Warp
1.	325 x 2,300	2	0
2.	250 x 1,370	2	2
3.	200 x 1,400	2	2
4.	200 x 600	2	2
5.	80 x 700	2	2

The mesh thickness ranged from very thin (0.0035 in., 325 x 2,300) to relatively thick (0.01 in., 80 x 700); all samples being dutch-twill weaves. After pleating, each sample was glued into place in a plastic frame (see Figure 39) using a commercial epoxy. Gluing permits the edge of the screen to be sealed to a supporting frame without introducing added physical damage which may effect the pore sizes.

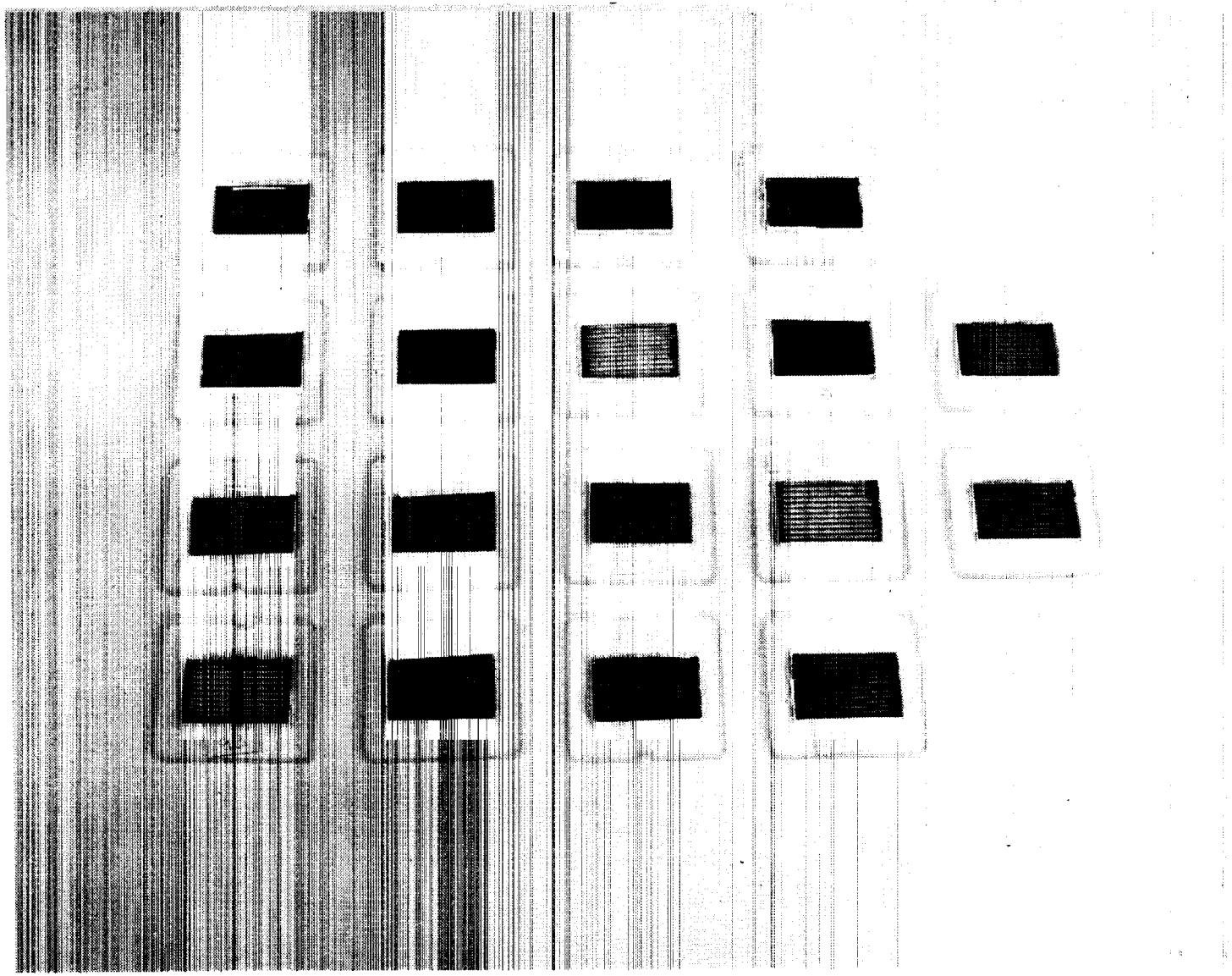

Figure 39. Pleated Screen Installed in Test Frames

The pleated screen samples have yet to be bubble-point checked in the pleated condition in isopropyl alcohol. These data were compared with the basic screen tests and are expected to give a measure of the loss in retentional capability that can be expected if pleating is required. These tests will be completed in April.

3.2.9 Test M—Wicking Experiments

No progress to date.

3.2.10 Test O—Screen Patching Evaluation

No progress to date.

3.2.11 Test P—TVS Heat Transfer Test

No progress to date.

REFERENCES

1. "Study and Design of a Cryogenic Propellant Acquisition System," First Quarterly Progress Report, MDAC Report MDC G2526, September 15, 1971.

2. "Study and Design of a Cryogenic Propellant Acquisition System," Second Quarterly Progress Report, MDAC Report MDC G2743. January 15, 1972.

3. "Lightweight Evacuated Multilayer Insulation Systems for the Space Shuttle Vehicle," Quarterly Technical Progress Report No. 2, Contract NAS 3-14369, Boeing Report, October 1, 1971.

4. "Pressure Sensing and Control Development for Pressurization and Venting Systems," NASA CR-72748, MDAC Report MDC G0933, March 1971.

5. L. J. Poth et al, "A Study of Cryogenic Propellant Stratification Reduction Techniques," GD/FW FZA-419-1, NAS 8-20330, September 15, 1967.

6. J. A. Start and M. H. Blatt, "Cryogenic Zero-Gravity Prototype Vent System," GD/C Report GDC-DDB67-006, October 1967.

7. W. H. Sterbentz, "Liquid Propellant Thermal Conditioning System," LMSC Report LMSC-A839783, (NAS CR-72113) April 1967.

8. Completion of Open Items from Conceptual Design Review Meeting, Rocketdyne letter 71R7134.

9. J. N. Castle, "Preliminary Experimental Evaluation in LH_2 of a Screen Surface Tension Acquisition Device," Report MDC G2452, August 1971.

10. J. N. Castle, "Heat Transfer Effects on Bubble Point Tests in Liquid Nitrogen," MDAC Report MDC G2653, January 1972.

11. J. N. Castle, "Cryogenic Bubble Point Testing of Selected Screens," MDAC Report MDC G2389, August 1971.

12. J. C. Armour and J. N. Cannon, "Fluid Flow Through Woven Screens," AIChE Journal, May 1968, pp 415-420.

13. "Low Gravity Propellant Control Using Capillary Devices in Large Scale Cryogenic Vehicles," related IRAD Studies, Contract NAS 8-21465, Report No. GDC-DDB70-009, August 1970.

14. G. F. Orton, "Simulated Flight Vibration Testing of a Surface Tension Propellant Expulsion Screen," MDAC Report MDC E0091, January 1970.